IN SITU IRON OXIDE EMPLACEMENT FOR GROUNDWATER ARSENIC REMEDIATION

A Dissertation

by

THOMAS SUNDAY ABIA II

Submitted to the Office of Graduate Studies of
Texas A&M University
in partial fulfillment of the requirements for the degree of

DOCTOR OF PHILOSOPHY

December 2011

Major Subject: Biological and Agricultural Engineering

In Situ Iron Oxide Emplacement for Groundwater

Arsenic Remediation

IN SITU IRON OXIDE EMPLACEMENT FOR GROUNDWATER ARSENIC REMEDIATION

A Dissertation

by

THOMAS SUNDAY ABIA II

Submitted to the Office of Graduate Studies of
Texas A&M University
in partial fulfillment of the requirements for the degree of

DOCTOR OF PHILOSOPHY

Approved by:

Co-Chairs of Advisory Committee,	Yongheng Huang
	Saqib Mukhtar
Committee Members,	Raghupathy Karthikeyan
	Bill Batchelor
Head of Department,	Steve Searcy

December 2011

Major Subject: Biological and Agricultural Engineering

ABSTRACT

In Situ Iron Oxide Emplacement for Groundwater Arsenic Remediation.

(December 2011)

Thomas Sunday Abia II, B.S., California State University – San Luis Obispo;

M.S., California State University – San Luis Obispo

Co-Chairs of Advisory Committee: Dr. Yongheng Huang
Dr. Saqib Mukhtar

Iron oxide-bearing minerals have long been recognized as an effective reactive media for arsenic-contaminated groundwater remediation. This research aimed to develop a technique that could facilitate in situ oxidative precipitation of Fe^{3+} in a soil (sand) media for generating a subsurface iron oxide-based reactive barrier that could immobilize arsenic (As) and other dissolved metals in groundwater. A simple in situ arsenic treatment process was successfully developed for treating contaminated rural groundwater using iron oxide-coated sand (IOCS).

Using imbibition flow, the system facilitated the dispersive transport of ferrous iron (Fe^{2+}) and oxidant solutions in porous sand to generate an overlaying blanket where the Fe^{2+} was oxidized and precipitated onto the surface as ferric oxide. The iron oxide (FeOx) emplacement process was significantly affected by (1) the initial surface area and surface-bound iron content of the sand, (2) the pH and solubility of the coating reagents, (3) the stability of the oxidant solution, and (4) the chemical injection schedule. In contrast to conventional excavate-and-fill treatment technologies, this technique could

be used to *in situ* replace a fresh iron oxide blanket on the sand and rejuvenate its treatment capacity for additional arsenic removal. Several bench-scale experiments revealed that the resultant IOCS could treat arsenic-laden groundwater for extended periods of time before approaching its effective life cycle. The adsorption capacity for As(III) and As(V) was influenced by (1) the amount of iron oxide accumulated on the sand surface, (2) the system pH, and (3) competition for adsorption sites from other groundwater constituents such as silicon (Si) and total dissolved solids (TDS). Although the IOCS could be replenished several times before exhaustion, the life cycle of the FeOx reactive barrier may be limited by the gradual loss of hydraulic conductivity induced by the imminent reduction of pore space over time.

DEDICATION

To my father, Thomas Sunday Abia I, a man who never took “no” for an answer during my upbringing. His hardline nurturing was the mental backbone that supported me through these nine (9) consecutive, tumultuous years of engineering school. This work resembles the uncompromising dedication and perseverance that he invested in me.

ACKNOWLEDGEMENTS

I am indebted to my advisory committee co-chairs, Dr. Yongheng Huang and Dr. Saqib Mukhtar, and committee members Dr. Raghupathy Karthikeyan, and Dr. Bill Batchelor, for their guidance and support throughout the course of this research. I am thankful to Dr. Huang for bringing me aboard this project when I first doubted myself as a research engineer. I would also like to thank Dr. Chunyan Wang for her unparalleled contributions to the execution of this project.

Thanks also to my friends, colleagues, and the department faculty and staff for making my time at Texas A&M University an unforgettable experience. I also want to extend my gratitude to the Texas Water Resources Institute, which provided the start-up funds, and the Texas A&M Office of Graduate Studies for their travel assistance to several research conferences. I would also like to acknowledge the support from the Hispanic Leadership in Agriculture and Environment (HLAE). I am grateful to the Texas A&M Wrestling Club and the National Collegiate Wrestling Association (NCWA) for providing me with a worthy distraction from my Ph.D. program. I could not thank you enough for giving me the opportunity to compete and grow as a wrestler in my final days as a scholar.

Lastly, thanks to my friends, old and new, and my family from home and abroad for their support, patience, and love during times of need. This has been the toughest phase for me in my life up to date, and I could not have done it without your endearing words and actions of encouragement.

NOMENCLATURE

ANOVA	Analysis of Variance
As	Arsenic
As(III)	Arsenite
As(V)	Arsenate
atm	atmosphere (pressure)
AWWA	American Water Works Association
BET	Brunauer, Emmett, and Teller
Ca^{2+}	Calcium ion
Cl_2	Chlorine Gas
Cl^-	Chloride ion
ClO_2	Chlorine Dioxide
cm	centimeter
Co^{2+}	Cobalt
CO_3^{2-}	Carbonate
Cu^{2+}	Copper
DDT	Dichlorodiphenyltrichloroethane (pesticide)
DMA	Dimethyl arsenate
DO	Dissolved oxygen
EBCT	Empty bed contact time
EDS	Energy dispersive spectroscopy

Fe	Elemental iron
Fe^{2+}	Ferrous iron
Fe^{3+}	Ferric iron
FeOx	Iron oxide
ft	foot
h	Hour(s)
H^+	Hydrogen ion
H_2O	Water
H_2O_2	Hydrogen Peroxide
$[H_2O_2 + OH^-]_{mix}$	Peroxide-alkalinity mixture
H_2SO_4	Sulfuric Acid
HCl	Hydrochloric Acid
HCO_3^-	Bicarbonate
HOC	Hydrophobic Organic Compound
HRT	Hydraulic Retention Time
in.	inch(es)
IOCS	Iron oxide-coated sand
kg	kilogram
K_H	Distribution coefficient (Henry's Law)
L	liter
lb_m	pound (mass)
M	Molarity

MCL	Maximum contaminant level
Mg^{2+}	Magnesium ion
$mg^{1}L^{-1}$	milligrams per liter (water)
mm	millimeter
MMA	Mono methyl arsenate
MnO_4^-	Permanganate
$mol^{1}L^{-1}$	Moles per liter (molarity)
MW	Molecular weight
N_2	Nitrogen gas
Na^+	Sodium ion
NaCl	Sodium chloride
NaOH	Sodium hydroxide
NAWQA	National Water Quality Assessment
NO_3^-	Nitrate ion
O_2	Molecular oxygen
O_3	Ozone
OCl^-	Hypochlorite ion
OH^-	Hydroxide ion (alkalinity)
OSHA	Occupational Safety and Health Administration
P	Elemental phosphorous
Pa	Pascal (pressure)
P_{O2}	Partial pressure of oxygen in water

PO_4^{3-}	Phosphate ion
ppb	parts per billion
PPE	Personal Protective Equipment
ppm	parts per million
psi	Pounds per square inch (pressure)
PVC	Polyvinyl chloride
PVCT	Pore volume contact time
SEM	Scanning Electron Microscopy
Si	Elemental silica
SiO_3^{2-}	Silicate
SO_4^{2-}	Sulfate
ST_{IOCS}	Iron Oxide-Coated Sand specific throughput
t	Adsorption time
t_{age}	Ageing time
$t_{breakthrough}$	Breakthrough time
t_{coat}	Coating time
WHO	World Health Organization
XRD	X-ray Diffraction
$\mu g^1 L^{-1}$	micrograms per liter
UR_{IOCS}	Iron Oxide-Coated Sand usage rate
USEPA	United States Environmental Protection Agency
USGS	United States Geological Survey

TABLE OF CONTENTS

CHAPTER Page

CHAPTER Page

CHAPTER Page

LIST OF FIGURES

FIGURE Page

FIGURE Page

LIST OF TABLES

TABLE Page

CHAPTER I

INTRODUCTION

PROBLEM STATEMENT

Arsenic Health Implications

Arsenic, a naturally-occurring pollutant with a vast array of pre-existing species, has acquired an unrivaled distinction as a poison. Ingestion of arsenic (As) can result in gastrointestinal irritation, thirst, abnormally low blood pressure, and convulsions (Viraraghavan et al., 1999). The lethal arsenic dose for adults has been observed between 1 and 4 mg As per kg body weight (Pontius et al., 1994). The toxicity scale of arsenic decreases in the order: arsine > inorganic As(III) > organic As(III) > inorganic As(V) > organic As(V) > arsonium compounds and elemental As (Subramanian, 1988). The toxicity is dependent on the oxidation state, chemical form, and solubility in the biological media. The As(III) toxicity exceeds As(V) toxicity by a magnitude of 10 (Pontius et al., 1994). Arsenic has been linked to other illnesses such as liver dysfunction, gangrene, and skin tumors (Hutton, 1987). Furthermore, a study focusing on the carcinogenic risks associated with arsenic-laden water concluded that cancers in the lung, kidney, bladder, and liver may result from consumption (Smith et al., 1992).

This dissertation follows the style of Water Research.

The study used estimated mortality rate ratios from Taiwan to extrapolate the As cancer risk in the United States. The results highlighted that the U.S. lifetime risk of dying from cancer in the bladder, kidney, lung, or liver at a consumption rate of 1 L per day of 50 micrograms per liter (μg^1L^{-1}) arsenic-laden water could be as high as 13 per 1000 persons. The study also concluded that over 350,000 people in the United States may be drinking water containing more than 50 μg^1L^{-1} arsenic and over 2.5 million Americans could be provided with water at a minimum arsenic concentration of 25 μg^1L^{-1}. At the time of this report, there was no accurate data on average arsenic levels in drinking water in the U.S. Some reports estimated between 2.0 and 2.5 μg^1L^{-1} (Life Systems Inc., 1989) while the average water intake was 1.6 L per day (Cotruvo, 1988). With these numbers, the lifetime risk of dying from cancer resulting from arsenic consumption in the United States was estimated at 1 per 1000 persons.

In 1999, the National Academy of Sciences carried out cancer risk assessments for arsenic ingestion from tap water consumption (Table 1) (NAS, 1999). These figures were based on a water consumption rate of 2 L per day per person.

Table 1: Tap Water As Cancer Risk[a] (NAS, 1999)

As level (μg^1L^{-1})	Cancer Risk[b]
0.5	1 in 10,000 people
1.0	1 in 5,000 people
3.0	1 in 1,667 people
4.0	1 in 1,250 people
5.0	1 in 1,000 people
10[c]	1 in 500 people
20	1 in 250 people
25	1 in 200 people
50	1 in 100 people

[a] Estimates in the United States
[b] Assume consumption of 2 L H_2O per day per person
[c] USEPA Drinking Water MCL for Arsenic

Tondel et al. (1999) proved that arsenic poisoning occurred by ingestion of arsenic-contaminated drinking water in Bangladesh. The study correlated the prevalence of skin lesions in males with arsenic intake at 150 μg^1L^{-1} and 1,000 μg^1L^{-1}. The results asserted that the prevalence of 150 μg^1L^{-1} and 1,000 μg^1L^{-1} arsenic in males was 18.6% and 37.0%, respectively. In a similar study by Smith et al. (2000) performed in Chile, the prevalence of skin lesions in males and females based on arsenic dosages between 750 μg^1L^{-1} and 800 μg^1L^{-1} were 66.6% and 16.6%, respectively.

Groundwater Arsenic Pollution Profile

There are many forms and sources of As contamination in the aquatic environment. In aqueous oxic environments, the predominant form of As is arsenate (As(V) as H_3AsO_4, $H_2AsO_4^-$, $HAsO_4^{2-}$, and $AsO4^{3-}$) (Oremland and Stolz, 2003). Arsenite (As(III) as H_3AsO_3 and $H_2AsO_3^-$) are prevalent in anoxic conditions. Arsenic naturally occurs in over 200 different mineral forms of which 60% are arsenates, 20% are sulfides and sulfosalts, and the remaining 20% are arsenides, arsenates, oxides, silicates, and elemental arsenic (Onishi and Wedepohl, 1969). Zerovalent arsenic (As^0) and As^{3-} rarely occur in aquatic environments (Mandal and Suzuki, 2002 and Goldberg and Johnstony, 2001). Organic arsenic compounds such as mono methyl arsenate (MMA) and dimethyl arsenate (DMA) have been observed in surface and groundwater supplies (Anderson and Bruland, 1991). Soil erosion and leaching are suspected of releasing dissolved and suspended arsenic into the oceans (Mackenzie et al., 1979). Table 2 identifies some of the various sources of arsenic contamination in groundwater.

Table 2: Groundwater Arsenic Contamination Sources (Mondal et al., 2006)

Source	Source Description	References
1	Dissolution of As from pyrite ores into H_2O by geological factors	Bureau of Reclamation, 2001
2	Ore processing for Cu, Au, Ni, Pb, and Zn	Leist et al., 2000
3	Insecticide and herbicide components	Korte and Fernando, 1991
4	Cotton and wool processing effluent streams	Chen et al., 1995
5	Arsenic-based wood preservatives	Bureau of Reclamation, 2001
6	Feed additives for metal alloys and in mining	Mandal and Suzuki, 2002
7	Seepages from hazardous waste sites	Bureau of Reclamation, 2001
8	Embalming fluids from cemetery burials (1880 – 1910)	Bureau of Reclamation, 2001
9	Power generation via combustion of As-laden coal	McNeill and Edwards, 1997
10	Effluent from semiconductor and glass manufacturing processes	Leist et al., 2000

[a] Natural source of As groundwater contamination (source #1 only)
[b] Anthropogenic source of As groundwater contamination (sources 2 – 10)

In January 2006, the United States Environmental Protection Agency (USEPA) lowered the maximum contaminant level (MCL) of As in drinking water from 50 $\mu g^1 L^{-1}$ to 10 $\mu g^1 L^{-1}$ (USEPA, 2006). The American Water Works Association (AWWA) conducted a survey for inorganic contaminants in water supply regions in the United States that identified 34 cases where As levels exceeded the MCL (AWWA Committee, 1985). Most of the violations were documented in New Mexico, Oklahoma, and Texas while separate cases were reported in Alaska, Illinois, New Hampshire, North Carolina, and Virginia. The USEPA identified 541 superfund sites across the country with As being the contaminant of concern in groundwater (USEPA OERR, 2009). Figure 1 shows an arsenic profile for approximately 31,350 groundwater wells in the United States, which was surveyed as part of the National Water Quality Assessment Program (NAWQA) (Ryker, 2001). The highest As discharge reported was an acid seep containing 850 $mg^1 L^{-1}$ As from the Richmond mine at Iron Mountain, CA (Nordstrom et al., 1999).

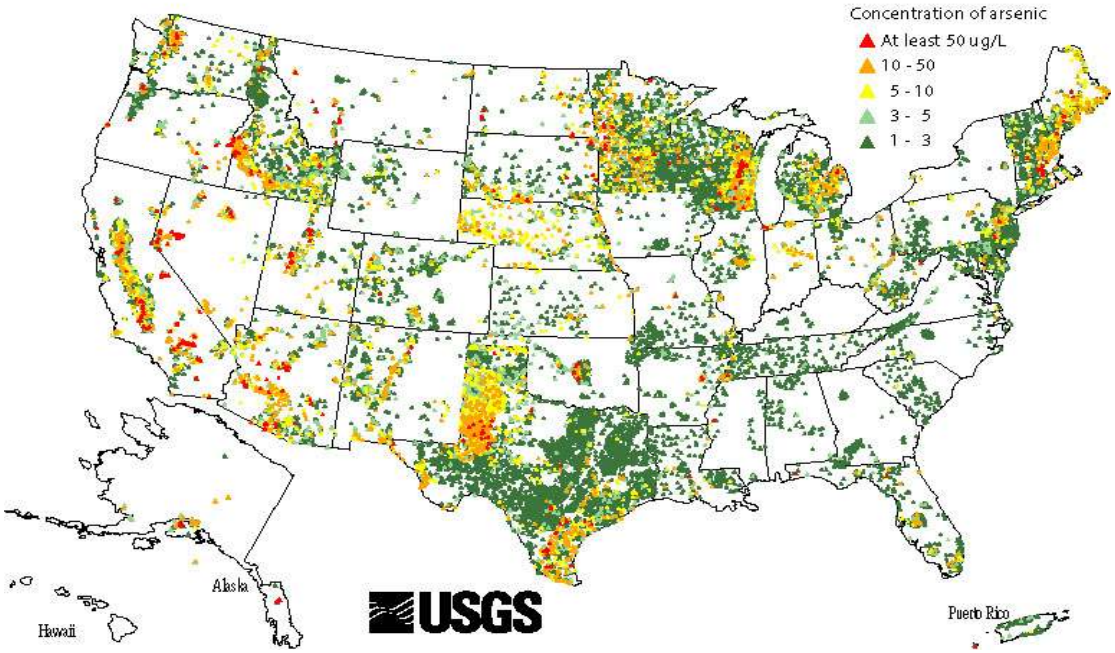

Figure 1: US Groundwater Arsenic Profile (Ryker, 2001)

Current Treatment Technologies for Heavy Metals

Interest in the development of dissolved metal and metalloids removal technology has been triggered by an increasing pool of toxicology reports linking arsenic pollution and domestic groundwater use in addition USEPA regulation of inorganic contaminants in drinking waters. In 1978, the USEPA reviewed arsenic treatment processes and summarized that coagulation with ferrous and aluminum salts and lime softening were the most successful methods for reducing arsenic in drinking water to the provisional primary regulations at 50 $\mu g^{1}L^{-1}$ (USEPA, 1978). Other conventional water treatment methods use mechanisms such as sorption and solid/liquid separation to reduce arsenic and other toxic metal ions. Such processes are employed by ion exchange, adsorption, reverse osmosis, and flocculation technology (Gupta et al. 2005). Table 3 characterizes

different types of chemical precipitation processes for heavy metal removal and their achievable minimum effluent concentrations.

Table 3: Heavy Metal Removal by Chemical Precipitation (Eckenfelder, 2000)

	Achievable Effluent			crystallizing agent					
Metal	**min[a]**	**max**	**Units**	**Al^{3+}**	**Fe^{3+}**	**OH^-**	**SO_4^{2-}**	**S^{2-}**	**removal process employed**
As	50		μg^1L^{-1}					x	filtration
	5		μg^1L^{-1}		x	x			coprecipitation
Ba	0.5		mg^1L^{-1}				x		precipitation
Cd	50		μg^1L^{-1}			x			precipitation at pH 10-11
	50		μg^1L^{-1}		x	x			coprecipitation
	8		μg^1L^{-1}					x	precipitation
Cu	20	70	μg^1L^{-1}			x			precipitation
	10	20	μg^1L^{-1}					x	precipitation
Hg	10	20	μg^1L^{-1}					x	precipitation
	1	2	μg^1L^{-1}	x					coprecipitation
	0.5	5	μg^1L^{-1}		x	x			coprecipitation
	1	5	μg^1L^{-1}						ion exchange
Ni	0.12		mg^1L^{-1}			x			precipitation at pH 10
Se	50		μg^1L^{-1}					x	precipitation
Zn	100		μg^1L^{-1}			x			precipitation at pH 11

[a] affected by type and strength of organic matter and water temperature

Some volatile metals in the water are highly hydrophilic and cannot be easily removed through oxidation, precipitation, or biological treatment while maintaining low operating costs and preserving environmental sustainability. Major problems with current treatment technology for dissolved metals are complex operations, extreme environmental conditions, single-contaminant treatment, use of expensive and toxic chemicals, and lack of re-usability. Among the listed advanced water treatment methods, adsorption has been consistently demonstrated as the best overall remediation process (Zhuang et al., 2007). Equipped with the ability to treat a wide range of compounds,

adsorption technologies can employ a variety of media and eliminate the need for additional treatment systems. Activated alumina sorption, anion exchange, zero-valent iron, polymeric ligand exchange, and iron oxide-coated sand (IOCS) are all examples of adsorption technologies. The high affinity of ferric oxides for metals and other inorganic pollutants suits its purpose as an alternative treatment method. In spite of this quality, its physical properties such as amorphousness, bulkiness, and low hydraulic conductivity have substantially limited its practicability (Benjamin et al. 1996).

Meng et al. (2004) undertook a study that evaluated a simple household bucket system for groundwater arsenic treatment in many villages of Chandpur District, Bangladesh. The system, which was capable of treating 16 L water containing 190 – 750 $\mu g^{1}L^{-1}$ arsenic at a time, comprised of the following: two 20-L plastic buckets, one with a spout mounted near the bottom, 2 g of ferric sulfate ($Fe_2(SO_4)_3$) and 0.5 g of calcium hypochlorite ($Ca(OCl)_2$), a piece of fabric, and some fine sand (Figure 2).

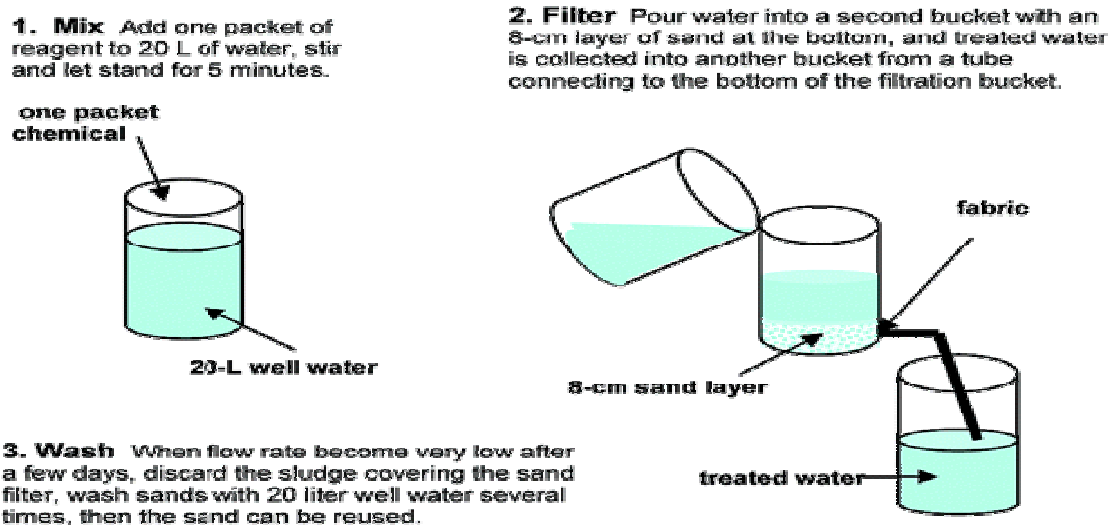

Figure 2: Simple Bucket System for As Treatment in Bangladesh (Meng et al., 2004)

The study reported that the arsenic-contaminated groundwater contained pre-existing amounts of iron (Fe) and phosphorous (P) at concentration ranges of 0.4 – 20 mg^1L^{-1} and 0.2 – 1.9 mg^1L^{-1}, respectively. Only 1 sample out of 72 total samples of treated water violated the Bangladesh drinking water standard of 50 μg^1L^{-1} arsenic (As). Although the As removal results of the study were satisfactory, the literature failed to develop a sufficient disposal protocol for the As-laden sludge. Citing concerns with high arsenic loading from soaring irrigation withdrawals, the authors resorted to spreading the sludge in the surrounding soil fields of the villages; stating the procedure would add less arsenic to the soil than prolonged irrigation with As-laden groundwater. While this method mitigated the impacts of arsenic application, the effects of sulfate (SO_4^{2-}) and hypochlorite (OCl^-) loading on soil were not effectively addressed in this study.

In West Bengal, India, a central facility containing 175 community-based well-head As removal units provides safe drinking water to approximately 150,000 people in the Sangrampur village (Figure 3). The units reduce groundwater As from 200 μg^1L^{-1} to less than 50 μg^1L^{-1} with iron oxide-coated activated alumina. Sarkar et al. (2008) studied and observed 2 regeneration cycles at this location over 5 years. The regeneration method applied sodium hydroxide (NaOH) and hydrochloric acid (HCl) to desorb the fixed As and refresh the spent alumina for additional As treatment. The As-laden sludge was treated with ferric chloride ($FeCl_3$) before aerated coarse-sand filtration for solids retention and storage. Despite the high chemical and operational complexities of this study, the literature cited As/FeOx sludge storage capabilities for at least 20 years with minimal arsenic leaching.

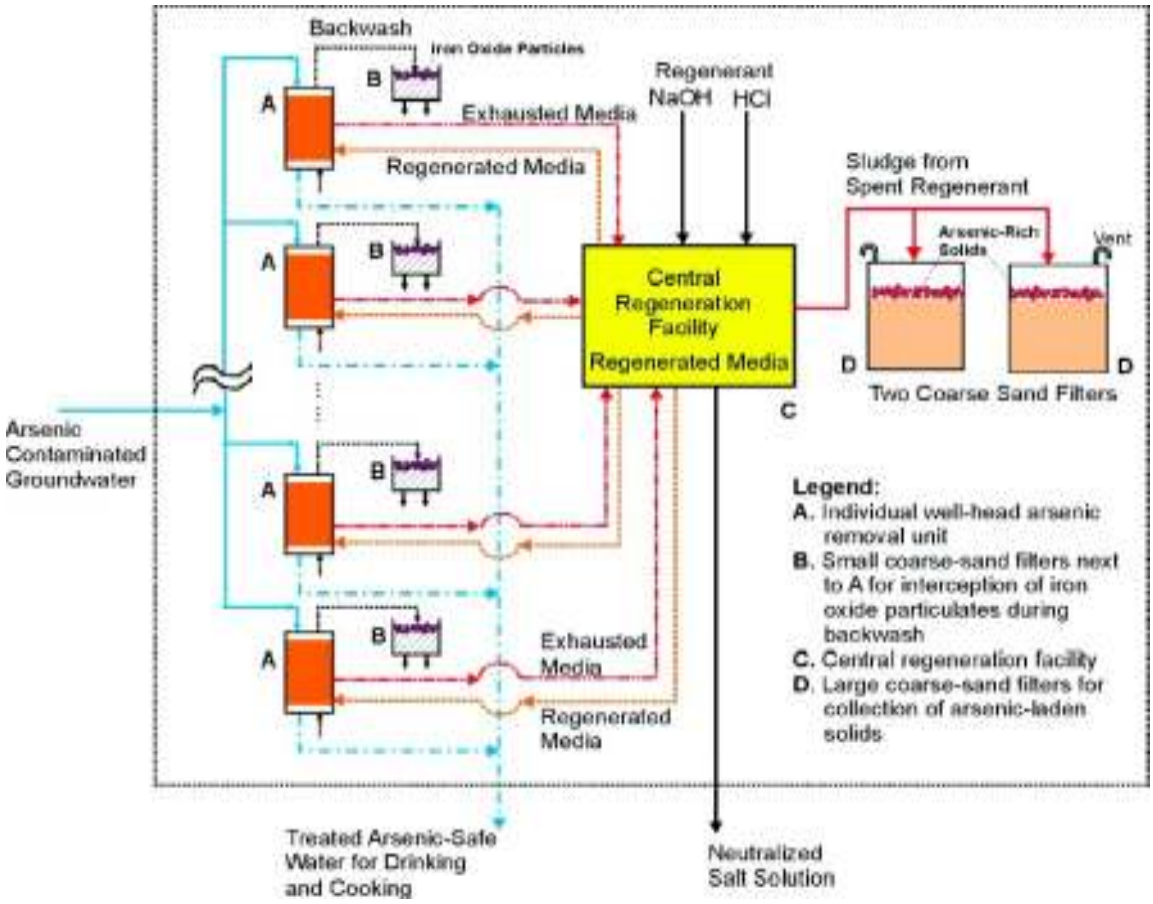

Figure 3: Centralized As treatment in West Bengal, India (Sarkar et al., 2008)

JUSTIFICATION FOR THE RESEARCH

Intellectual Merit

Although several methods have been developed to remediate arsenic from groundwater using ferric oxides and sand, they require additional effort for regeneration and sludge disposal; consequently complicating operational configuration, costs, and accessibility. The concept of arsenic adsorption by iron oxide-coated sand (IOCS) has been proven by the USEPA and a variety of studies. This research proposes to study the oxidative precipitation of Fe^{3+} in a soil (sand) matrix using diffusive transport of ferrous

iron (Fe^{2+}) and oxidant to create an iron oxide-based adsorptive barrier that could be continuously refreshed upon exhaustion. The resulting IOCS could surround a groundwater well and passively immobilize arsenic (As) in subsurface aquatic environments to a considerable extent; further restoring one of the many crippled, yet highly demanded sources of drinking water. The use of non-toxic chemicals in this process could mitigate the anticipation of occupational hazards and health effects; further increasing the accessibility and practicability of this technology for under-resourced communities. The employment of this process for extensive groundwater As remediation has the potential to address the economic and operational concerns of mainstream arsenic groundwater remediation. The elimination of soil excavation, hazardous synthetic chemicals, and sludge disposal could simplify the installation and operation efforts of this technology onto an existing groundwater well. The use of a simple injection scheme, combined with the treatment versatility of iron oxide (FeOx) on a variety of pollutants, could warrant the feasibility of IOCS in rural groundwater As treatment. Moreover, the in situ application may simplify the chemical maintenance and iron oxide (FeOx) refreshment requirements while sustaining a high adsorption capacity; thus extending the treatment life of the IOCS.

Nonetheless, there are challenges that may impede the applicability of the in situ iron oxide sand coating technique in a subsurface environment. The complications associated with the groundwater conditions may adversely affect the As adsorption performance of the IOCS. The ionic conditions could significantly impact the ability of the dissolved As ions to attach to the FeOx crystals on the sand surface. The anticipated complex soil

conditions such as the asymmetrical soil porosities could significantly influence the media hydraulic conductivity; consequently impacting the possibility of in situ regenerating the iron oxide sand. Although IOCS has been proven to remove As and other groundwater contaminants, it remains to be seen whether the long-term stability of the iron oxide and adsorbed arsenic can be established. Accordingly, an investigation into a simple, inexpensive, and sustainable production method for IOCS is necessary to address these concerns and supplement its merit in the drinking water industry.

Broader Impacts

The outcomes of this study will be of significant value not only to groundwater engineers and scientists who are interested in the fate and transport of dissolved metals, but to groundwater industry professionals, regulatory agencies, environmental planners, and ultimately the residents of low-income communities. It is expected that the results of this undertaking will lead to the development of a cutting-edge technology that is within reach for communities that do not have the appropriate means to employ conventional arsenic groundwater remediation. Better understanding of this research with novel modeling tools will help these communities install an appropriate defense against arsenic-contaminated groundwater. The successful implementation of this remarkable, yet simple treatment technology would improve water quality, enhance aquatic public health and safety, and promote social ecology over extended periods of time.

RESEARCH HYPOTHESES

The conditional propositions of this investigation are the following: (1) The initial condition of the sand surface may be directly related to the quality and quantity of the iron oxide (FeOx) coating process. (2) Dispersive-adsorptive and/or dispersive-reactive transport of Fe^{2+} in a homogeneous saturated soil (sand) matrix, concurrent with the use of a water buffer and the controlled supply of an oxidant, may facilitate the precipitation of FeOx at a desired destination from the injection point. (3) The re-emplacement of a new FeOx layer following arsenic (As) saturation on the previously deposited FeOx could encapsulate the immobilized As and thus prevent leaching in landfill conditions over extended time periods. The refreshed iron oxide could also adsorb additional arsenic from contaminated groundwater; effectively extending the life cycle of the iron oxide-coated sand and subsequently producing more drinking water for consumption.

RESEARCH OBJECTIVES

The research proposes to: (1) correlate the migration of sand surface colloids at hydrological interfaces to the quantity and quality of the subsequent FeOx coating process, (2) develop an in situ iron oxide coating procedure and quantify/qualify the FeOx deposits accumulated on the sand, and (3) characterize arsenic (As) removal with respect to groundwater conditions based on the quantity and nature accumulated on the IOCS.

CHAPTER II

IN SITU OXIDATIVE PRECIPITATION OF IRON OXIDES ON POROUS SAND MEDIA: A NEW APPROACH TO IOCS FABRICATION

LITERATURE REVIEW

Mechanism and Kinetics of Ambient Iron Oxide Formation in Aqueous Fe^{2+} Systems

Iron oxides (FeOx) are composed of elemental iron (Fe) together with elemental oxygen (O) and/or alkalinity (OH^-). The ionic strength of the environment significantly impacts iron oxide formations. In aqueous Fe^{2+} systems, the oxidation of Fe^{2+} to ferric iron (Fe^{3+}) has been observed at pH levels as low as 4 and as high as 10 (Cornell and Schwertmann, 2003). However, the oxidation rate of O_2 is severely retarded by the increasing concentration of hydrogen (H^+) ions in acidic conditions ($2.5 \leq pH \leq 4$) (Millero et al., 1987). The conversion of Fe^{2+} to Fe^{3+} produces iron oxides, iron hydroxides, and/or iron oxide-hydroxides, which can be generally described by one of the following reactions:

$$4Fe^{2+} + O_2 + 8OH^- \rightarrow 2Fe_2O_3 + 4H_2O \quad (1)$$

$$4Fe^{2+} + O_2 + 6H_2O \rightarrow 4FeOOH + 8H^+ \quad (2)$$

Equation 1 represents the formation of ferric oxide, e.g. hematite (α-Fe_2O_3), as the end product. In Equation 2, the oxidation of Fe^{2+} produces iron oxyhydroxide (e.g. lepidocrocite Υ-FeOOH), which results from oxygen-induced oxidation followed by hydrolysis (Tamura et al., 1976; Sung and Morgan, 1980; Vracar and Cerovic, 1997; and Rose and Waite, 2002). The oxidation of one Fe^{2+} to ferric oxide or ferric oxyhydroxide

will produce 2 H^+, thus both reactions (Eqns 1 and 2) will consume a significant amount of alkalinity or lower the pH.

Houben (2004) discussed the hydro-chemical background of iron oxide formation in aqueous Fe^{2+} systems. At near-neutral pH, the rate of Fe^{2+} oxidation is first order with respect to the Fe^{2+}concentration and second order with respect to the hydroxide ion concentration (Stumm and Lee, 1961):

$$R = k_1*[Fe^{2+}]*P_{O2}*[OH^-]^2 \quad (3)$$

where R is the reaction rate for Fe^{2+} oxidation (mol^1min^{-1}), k_1 is the rate constant ($mol^{-2}atm^{-1}min^{-1}$ or $mol^{-3}min^{-1}$), $[Fe^{2+}]$ is the ferrous iron concentration (mol^1L^{-1}), P_{O2} is the partial pressure of dissolved oxygen (atm^1L^{-1}), and $[OH^-]$ is the hydroxide ion concentration (mol^1L^{-1}). Previous studies determined k_1 at 25 ^oC to be 1.8 x 10^{13} $mol^{-2}atm^{-1}min^{-1}$ (1.4 x 10^{16} $mol^{-3}min^{-1}$ when using oxygen solubility) (Tamura et al., 1976) and 8.0 ($\pm$ 2.5) x 10^{13} $mol^{-2}atm^{-1}min^{-1}$ (6.0 x 10^{16} $mol^{-3}min^{-1}$ when using oxygen solubility) (Stumm and Morgan, 1996). Millero (1985) and Wehrli (1990) found that Fe^{2+} and oxygen interacted rapidly in the presence of hydroxyl groups; leading to a higher oxidation rate that most likely resulted from enhanced electron transfer capabilities. The partial pressure of oxygen can be expressed as dissolved oxygen (DO) concentration using Henry's Law:

$$K_H = [O_2]/P_{O2} \quad (4)$$

where K_H is the temperature-dependent distribution coefficient (mol^1atm^{-1}) and $[O_2]$ is the DO concentration in water (mol^1L^{-1}). Stumm and Morgan (1996) found that the K_H values at 25 ^oC and 10 ^oC were 1.26 x 10^{-3} mol^1atm^{-1} and 1.32 x 10^{-3} mol^1atm^{-1},

respectively. Substituting Equation 4, the dissociation constant for water ($K_w = [OH^-]*[H^+] = 1 \times 10^{-14}$ mol^2L^{-2}), and the exponential relationship between pH and hydrogen concentration ($[H^+] = 10^{-pH}$) into Equation 3, the aerial Fe^{2+} oxidation rate can be rearranged into a more suitable function of O_2 concentration and pH:

$$R = k_1*[Fe^{2+}]*([O_2]/K_H)*(K_w/10^{-pH})^2 \quad (5)$$

where K_H and K_w are temperature-dependent constants and R is now second order with respect to the pH and first order to the Fe^{2+} and O_2 concentrations (mol^1L^{-1}).

Tamura et al. (1976) found that initially deposited iron oxide had a catalytic effect on the subsequent oxidation of Fe^{2+}. The literature established a direct relationship between the total Fe^{2+} oxidation rate and increasing iron oxide (FeOx) concentration at pH 6.2. This finding was attributed to the sorption of Fe^{2+} onto the precipitated FeOx followed by surface oxidation. The adsorption of Fe^{2+} onto the FeOx surface was found to have increased with rising pH due to the elevated negative surface charge of the oxide. Additionally, Equation 3 was expanded by Tamura et al. (1976) to account for the oxidation rate of the Fe^{2+} on the FeOx:

$$R = k_1*[Fe^{2+}]*P_{O2}*[OH^-]^2 + k_2*[Fe^{2+}]*[Fe^{3+}]*P_{O2}*[OH^-]^2 \quad (6)$$

where $[Fe^{3+}]$ is the precipitated iron oxide concentration (mol^1L^{-1}) and k_2 is the Fe^{2+} oxidation rate on the iron oxide surface ($mol^{-2}atm^{-1}min^{-1}$ or $mol^{-3}min^{-1}$). The first half of Equation 6 was defined as the homogeneous oxidation of Fe^{2+} in aqueous phase as described by Equations 3 or 5 while the second half was referred to as the heterogeneous oxidation of Fe^{2+} on the FeOx surface. The pH was determined to be a more formidable obstacle to the homogeneous reaction at high acidic levels. Hence, the heterogeneous

oxidation of Fe^{2+} was found to be insignificant at levels below 3 $mg^{1}L^{-1}$ Fe^{2+} (0.05 x 10^{-3} $mol^{1}L^{-1}$) where the iron oxides are incapable of providing sufficient catalytic surface (Tamura et al., 1976).

RESEARCH OBJECTIVES

The study described in this chapter was aimed at developing a novel technique that could in-situ emplace iron oxides onto soil media under ambient environments and mild chemical conditions. An exhaustive literature review revealed that no method of the like or similar has been previously reported or knowingly used. The technique involved the employment of dispersive, adsorptive, and reactive chemical/hydraulic processes to transport Fe^{2+} and oxidant (e.g., dissolved oxygen) through porous media to the desired location, upon which Fe^{2+} reacted with the oxidant and precipitated onto the soil grain surface. The study focused on elucidating the mechanism and evaluating the factors that influenced the in-situ FeOx coating process.

MATERIALS AND METHODS

Materials

During reagent preparation, separate 20-L Nalgene carboy tanks filled with water were first titrated with HCl or NaOH solutions to their desired pH ranges and purged with 95%-purity compressed nitrogen or 97%-purity oxygen. 19 M sodium hydroxide (NaOH) and 6 M hydrochloric acid (HCl) solutions were used for pH adjustments. The reagents in granular form were then added to the water solutions following oxygen removal. Two types of silica sand were procured from an indigenous manufacturer of industrial minerals (AGSCO Corporation, Wheeling, Illinois, United States). The sands

each had a geometric size range between 0.42 and 0.59 mm (30 x 40 US mesh), bulk density of 1605 $kg^{1}m^{-3}$, and a bulk porosity of 38%. A Brunauer, Emmett, and Teller (BET) analysis measured the sand surface area at 1.20 $m^{2}g^{-1}$.

Equipment and Wet Chemistry Analyses

Outgoing samples from column tests were collected using two Spectrum Chromatography 141200 IS-95 Fraction Collectors (Spectrum Chromatography, Houston, Texas). Wet chemistry analyses were referenced from methods published by the American Public Health Association (APHA), American Water Works Association (AWWA), or the Water Environment Federation (WEF) (APHA et al., 1995).

pH measurements were conducted using a Thermo Scientific 5000 pH meter (Thermo Scientific, Singapore). Atomic absorption readings for total Fe (flame method at 248 nm), As(III) (mercury hydride method at 193 nm), and total As (mercury hydride method at 193 nm) were acquired using a PerkinElmer AAnalyst400 Atomic Absorption Spectrometer (PerkinElmer, Connecticut). Spectrometric analyses for turbidity (250 nm) and Fe^{2+} (510 nm) were carried out using a PG T80+ UV/IVS Spectrometer (PG Instruments, Wibtoft Lutterworth, Leicestershire, United Kingdom). Scanning Electron Microscopy (SEM) and X-ray Diffraction (XRD) were used to characterize the surface properties of sand and emulsified mixtures (Ellis and Pendleton, 2007). Energy Dispersive Spectroscopy (EDS) was employed to mathematically compute the elemental composition on the sand using dispersive energy plots. A Quantachrome NOVA 4200e Surface Area and Pore Size Analyzer was determined the specific surface area of the sand via N_2 gas adsorption (Quantachrome Instruments, Boynton Beach, Florida).

Sand Purification Chemical Components

Preparation of Hydrochloric Acid (HCl) Solution

3 mL of 1.00 M HCl was diluted with de-ionized water (DI H_2O) to 3 L to produce 1.00 mM stock H^+.

Preparation of Sodium Hydroxide (NaOH) Solution

3 mL of 1.00 M NaOH was diluted to 3 L to produce 1.00 mM stock OH^-.

Preparation of Sodium Chloride (NaCl) Buffer Solution

3 mL of 1.00 M NaCl was diluted to 3 L to produce 1.00 mM stock NaCl.

Iron Oxide (FeOx) Chemical Components

Preparation of Dissolved Oxygen (DO) Solution

According to Henry's Law described in Equation 4, the dissolved oxygen concentration in water is proportional to the partial pressure of the system. The solubility of oxygen (O_2) in water descends from 0.28 to 0.26 mM ($9.1 \leq DO \leq 8.3$ mg^1L^{-1} O_2) when equilibrated in open air (101 kPa) at temperatures between 20 and 25 ^oC (Millero et al., 1987). Accounting for only 21% of the dissolved air in water by volume (Emsley, 2001; Dole, 1965; Cook, 1968; Cotton and Wilkinson, 1972) the solubility of O_2 in water can be elevated between 1.23 and 1.35 mM ($39.6 \leq DO \leq 43.3$ mg^1L^{-1} O_2) when equilibrated with compressed oxygen in similar environmental conditions. Hence, 10 L of DI H_2O was oxygenated and augmented with. 9.84 mM (167 mg^1L^{-1}) of NaOH to produce an oxidant/alkalinity supply mixture ($[O_2 + OH^-]_{mix}$) that would facilitate Fe^{3+} precipitation.

Preparation of Ferrous Iron (Fe^{2+}) Solution

Referring to Equations 1 and 2, the Fe^{2+} and alkalinity concentrations were designed to react with the maximum DO concentration in water. To account for the frequent temperature fluctuations (23 $\pm$ 2 ^{o}C) during the study, a maximum 19.5 g of ferrous chloride tetrahydrate ($FeCl_2 \cdot 4H_2O$) was dissolved in 20 L of DI H_2O to produce 4.92 mM Fe^{2+} stock (275 mg^1L^{-1} Fe^{2+}) that would react with 1.23 mM DO at 25 ^{o}C. HCl was used to adjust the solution within a pH range that prohibited Fe^{2+} and Fe^{3+} precipitation in the storage tank.

Preparation of Water Buffer Solution

Oxygen-depleted DI H_2O was also used as a barrier to avoid contact between the Fe^{2+} and $[O_2 + OH^-]_{mix}$ plumes in the conveyance system.

Design of Column Experiments

All experiments were constructed and operated indoors (23 $\pm$ 2 ^{o}C at 101 kPa). A series of column trials were conducted to devise a proper injection scheme that would maximize iron oxide (FeOx) precipitation on the sand. To avoid air bubble formation, the sand was wet-packed into clear polyvinyl chloride (PVC) columns that were acquired from a local manufacturer (Boedeker Plastics Inc., Shiner, Texas, United States). The columns each were 91 cm long with an inside diameter (ID) of 2.54 cm; converting to a sand volume and mass of 287 mL and 477 g, respectively. A minimum pore volume contact time (PVCT) of 30 minutes was sustained by pumping 5.6 mL^1min^{-1} feed water using a peristaltic pump (Masterflex Model # 7519-15, Vernon Hills, IL, USA). Daily water pressure (10 $\pm$ 0.7 kPa) and reagent pH readings were also recorded.

Surface-bound Iron Extraction and Analyses

Two extraction procedures were carried out to characterize (1) the surface-bound, pre-existing iron (Fe^{2+}) on the sand prior to iron oxide coating and (2) the subsequently emplaced iron oxide.

For the Fe^{2+} extraction procedure, a mass-based liquid-solid ratio of 10:1 was used to determine the proper amount of extraction liquid required for each sand batch (Lee et al., 2007 and Lee et al., 2009). 60 mL of hydrochloric acid (HCl at 6 M) was mixed with 6 g sand; sustaining a pH of 0.78 $\pm$ 0.03. Iron extraction experiments were performed under constant agitation in rubber-sealed 70-mL beakers in a rotating arm shaker (29 rpm) for 24 h. Supernatant samples were individually filtered through a 0.45 μm cellulose acetate filter and analyzed for Fe^{2+} via UV/IVS Spectrometry.

Sand samples were collected before wet-packing, after purification, and after iron oxide (FeOx) coating for spectrometric surface imaging analyses in the FeOx extraction procedure. Ferrous iron (Fe^{2+}) breakthrough profiles were acquired before and after FeOx sand coating to evaluate Fe^{2+} transport behavior in the sand column. The 91-cm columns were then dismantled into 15-cm portions, rinsed with DI H_2O, and air-dried in depth-coded petri dishes for 48 hours before undergoing imaging and/or aqueous extraction. 5 g of dried, well-mixed iron oxide-coated sand (IOCS) from each petri dish was placed in separate 10-mL glass vials, mixed with 10 mL of 6 M HCl, sealed with a rubber top, and agitated in a rotating arm shaker (29 rpm) for 24 h to obtain an aqueous solution. Each solution was then filtered through a 0.45 μm cellulose acetate filter and analyzed for Fe^{2+} and total iron. The Fe^{2+} and total Fe concentrations were used to

quantify the FeOx accumulation on the sand (mg^1g^{-1}) with respect to column depth and were subsequently arranged into an FeOx concentration profile.

RESULTS AND DISCUSSION

Sand Purification

Using imbibition flow, the sand was injected with HCl and NaOH to remove pre-existing excess surface colloids following wet-packing. Sodium chloride (NaCl) was used as a buffer to separate the HCl and NaOH plumes in the conveyance system. The PVCT for this procedure was 60 minutes. The sand was first rinsed with DI H_2O to remove loosely suspended particles resulting from wet-packing. The acid/base injection scheme proceeded in the following format:

$$HCl \rightarrow NaCl \rightarrow NaOH \rightarrow NaCl \quad (7)$$

where the dissociated hydrogen ion (H^+) from the HCl replaces the bridging bonds (Ca^{2+} or Mg^{2+}) between the surface minerals and the sand grain with two hydrogen bonds; resulting in a weaker binding strength. The hydroxide ions (OH^-) from the NaOH generate a repulsive force that overcomes the weak H^+ attraction and detaches the degraded impurities from the sand (Huang, 2009). Table 4 and Figure 4 discuss the chemistry and operation of the purification procedure in the sand columns.

Table 4: Sand Purification Operation[a]

Chemical	pH	Molar Concentration	Mass Concentration	Injection Time[b]
HCl	~3.00	1.00 10^{-3} M	1.00 mg^1L^{-1}	60 minutes
NaCl	~8.35	1.00 10^{-3} M	58.4 μg^1L^{-1}	60 minutes
NaOH	~11.0	1.00 10^{-3} M	17.0 mg^1L^{-1}	60 minutes
NaCl	~8.35	1.00 10^{-3} M	58.4 μg^1L^{-1}	60 minutes

[a] sand column PVCT = 60 minutes
[b] Sum of injection times is equal to one conditioning cycle

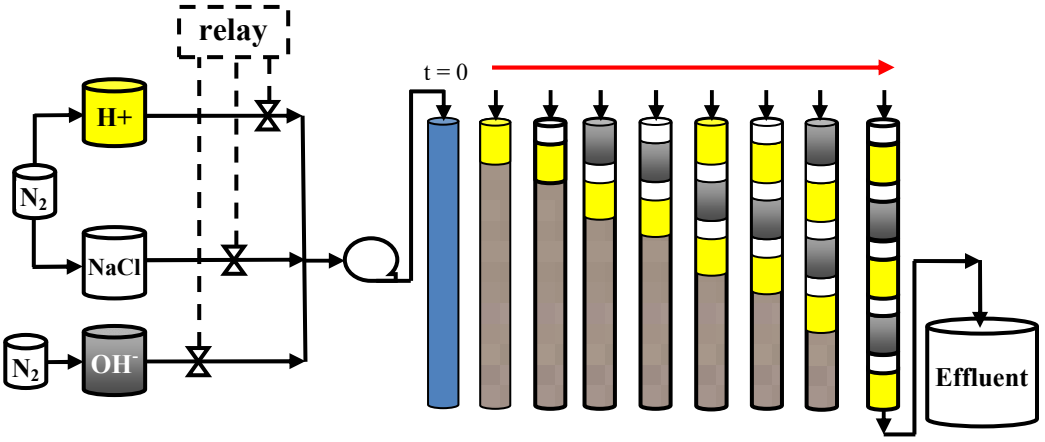

Figure 4: Sand Purification Procedure

Each conditioning cycle lasted 4 hours and experiments were performed to evaluate the changes in sand properties for up to 4 conditioning cycles. SEM imaging (Figure 5) revealed that the original silica sand surface was laden with clays and colloids before the conditioning phase was initiated. After the conditioning chemicals were applied, the rugged surface of the original silica sand was converted to a smooth exterior with a smaller amount of colloids remaining (Figure 6).

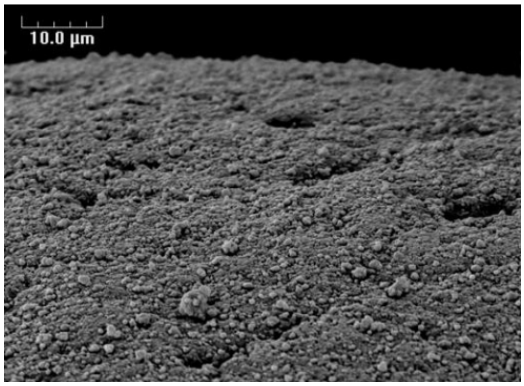

Figure 5: Initial Sand Surface

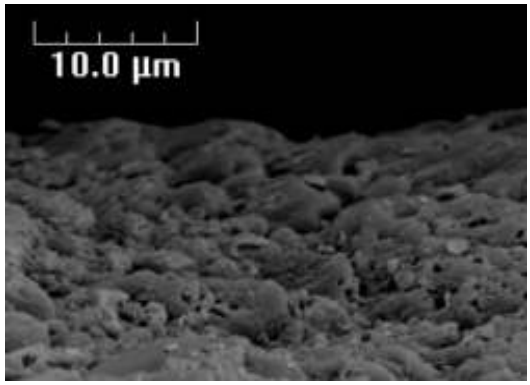

Figure 6: Surface of Cleaned Silica Sand

Turbidity release profiles were sporadically composed in between each of 4 purification cycles on a single sand column to establish a relationship between colloid migration and increasing acid/base applications. The exiting turbidity was plotted with respect to each injection cycle (Figure 7).

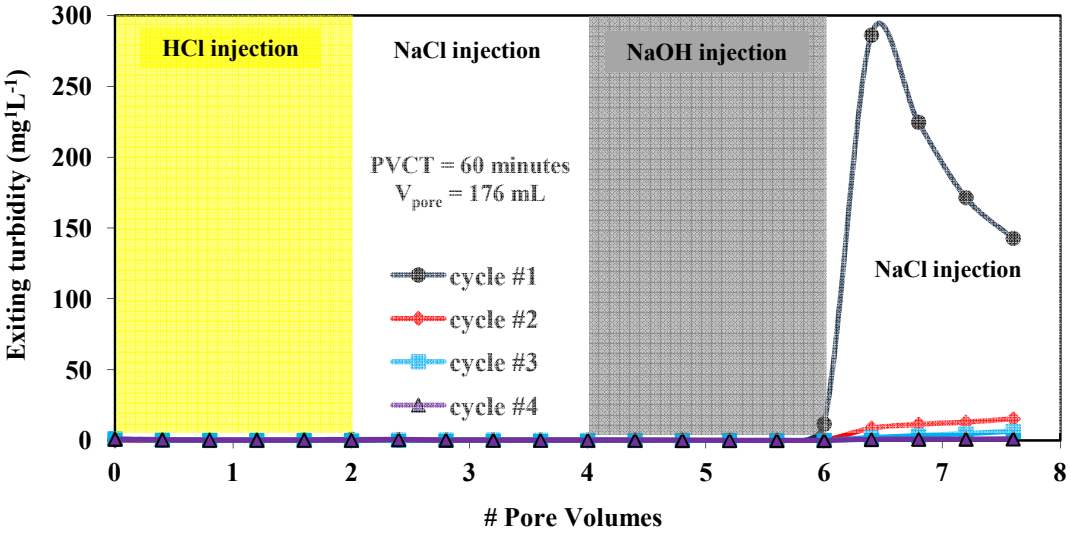

Figure 7: Turbidity release during Sand Purification

Figure 7 indicated that colloid release was significantly reduced after the 1st purification cycle. X-ray Diffraction (XRD) analyses revealed that colloidal particle matter released from the sand cleaning process was predominantly kaolinite and muscovite, two of the most common clay minerals. Energy Dispersive Spectroscopy (EDS) analysis further corroborated the effectiveness of the sand purification process as the silicon content generally increased with additional conditioning cycles (Table 5). BET analyses were also performed to examine how the sand surface cleaning process

will change the specific surface area of the sand. The analyses concluded that the BET surface area of the sand increased with additional purification cycles. The upsurge in the specific surface area could provide additional emplacement surface for iron oxides and yield a higher concentration on the sand; ultimately increasing the adsorption capacity of the sand for dissolved metallic ions.

Table 5: Sand Physical Parameter Analyses (EDS and BET)

		Purification cycles					
Sand Parameter	**Sand[a]**	**1**	**2**	**3**	**units**	**Δ_{max}[b]**	**Cycle[c]**
Silicon (Si) content	82.7	88.7	91.1	85.3	% weight	10.1%	2
Iron (Fe) content	5.75	1.10	1.42	1.43	% weight	-80.8%	1
Oxygen (O) content	3.11	3.92	2.13	4.36	% weight	40.2%	3
BET Surface Area	1.20	2.39	3.67	5.37	m^2g^{-1}	348%	3

[a] Physical analysis of original sand condition before purification
[b] Maximum upward or downward percentage change from original sand
[c] Corresponding cycle to where Δ_{max} occurred

The availability of surface colloids on the media prior to iron oxide coating was found to affect the ability of the Fe^{2+} to adhere to the sand before induced O_2 oxidation. An Fe^{2+} transport profile analysis was carried out to compare Fe^{2+} adsorption on original sand against purified sand of various conditions. Following sand purification, aqueous Fe^{2+} was continuously pumped through the sand filter (2 hours) in conjunction with intermittent water injections (1 hour) and analyzed for a change between the initial and final concentrations (Figure 8). The proceeding concentrations (C_{out}) were divided by the fixed feed (C_{in}) to yield the fraction of Fe^{2+} passing through the filter (C_{out}/C_{in}). A low C_{out}/C_{in} suggested high Fe^{2+} retention (adsorption) on the sand. A fraction yield value above 1 indicated desorption of pre-existing Fe^{2+} on the sand.

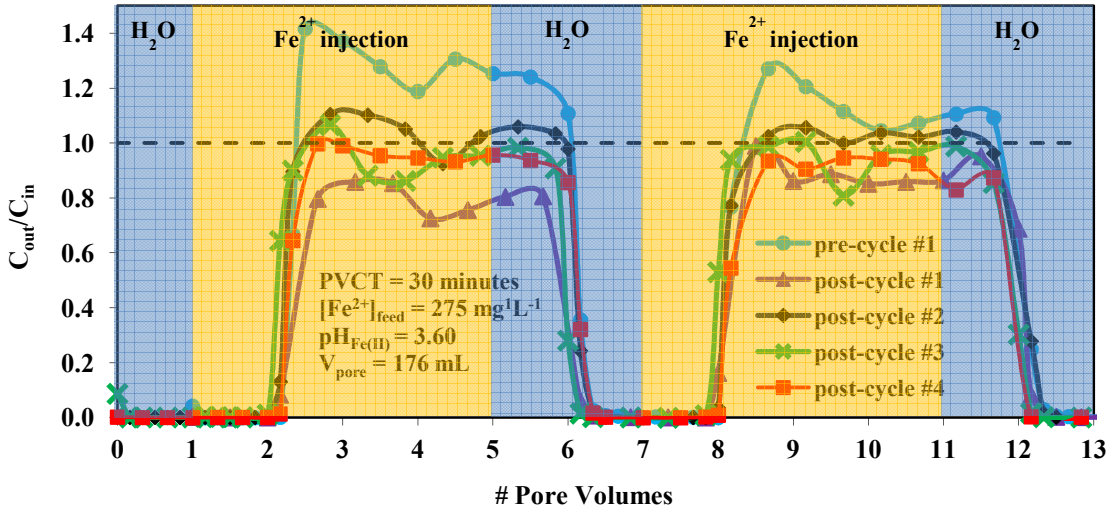

Figure 8: Sand column Fe^{2+} Breakthrough Curves with or without Prior Cleaning

The breakthrough analysis revealed that Fe^{2+} adhesion on sand peaked after the first purification cycle (post-cycle #1 curve, 27% after 4 pore volumes) while Fe^{2+} desorption was greatest before any purification was carried out (pre-cycle #1 curve). This finding further insinuates that the sand contained some surface-bound iron prior to cleaning. The reduction in Fe^{2+} breakthrough after the first cycle could be attributed to the upsurge in adsorption sites resulting from the twofold increase in specific surface area. Furthermore, the purification procedure may have significantly diminished Fe^{2+} adsorption by removing a considerable amount of iron from the sand (maximum loss of 81% after 1st cycle). Although no specific relationships between the surface colloids and the iron content of the sand have been established, the data suggested that the iron content reduction is a direct result of colloid migration. As such, the sand surface minerals may have contained iron in addition to clay particles. To that effect, total colloid removal must be avoided to allow for sufficient Fe^{2+} availability.

Iron Oxide Sand Coating Performance

The sand was first rinsed with water to remove any remaining debris from the conditioning procedure and stabilize the system to near-neutral pH. Using imbibition flow, the sand was then sequentially eluted with ferrous chloride ($FeCl_2$ as Fe^{2+} source) and oxygenated sodium hydroxide ($[O_2 + OH^-]_{mix}$) to precipitate iron oxide (FeOx) crystals on the sand surface. Intermittent injections of de-oxygenated water were used as buffers to separate the Fe^{2+} and $[O_2 + OH^-]_{mix}$ plumes in the conveyance system. The PVCT for this procedure was 30 minutes. The proceeding injection scheme follows:

$$Fe^{2+} \rightarrow H_2O \rightarrow [O_2 + OH^-]_{mix} \rightarrow H_2O \quad (8)$$

where the duration of the H_2O injection dictated the depth at which FeOx (Fe^{3+}) was formed in the column. FeOx in the sand column could be produced by two different mechanisms: (1) Direct oxidation of aqueous Fe^{2+} ions by dissolved oxygen under favorable pH to precipitate Fe^{3+} particles and adsorb onto the sand grain surface (dispersive-reactive Fe^{2+} transport). In this mechanism, the formation of FeOx results from a homogeneous reaction where both Fe^{2+} and $[O_2 + OH^-]_{mix}$ were in aqueous phase. Although the Fe^{2+} and O_2 were injected into the sand column separately with a H_2O buffer in between, the two chemicals may have diffused towards each other as they moved through the porous sand bed and come into contact eventually. (2) In the second mechanism, FeOx is formed by the direct oxidation of surface-adsorbed Fe^{2+} when a DO plume passes through. In this case, the reaction is a surface-mediated heterogeneous reaction. The efficiency of this mechanism depends on the adsorption of Fe^{2+} onto the sand (dispersive-adsorptive Fe^{2+} transport). To ensure sufficient oxidation of Fe^{2+} in the

sand column, the $[O_2 + OH^-]_{mix}$ injection slightly exceeded the Fe^{2+} injection; providing additional alkalinity and oxidant supply. A series of preliminary experiments were conducted to establish optimum pH ranges for the coating reagents and ascertain proper in situ injection scheme. Table 6 and Figure 9 discuss the chemistry and operation profiles of the FeOx coating technique, which was successfully capable of precipitating Fe^{3+} onto silica sand under ambient temperature and pressure conditions (Figure 10).

Table 6: Iron Oxide Coating Chemistry Profile and Operation[a]

Reagent(s)	pH	Molar Concentration	Mass Concentration	Injection Time[b]
Fe^{2+} H^+	~4.00	4.92 10^{-3} M 100 10^{-6} M	275 mg^1L^{-1} 100 μg^1L^{-1}	4 minutes
H_2O	~6.00	1.00 10^{-6} M	1.00 μg^1L^{-1}	10 minutes
O_2 OH^-	~12.0	~1.23 10^{-3} M $\leq$9.84 10^{-3} M	~39.4 mg^1L^{-1} $\leq$167 mg^1L^{-1}	6 minutes
H_2O	~6.00	1.00 10^{-6} M	1.00 μg^1L^{-1}	10 minutes

[a] PVCT = 30 minutes

[b] Sum of injection times is equal to one FeOx injection cycle

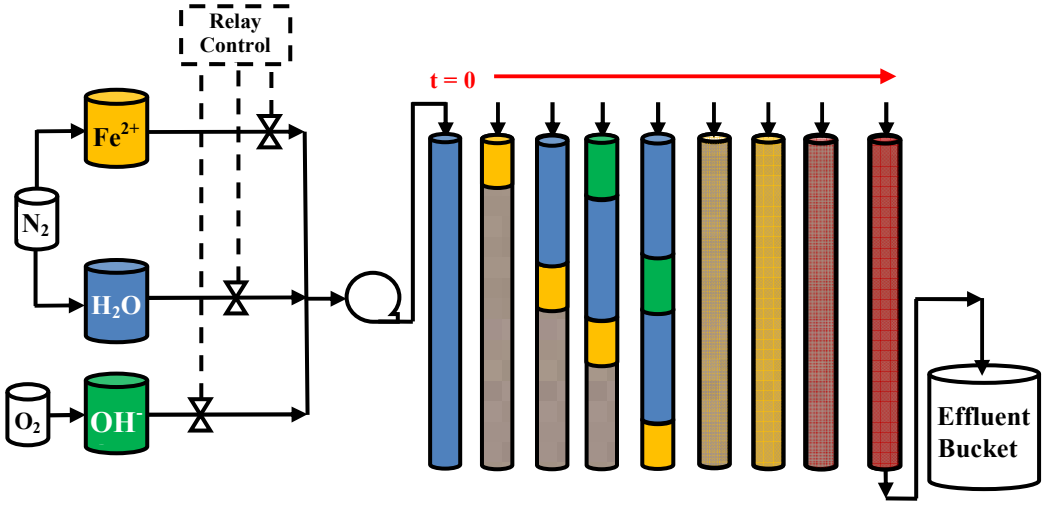

Figure 9: FeOx Sand Coating Procedure

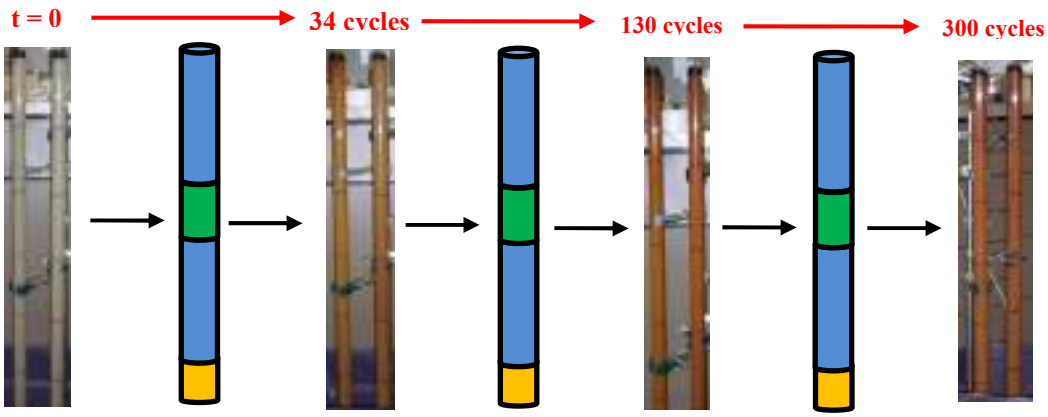

Figure 10: FeOx Sand Coating Performance

It was observed that FeOx precipitation was prohibited or severely delayed when there was little or no pre-existing iron in the sand. The sands in this study were analyzed to identify initial Fe^{2+} content through acid extraction experiments prior to FeOx coating in the column. The Agsco white sand (high quality grade), which did not yield surface-bound iron oxide formation even after 5 days of coating, had an initial Fe^{2+} composition of 0.06 $mg^{1}kg^{-1}$. Conversely, FeOx was observed after the 1st day of coating on the Agsco beige sand (low quality grade), which initially consisted of 0.18 $mg^{1}kg^{-1}$ Fe^{2+}. The data suggests that FeOx precipitation on the sand was accelerated with increasing surface-bound Fe^{2+} content.

The dispersive-adsorptive transport profile of Fe^{2+} prior to FeOx coating was illustrated in Figure 8. The small quantity of Fe^{2+} adsorbed, combined with the initial iron in the sand, may have been oxidized concurrently by the introductory $[O_2 + OH^-]_{mix}$ plume to form the initial FeOx layer on the sand grain. The subsequent accumulation of FeOx was examined by elucidating the interactions between the Fe^{2+} and $[O_2 + OH^-]_{mix}$

in the sand. Herein, the effluent Fe^{2+} and $[O_2 + OH^-]_{mix}$ plumes were collected and profiled with their respective pH values for the initial three injection cycles (Figure 11).

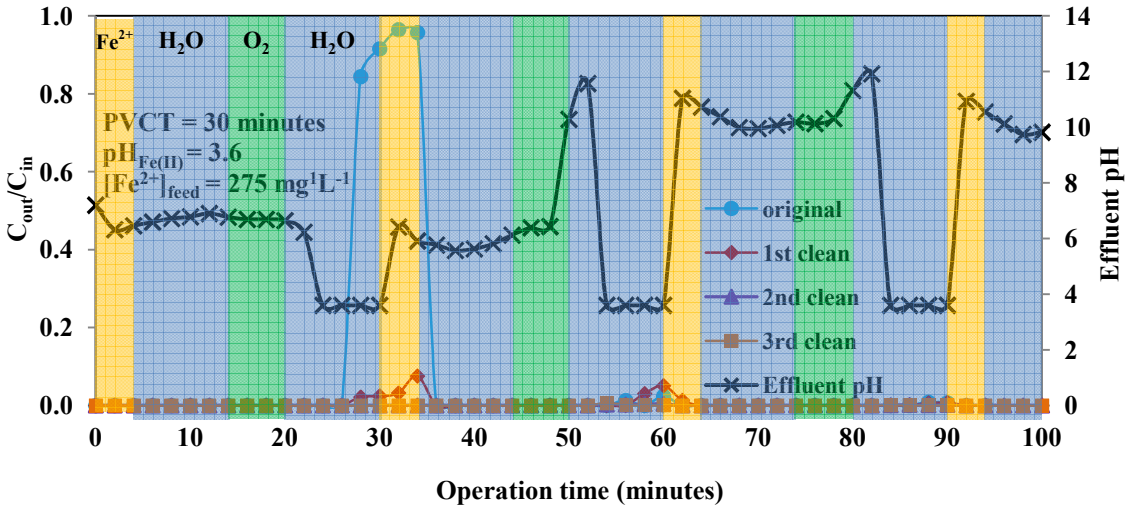

Figure 11: FeOx Sand Coating Reaction Progress

Outflow samples were collected every 2 minutes and analyzed for pH or Fe^{2+}. Effluent pH was not recorded during the time intervals between 28 – 34 minutes, 56 – 62 minutes, and 84 – 90 minutes because the outflow samples were preserved with acid and analyzed for Fe^{2+} only. The first coating cycle displaced water that was used to rinse the system after sand purification; accounting for the near-neutral effluent pH in the first 28 minutes of operation. The elevated pH in the final 50 minutes demonstrates the sustained prevalence of the $[O_2 + OH^-]_{mix}$; implying that significant Fe^{2+} oxidation may have been achieved in the sand column. The non-purified sand (original sand) recorded significant Fe^{2+} in the outflow at the beginning of the 2nd coating cycle; accounting for the pre-

existing Fe^{2+} in the system prior to FeOx coating. Oxygen and alkalinity were not introduced into the column until after the first Fe^{2+} and H_2O buffer injections; making it possible for the first Fe^{2+} injection to pass through the sand column un-oxidized. The cleaned sand columns did not bleed more than 8% of the injected Fe^{2+} during their first 100 minutes of operation; suggesting that the Fe^{2+} was either retained in the sand column or precipitated to FeOx.

Additional breakthrough curves of a continuous Fe^{2+} injection were obtained during progressive stages of the FeOx coating process to evaluate how the adsorptive-diffusive transport of Fe^{2+} through the sand media would be affected by the presence of an increasing amount of FeOx in the media (Figure 12).

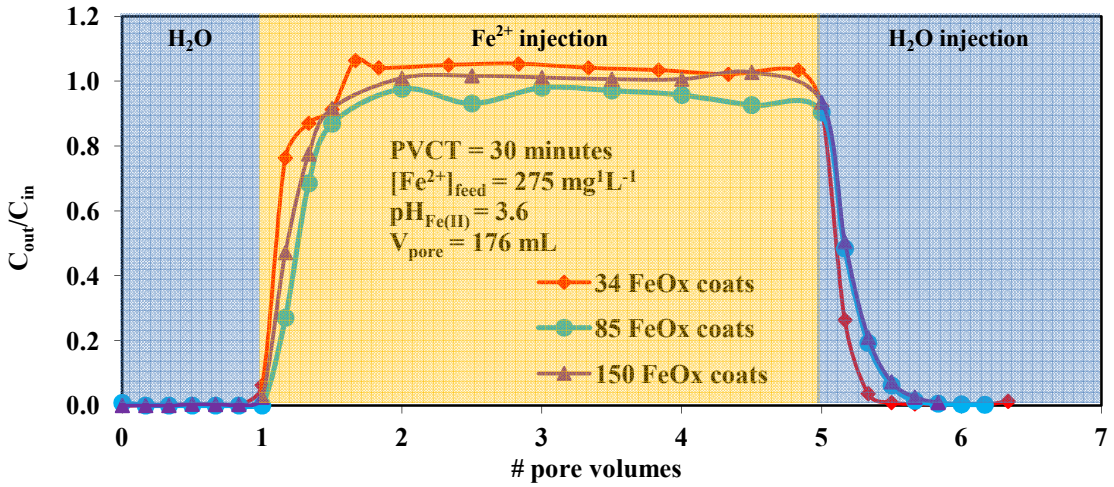

Figure 12: Fe^{2+} Mobility in Sand Filter with Increasing FeOx Coating

The steadily weak Fe^{2+} adsorption with increasing FeOx precipitation alluded to diffusive-reactive transport as the dominant Fe^{2+} conveyance mechanism in the coating

process; attributing to the repulsion between Fe^{2+} and FeOx induced by the low $pH_{Fe(II)}$ of 3.6. The migrated Fe^{2+} ions were most likely oxidized by the $[O_2 + OH^-]_{mix}$ plume prior to sorption onto the FeOx surface.

Iron Oxide Sand Coating Control Variables

The development of the FeOx emplacement technique was not entirely flawless. Several operating factors were encountered and documented throughout the course of several trial-and-error experiments before the appropriate FeOx coating sequence was successfully devised. The varying magnitudes of impact inflicted by these variables were critical to properly depositing FeOx on the sand, yet simple to control.

The preparation of the FeOx chemical reagents was found to affect the coating process. The FeOx chemicals reacted in the conveyance system and subsequently precipitated Fe^{3+} before reaching the injection point; leading to clogging and a reduced hydraulic conductivity at the top of sand column (Figure 13). This phenomenon was attributed to the pre-existing oxygen (5.7 mg^1L^{-1} O_2) in the reagent water. Thus, the design of the FeOx coating experiment required de-oxygenation of the Fe^{2+} and H_2O buffer solutions before injection initiation.

Figure 13: Iron Oxide Slurry-induced Clogging

While the composition of the FeOx reagents controlled their behavior in the conveyance system, their delicate chemistry profiles were fundamentally crucial to their performances in the sand column. It was observed early in the study that the FeOx reagents necessitated pH ranges where (1) encrustation of stored Fe^{2+} was circumvented, (2) over-lapping between the Fe^{2+} and $[O_2 + OH^-]_{mix}$ plumes was averted during single-line conveyance, and (3) sufficient deposition of Fe^{3+} was achieved in the sand column by the $[O_2 + OH^-]_{mix}$. In essence, the most ideal ionic conditions for this study would delay FeOx formation until the endpoint (sand column) was reached. Table 7 lists the various FeOx chemicals, their conditions, and their respective system responses.

Table 7: FeOx Reagent Ionic Conditions and Observed System Responses

Agent	Condition(s)*	Storage	Transport	Column	Response Comments**
Fe^{2+}	+33.3 mL 6M HCl: pH ≈ 2.0	A	A	C**	retardation of FeOx precipitation
	+3.32 mL 6M HCl: pH ≈ 3.0	A	B**	A	slight FeOx formation
	+1.96 mL 1M HCl: pH ≈ 4.0	A	B**	A	slight FeOx formation
	+0.16 mL 1M HCl: pH ≈ 5.0	A	C**	~	vulnerability to ionic penetration
	no modification: pH ≈ 6.0	B**	B	B	Fe^{3+} sediments observed after 24 h
H_2O	+33.3 mL 6M HCl: pH ≈ 2.0	A	A	C**	inhibition of FeOx precipitation
	+0.33 mL 6M HCl: pH ≈ 4.0	A	A	C**	decelerated FeOx formation
	+0.16 mL 1M HCl: pH ≈ 5.0	A	A	A	No adverse response observed
	no modification: pH ≈ 6.0	A	B**	A	Slight Fe^{3+} precipitation
	$+2E^{-3}$ mL 1M NaOH: pH ≈ 7.0	A	C**	~	Lack of $H^+ \rightarrow$ ineffective barrier
	+0.02 mL 1M NaOH: pH ≈ 8.0	A	C**	~	accelerated FeOx formation
	+2 mL 1M NaOH: pH ≈ 10	A	C**	~	accelerated FeOx formation
O_2	+2 mL 1M NaOH: pH ≈ 10	A	A	B**	insufficient alkalinity supply
	+20 mL 1M NaOH: pH ≈ 11	A	B**	A	slight FeOx formation
	+33.3 mL 6M NaOH: pH ≈ 12	A	B**	A	slight FeOx formation
	+105 mL 19M NaOH: pH ≈ 13	A	B	C**	black Fe deposits in sand column

* Change in pH of DI water ($pH_{initial} = 5.70 \pm 0.15$ and $V_{water} = 20$ L) using HCl and NaOH to adjust

** Comments pertain to side effects resulting from the least favorable response recorded

A slight response with minimal side effects, overall process is unaffected, best conditions

B moderate response with discomfort to overall process, conditions are tolerable with caution

C significant response with detrimental side effects to overall process, conditions not suitable

Fe^{2+} sediments were observed in the storage tank at pH 6, but FeOx sedimentation in the sand column was severely retarded at an Fe^{2+} storage pH below 2.0. As such, the Fe^{2+} solution pH was maintained between 3 and 4 to minimize the sensitivity to ionic changes. The use of a strong acid or strong base as a buffer agent can significantly hinder or rapidly accelerate Fe^{3+} formation upon contact with the Fe^{2+} plume, respectively. The installation of a weak alkaline buffer resulted in the instantaneous precipitation of Fe^{2+} and/or Fe^{3+} in the conveyance system, likely due to the chemical reaction between the alkalinity and the Fe^{2+}. However, minimal Fe^{2+} and/or Fe^{3+} sedimentation was observed in the conveyance system with the installation of a weak acid buffer; keeping the Fe^{2+} and $[O_2 + OH^-]_{mix}$ plumes intact until diffusion into the sand column was attained. Accordingly, the water buffer was preserved between pH 5.0 and pH 6.0. To accommodate the high demand for alkalinity, the oxygenated water was augmented with 167 mg^1L^{-1} OH^- (9.84 mM OH^- at pH 12), which provided sufficient alkalinity for oxidative precipitation of Fe^{2+} in the sand column, as demonstrated in Equations 1 and 2. However, an $[O_2 + OH^-]_{mix}$ injection with pH at 13 precipitated black and/or slurry iron in the sand column likely as a result of excess alkalinity in the system. The $[O_2 + OH^-]_{mix}$ performed best at a pH range between 11 and 12 as opposed to pH 10, where FeOx precipitation was slightly delayed due to insufficient alkalinity supply. The Fe^{2+} and H_2O buffer solutions were henceforth purged with nitrogen and titrated to their respective pH ranges prior to reagent addition for all subsequent experiments.

A correlation between sand surface area and FeOx sand coating distribution was developed. After each subsequent sand purification cycle, several sand filters in parallel

operation were continuously coated in FeOx for a total of 384 coating cycles per column. FeOx concentration profiles were constructed by separating the columns into 6 segments and analyzing them for Fe^{3+} concentrations on the sand ($[FeOx]_{0 - 15}$, $[FeOx]_{15 - 31}$, $[FeOx]_{31 - 46}$, $[FeOx]_{46 - 61}$, $[FeOx]_{61 - 76}$, and $[FeOx]_{76 - 91}$) in the following manner:

$$\sigma_n^2 = ([FeOx]_{avg} - [FeOx]_{depth})^2 \quad (9)$$

$$\sigma_{uniformity} = (\sum \sigma_n^2/6)^{0.5} \quad (10)$$

where $[FeOx]_{avg}$ is the mean FeOx concentration of each column (mg^1g^{-1}), $[FeOx]_{depth}$ is the depth-specific FeOx concentration (mg^1g^{-1}). The uniformity of FeOx coating ($\sigma_{uniformity}$) is equal to the standard deviation of each column. A low $\sigma_{uniformity}$ (mg^1g^{-1}) indicates a higher degree of uniform coating on the sand (Figure 14).

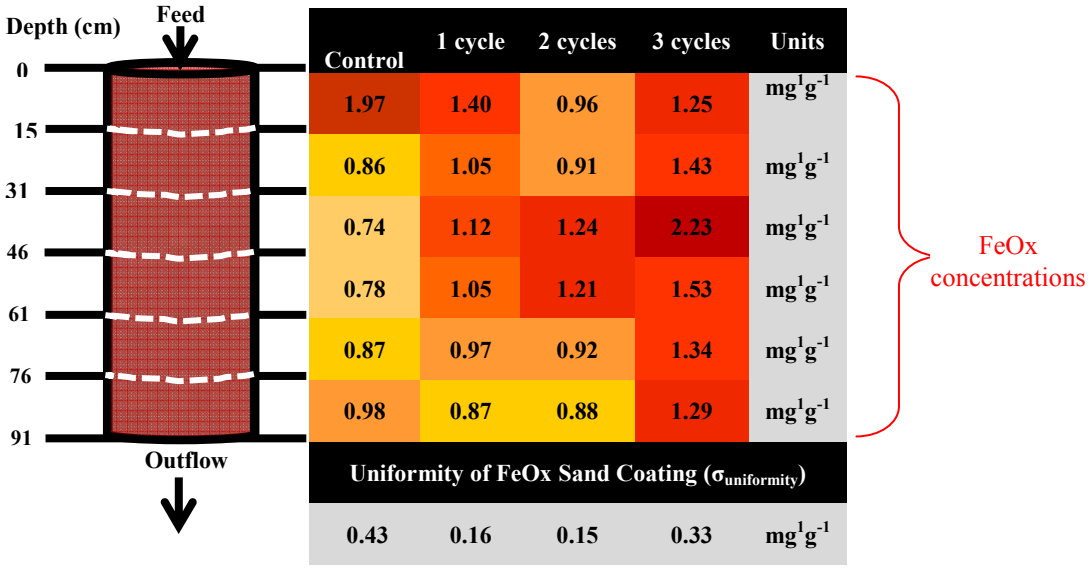

Figure 14: FeOx Sand Coating Concentration Profiles

The data shows that the non-purified (control) sand column, had the most uneven FeOx distribution (highest $\sigma_{uniformity}$). The concentration of the precipitated Fe^{3+} in the top 15 cm of the control column was more than twice of any of its other sections. The preferred deposition of FeOx in the inlet increased the likelihood of clogging at the injection point that could subsequently result in reduced hydraulic conductivity. Similar effects of lesser extent were observed after 1 purification cycle where the $[FeOx]_{0 - 15}$ surpassed the [FeOx] at the lower depths by a maximum magnitude of 1.61; highlighting the reduced but significant potential for clogging. The data further illustrates that the FeOx concentrations on the sand increase as the surface area also increases. The likelihood of induced head loss at the injection point was lowest after 2 sand purification cycles, and henceforth all further FeOx sand coating experiments were preceded with this procedure.

The injection schedule for applying the FeOx coating chemicals were based on an operating PVCT of 30 minutes. The injection point was at the top of the sand column with the FeOx coating configured to initially coat the bottom portion to prevent loss of hydraulic conductivity early in the experiment. The duration of the H_2O buffer injection was initially suspected of influencing the depth at which FeOx deposits would be retained in the sand column. Figure 15 demonstrates how the duration of the water plug between the Fe^{2+} and $[O_2 + OH^-]_{mix}$ insertions controlled the depth at which the migrating Fe^{2+} was oxidized by the O_2 and retained in the sand column. The top graph shows the injection depths of each chemical in a single coating cycle and the bottom graph shows the observed coating progress over time with respect to the injection scheme and number of FeOx coating cycles. Previous FeOx coating trials have shown

that an elongated water buffer elution would increase the depth at which Fe^{3+} precipitation would occur; substantiating the applicability Fe^{2+} oxidation at controlled depths. The water buffer could also be reduced to coat the sand at shorter distances from the injection point, but was not necessary upon acquisition of uniform coating in the column. The H_2O buffer was ineffective as an ionic barrier at an elution time under 5 minutes at the PVCT of 30 minutes, leading to the results of the control column in Figure 13. The $[O_2 + OH^-]_{mix}$ injection slightly exceeded the Fe^{2+} injection to optimize Fe^{3+} precipitation (Table 12). The injection schedule remained constant throughout the coating process for all columns since uniform coating was achieved (Figure 10). The coating depth was first observed between 18 and 30 inches shortly after commencement. Despite uniform FeOx emplacement in all regions of the column, the aforementioned depth continued to accumulate more Fe^{3+} than the other zones throughout the coating process; resulting in the low Fe^{2+} effluent concentrations acquired in Figure 11.

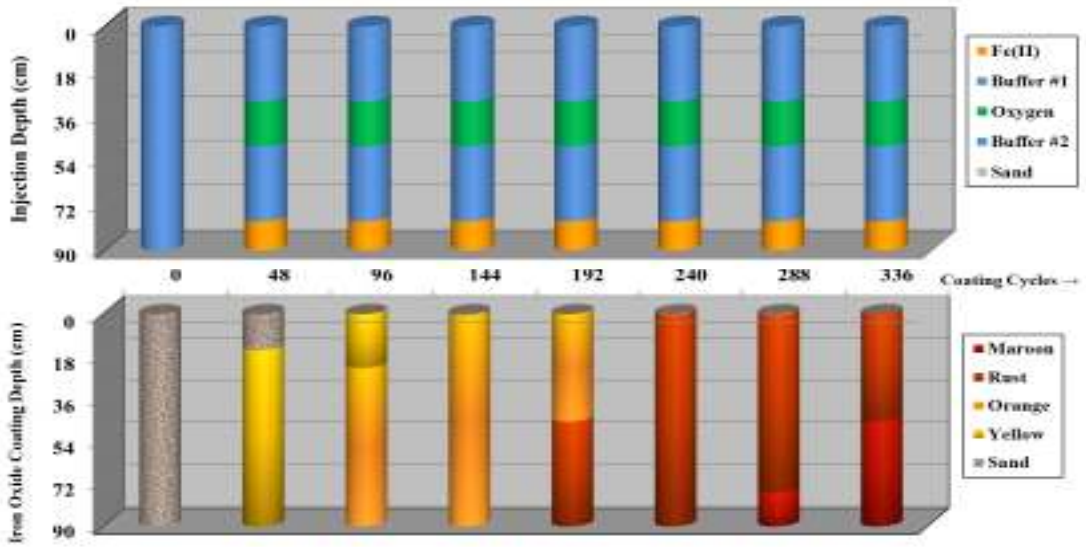

Figure 15: FeOx Sand Coating Profile

SUMMARY

Silica sand packed under saturated conditions was coated with iron oxide using an extensive in situ preparation process. The sand was purified with acid and base to remove surface minerals; thus converting the complex initial surface with various clay minerals to a more uniform and pure silica surface. It was discovered that an adequate amount of remaining colloids allowed for uniform iron oxide coating despite lacking superior Fe^{2+} adsorption.

After several preliminary trial-and-error experiments, the in situ iron oxide sand coating process was successfully developed and optimized using two-step diffusive transport of Fe^{2+}, water buffer, and oxidant. The in situ iron oxide coating process was influenced by the (1) physical preparation of the coating agents, (2) reagent pH, (3) initial sand condition, and (4) coating schematic. The de-oxygenated Fe^{2+} and water buffer solutions maintained delicate pH ranges for optimum coating performance. The Fe^{2+} solution could have a minimum pH of 3 to sufficiently attach onto the surface minerals of the silica sand and a maximum pH of 4 for simultaneously prevention of pre-oxidative precipitation in the storage tank. The oxygen-depleted water buffer was successfully capable of averting Fe^{2+} oxidation in the conveyance system while promoting Fe^{3+} sedimentation in the sand column using a pH range between 5.0 and 6.0.

CHAPTER III

ADSORPTIVE FILTRATION OF GROUNDWATER ARSENIC BY IRON OXIDE-COATED SAND (IOCS)

LITERATURE REVIEW

Physiochemical and Sorption Properties of Iron Oxides

The characterization of iron oxides has been critical in understanding their capacity for metallic adsorption. Cornell and Schwertmann (2003) discussed the complex physiochemical and sorption properties of iron oxides (FeOx). They are predominantly composed of iron (Fe) together with elemental oxygen (O) and/or hydroxide (OH^-) and generally have low solubility, which contributes to their high stability in precipitated form. The iron content in the compounds can either be ferrous (Fe^{2+}), ferric (Fe^{3+}), or a mixture of both. The performance of iron oxides as sorption mediums for contaminant removal are affected by several characteristics such as specific surface, porosity, heating temperature and time, evolving crystal morphology, competition for adhesion sites by various ions, and electronic properties. For example, the adsorption of arsenic on FeOx is influenced by the rate of transfer of the outermost pair(s) of electrons to the FeOx surface. The electron configuration of the Fe^{3+} ion is $1s^2\ 2s^2\ 2p^6\ 3s^2\ 3p^6\ 3d^5$ where the 5 unpaired electrons in the 3d orbital highlight the unique affinity for anionic and/or cationic covalent bonding.

Anionic adsorption, the mechanism behind arsenic uptake by iron oxides, involves the oxidation of ligands. Ligands are ions that have at least one atom with a lone pair of

electrons so that they can function as electron donors (Cornell and Schwertmann, 2003). Iron, a transition metal, serves as the electron acceptor that oxidizes and adsorbs the ligand, such as arsenic. For groundwater remediation, common ligands such as chlorides (Cl^-) and nitrates (NO_3^-), even at high concentrations, are slightly unfavorable to arsenic adsorption onto iron oxides due to their weak net charge (Dzonmabk and Morel, 1990). On the other hand, phosphates (PO_4^{3-}), sulfates (SO_4^{2-}), carbonates (CO_3^{2-}), and silicates (SiO_3^{2-}) at elevated concentrations increase arsenic mobility significantly. The groundwater pH also affects As adsorption onto iron oxides. As(V) adsorption is greatest under acidic conditions whereas As(III) adsorption is superior in alkaline conditions. At an ambient pH around 7, the adsorption capacities of As(V) and As(III) will overlap due to the different surface complexes resulting from the two oxidation states (Cornell and Schwertmann, 2003). The dynamics of anionic adsorption on FeOx follow a two-step process beginning with the rapid diffusion of the anion to the immediately available adsorption sites on the FeOx surface. The time-consuming second phase of adsorption can be attributed to (1) the diffusion into particle aggregates (Willet et al., 1988 and Fuller et al., 1993) or crystal micropores and (2) surface complexation.

RESEARCH OBJECTIVE

The present research was designed to evaluate the newly devised iron oxide-coated sand (IOCS) as an adsorbent for groundwater As(III) and As(V) remediation. The resulting development could provide a long-term and feasible solution to groundwater arsenic remediation.

MATERIALS AND METHODS

Materials

All materials used in this study were duplicated in the same manner from Chapter II.

Equipment and Wet Chemistry Analyses

All equipment and wet chemistry analyses performed in this study was duplicated in the same manner from Chapter II.

Preparation of IOCS

The iron oxide sand coating results obtained from Chapter II was replicated in this study to prepare the iron oxide-coated sand (IOCS).

Preparation of Synthetic Arsenic Samples

Synthetic sodium arsenite ($NaAsO_2$ at 0.5% weight by volume or 5,000 mg^1L^{-1}) and sodium hydrogen arsenate heptahydrate ($Na_2HAsO_4{\cdot}7H_2O$) were used as the As(III) and As(V) supplies, respectively. 1.00 g of $Na_2HAsO_4{\cdot}7H_2O$ was dissolved in 1 L DI H_2O to produce a stock solution of 240 mg^1L^{-1} As(V). 54 mL of $NaAsO_2$ was diluted with 946 mL DI H_2O to make an As(III) stock supply of 270 mg^1L^{-1}.

Design of Batch Experiments

Batch experiments were carried out indoors (22 $\pm$ 3 ^oC at 101 kPa) with virgin materials to investigate the effects of water pH ($pH_{solution}$), adsorption time ($t_{adsorption}$), initial As concentration (isotherms), iron oxide (FeOx) dosage ($[FeOx]_{sand}$), and groundwater constituents (anions) on As(III) and As(V) adsorption by iron oxide-coated sand (IOCS). The working sand volume and mass in each batch sample was 3.12 mL and 5 g, respectively. To study the effects of FeOx dosage on As uptake, experiments were

performed with fixed arsenic concentrations of 3 mg^1L^{-1} and varying FeOx concentrations on the sand (0.74 - 2.26 mg^1g^{-1} or 0.4 – 1.23 g^1L^{-1}). In order to maintain a relatively constant FeOx dosage in the remaining experiments, IOCS with FeOx concentrations ranging from 1.37 to 1.51 mg^1g^{-1} (0.74 – 0.82 g^1L^{-1}) was used for the batch samples. The concentration for each As influent sample during the $pH_{solution}$, $t_{adsorption}$, $[FeOx]_{sand}$, and anion batch experiments was 3 mg^1L^{-1} while the adsorption isotherm studies ranged between 1 and 20 mg^1L^{-1} influent As(III) or As(V). All batch samples were placed in 10-mL vials with re-sealable rubber stoppers and agitated in a rotating arm shaker for mixing. Excluding the $t_{adsorption}$ and $pH_{solution}$ experiments, all batch samples were shaken over a pristine period of 24 h at near-neutral pH (pH = 7.0 $\pm$ 0.2), respectively. After arm-shaking rotation (29 rpm), the supernatant was extracted using a syringe, filtered through a 0.45-micrometer (μm) cellulose acetate filter, and analyzed for final As(III) or As(V) concentrations via atomic absorption.

Design of Column Experiments

Column experiments, replicating the experimental set-up from Chapter II, were designed to develop a feasible operational format and assess the longevity of As adsorption by the IOCS. A PVCT of 30 minutes was sustained by pumping feed water through the column at a flow rate of 5.6 mL^1min^{-1}. Initial and subsequent As removal trials were evaluated using DI H_2O water spiked with varying influent As concentrations (1.87 – 3.00 mg^1L^{-1} As(III) or As(V) at pH = 7.0 $\pm$ 0.2). Effluent samples were regularly collected and analyzed for As(III) or As(V) via atomic absorption. The working water pressure was 10.3 $\pm$ 0.7 kPa at the injection point of each column.

Surface-bound Iron and Arsenic Analyses

Laboratory analyses of the FeOx accumulated on the sand surface encompassed a sequence of procedures that accommodated time-sensitive situations. Iron oxide quantification and qualification on the sand surface was conducted using extraction and imaging procedures replicated from Chapter II. The routine incorporated the extraction and analyses of the adsorbed arsenic in addition to quantifying iron oxide accumulation on the sand surface. Arsenate (As(V)) and arsenite (As(III)) breakthrough profiles were obtained after FeOx sand coating to assess the adsorption capacity of the IOCS for As. The IOCS was aged in the column before rinsing with water to ensure maximum uptake of arsenic. The 91-cm columns were then dis-mantled into 15-cm portions, rinsed with DI H_2O, and air-dried in section-coded petri dishes for 48 hours before undergoing imaging and/or aqueous extraction. 5 g of dried, well-mixed iron oxide-coated sand (IOCS) from each petri dish was placed in separate 10-mL glass vials, mixed with 9.5 mL of 6 M HCl, sealed with rubber top, and agitated in a rotating arm shaker (29 rpm) for 24 h to obtain an aqueous As-FeOx mixture. Each solution was then filtered through a 0.45 μm cellulose acetate filter and analyzed for As(III) or As(V) (J) and total iron. Mass balances were used to compute the amount of As adsorbed on the sand ($\mu g^1 g^{-1}$) with respect to FeOx dosage ($mg^1 g^{-1}$) and column depth.

Toxicity Characteristic Leaching Procedure (TCLP)

The TCLP was established by the US Environmental Protection Agency in response to the 1984 Hazardous and Solid Waste Amendments (HSWA), which resulted from the Resource Conservation and Recovery Act (RCRA) (USEPA, 1986). The test was used to

simulate leaching of arsenic in a municipal landfill and categorize solid materials as inert or mobile with regard to the Maximum Concentration of Contaminants for Toxicity Characteristics (MCCTC). The TCLP was applied to the spent iron oxide-coated sand (IOCS) from the column experiments. Herein, 5.7 mL of glacial acetic acid (CH_3COOH at 17 M) was diluted to 1 L with anaerobic DI H_2O; sustaining a pH of 2.88 $\pm$ 0.03. A mass-based liquid-solid ratio of 20:1 was used to determine the proper amount of extraction liquid required for each As-saturated IOCS column. Samples were collected at regular intervals, individually filtered through a 0.45 μm cellulose acetate filter, and analyzed for As(III) or As(V) via atomic absorption.

Sorption Data Analyses

Two adsorption characteristics were adopted to evaluate As adsorption during the experiments. The mass of As accumulated on the sand, q_{As} (μg As per g IOCS), was calculated by analyzing the corresponding aqueous As concentration before and after IOCS adsorption and accounting for the sand mass using the following equation:

$$q_{As} = ((C_o - C_e)*V_s)/M_{IOCS} \quad (11)$$

where C_o and C_e are the initial and final As concentrations (mg^1L^{-1}), V_s is the solution sample volume (L), and M_{IOCS} is the mass of the IOCS (g).

The first adsorption classification used to characterize As uptake on the IOCS was the Freundlich isotherm, which uses the non-linear function below:

$$q_{As} = K*C_e^{(1/n)} \quad (12)$$

where K and n are empirical constants determined from laboratory studies evaluating As adsorption capacity based on FeOx accumulation on sand. K is related to the quantity of

sorbate associated with the sorbent and n is linked to the strength of the sorption process. The Freundlich adsorption approximation insinuates that the iron oxide surface is heterogeneous, such as various sizes of micro-particles (Zhuang et al., 2008). The Freundlich adsorption mechanism in this study is illustrated by plotting q_{As} on the y-axis against C_e on the x-axis.

The second adsorption classification used to quantify As adsorption on the IOCS in this study was the Langmuir isotherm, which relates adsorption and As concentration:

$$q_{As} = q_m * [(b*C_e)/(1 + b*C_e)] \quad (13)$$

where q_m is the maximum (saturated) monolayer adsorption capacity ($\mu g^1 g^{-1}$) and b is the Langmuir constant (μg^{-1}). The Langmuir constant corresponds to the affinity between the arsenic and the iron oxide at specific conditions. The Langmuir adsorption mechanism in this study is demonstrated by also plotting q_{As} on the y-axis against C_e on the x-axis. The Langmuir model operates on the following assumptions: (1) homogeneous sorbent surface where all adsorption sites are uniform, (2) the sorption mechanism is the same for all sorbates, (3) there are no interactions between the adsorbed molecules, and (4) sorption occurs only on free surface sites (monolayer) and is reversible when maximum adsorption is achieved (LaGrega et al., 2001).

Non-linear generalized reduced gradient (GRG) analyses was conducted on the adsorption data. The experimental data was correlated with the model (predicted) data to assess the data suitability. The plots with the best fit (highest r^2 values) for As(III) and As(V) adsorption were used to describe the immobilization process of As by the iron oxide-coated sand.

RESULTS AND DISCUSSION

Batch Tests

Effects of pH

The effect of variation of the solution initial pH (2 – 12) on As(III) and As(V) adsorption is shown in Figure 16. The data noted that As(III) adsorption on the coated sand at pH 2.0 and pH 3.0 was inferior to As(V) uptake, but remained parallel or superior thereafter. The maximum adsorption efficiency for As(III) was 99.9% at pH 7; complying with a previous study using iron oxide-coated sand (IOCS) (Thirunavukkarasu et al., 2003). While As(V) adsorption also peaked at 99.9% at pH 7, it was reduced at elevated alkaline levels (pH 9 – pH 12). This is similar for As(III) adsorption at pH levels above 11. These data suggests that As(III) and As(V) adsorption by IOCS was weak under strong basic conditions due to the repulsive force induced from the net negative surface charge of the iron oxide crystals. Collectively, As(III) and As(V) adsorption was greater than 98% between pH 4 and pH 9, but did not breach 69% removal at pH 12. Excluding the data at pH 12, these findings are consistent with Cornell and Schwertmann (2003), Raven et al. (1998), and Gupta et al. (2005).

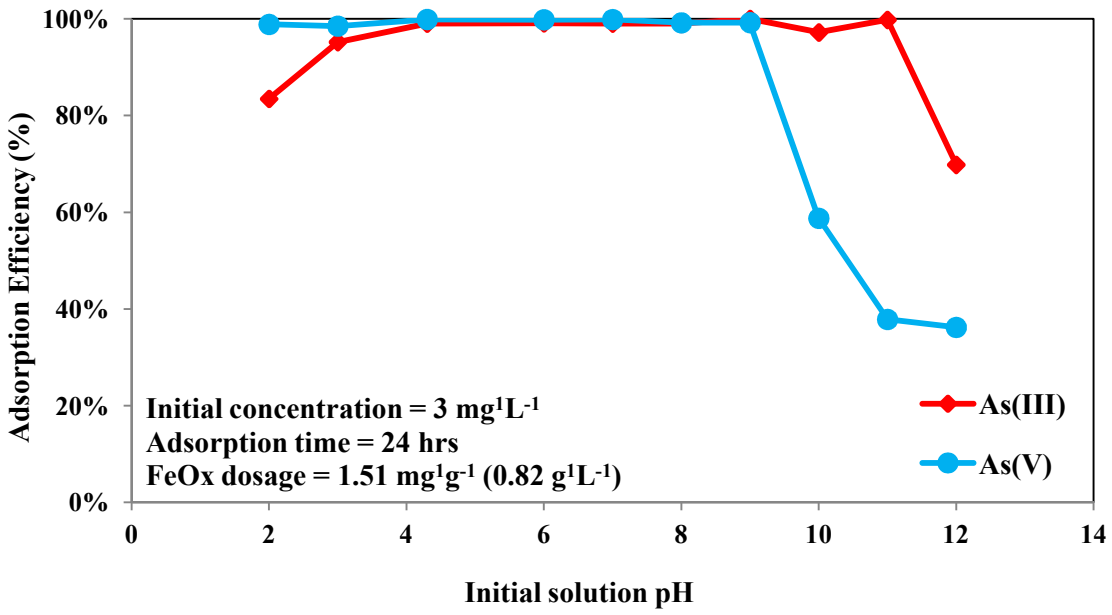

Figure 16: pH-induced As(III) and As(V) adsorption

The change in solution pH during adsorption was also recorded to identify a stable pH range complementary to As(III) and As(V) uptake by iron oxide (Figure 17). The pH generally increased in acidic conditions with a maximum jump of +1.84 at pH 4 for both species. At basic levels, the pH dropped with a maximum reduction of -1.72 at pH 9 and -1.84 at pH 10 for As(III) and As(V), respectively. The data suggests that neutral pH conditions provided a balanced net surface charge in order to accommodate simultaneous As(III) and As(V) adsorption. Additionally, there was no change in pH during As adsorption at neutral conditions; further corroborating the need for a balanced acidity/alkalinity environment for As(III) and As(V) removal from water using IOCS. Maximum As(III) and As(V) uptake were observed at pH 7, and henceforth all further batch experiments were carried out at near-neutral conditions.

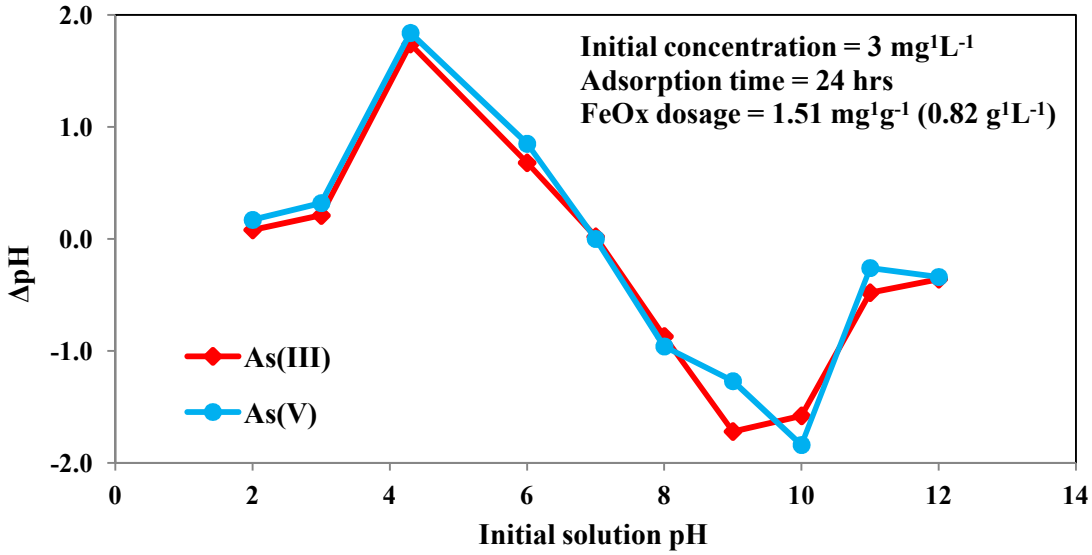

Figure 17: Change in pH resulting from As adsorption

Adsorption Dynamics

The effect of contact time (5 – 510 minutes) on the adsorption of As(III) and As(V) by IOCS is demonstrated in Figure 18. The rapid removal of As(III) and As(V) throughout the experiment could be attributed to the co-precipitation on the FeOx surface resulting from ferric hydroxide formation that selectively adsorbed As(III) and As(V) at near-neutral pH (Gupta et al., 2005 and Sarkar et al., 2008). It is also suspected that the As and FeOx were bound by inner-sphere complexes where the FeOx served as an electron-receiving transition metal (Dzonmabk and Morel, 1990). During the first 210 minutes of contact, As(III) adsorption exceeded As(V) removal on 11 out of the first 12 time intervals. After 210 minutes of adsorption, As(III) and As(V) removal were parallel at 95.0% before As(V) achieved superior uptake thereafter. As(III) and As(V) adsorption peaked at 96.5% and 97.8% respectively at a contact time 510 minutes.

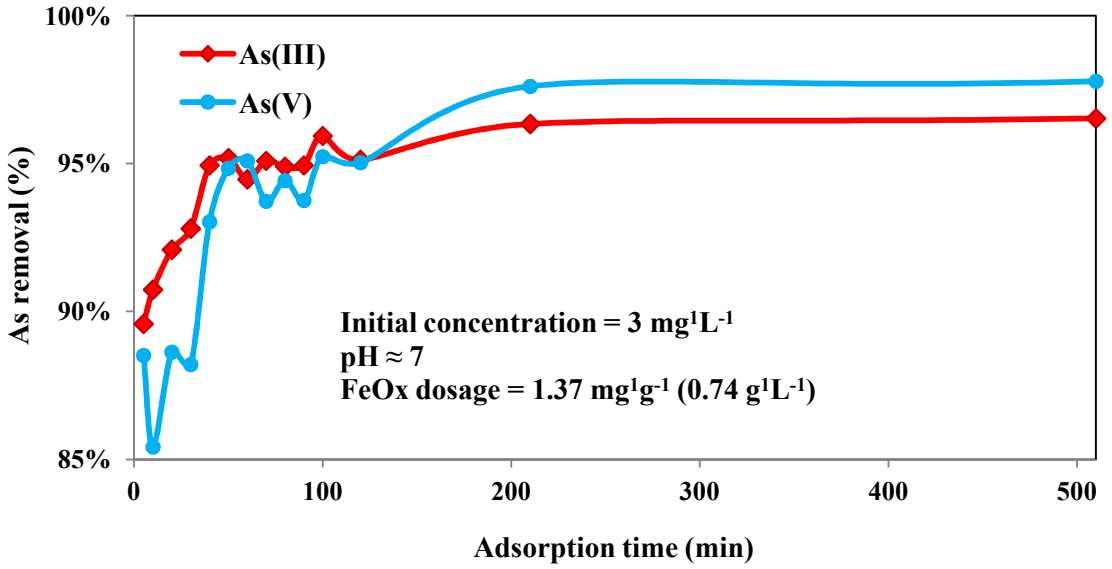

Figure 18: Adsorption Dynamics of As(III) and As(V)

Effects of Initial As Concentration (Adsorption Isotherms)

Figure 19 illustrates the effect of initial arsenic concentration (1.0 – 20 mg^1L^{-1}) on As(III) and As(V) adsorption by iron oxide-coated sand (IOCS). The data reveals that the adsorption efficiencies were highest for As(III) (above 97% up to 2 mg^1L^{-1}) and As(V) (above 99% up to 6 mg^1L^{-1}) when the As levels were initially low; followed by a gradual decrease in uptake as the feed concentration increased. The adsorption efficiency at 20 mg^1L^{-1} was 59.7% for As(III) (20.7 μg adsorbed per g sand) and 66.9% for As(V) (24.6 μg adsorbed per g sand). The decrease in uptake capacity at higher concentrations could be attributed to the imminent saturation of the fixed supply of adsorption sites with the affixed arsenic. However, additional As in the solution was shown to increase the amount adsorbed on the sand significantly; likely stemming from the increased As availability for additional adsorption (Figure 20).

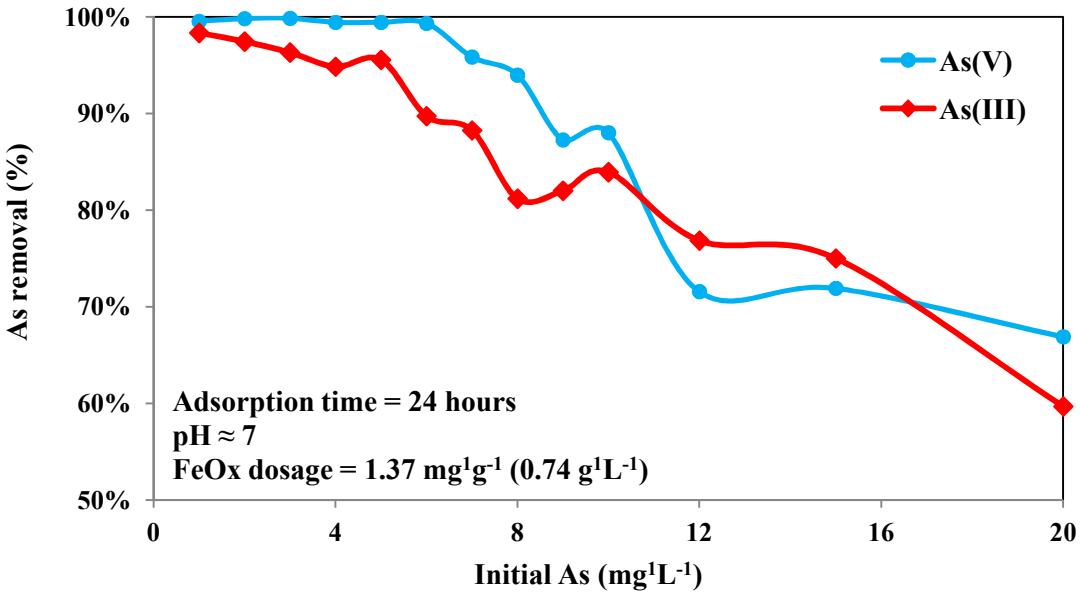

Figure 19: Effects of Initial Concentration on As(III) and As(V) Adsorption

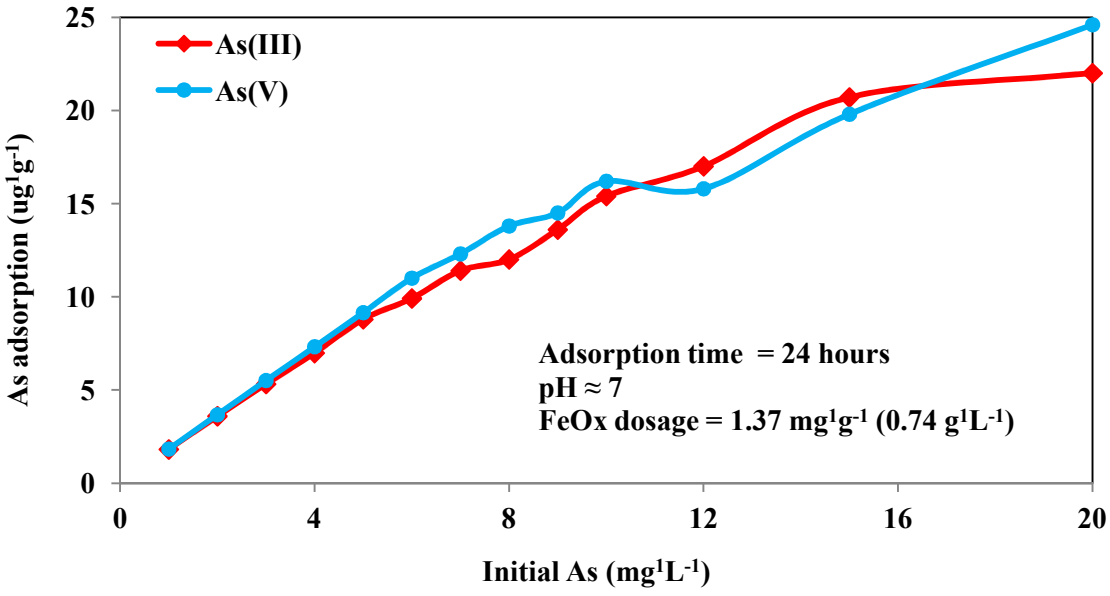

Figure 20: As(III) and As(V) Mass-based Adsorption

The Freundlich (Figure 21) and Langmuir (Figure 22) sorption models were adopted to estimate the maximum arsenic uptake at different influent concentrations. The correlation between the experimental data and predicted (model) data revealed that the Freundlich model ($r^2_{As(III)}$ = 0.96 and $r^2_{As(V)}$ = 0.91) defined the adhesion of As onto the iron oxides better than the Langmuir model ($r^2_{As(III)}$ = 0.92 and $r^2_{As(V)}$ = 0.81). This outcome, combined with the increased uptake capacity resulting from higher As loadings on the fixed number adsorption sites (Figure 20), suggest that there may have been other factors contributing to the adsorption of As onto FeOx (i.e. interaction between adsorbed As molecules, heterogeneity of FeOx surface highlighted by different charge densities and concentrations, deposition of As onto previously adsorbed As, etc.).

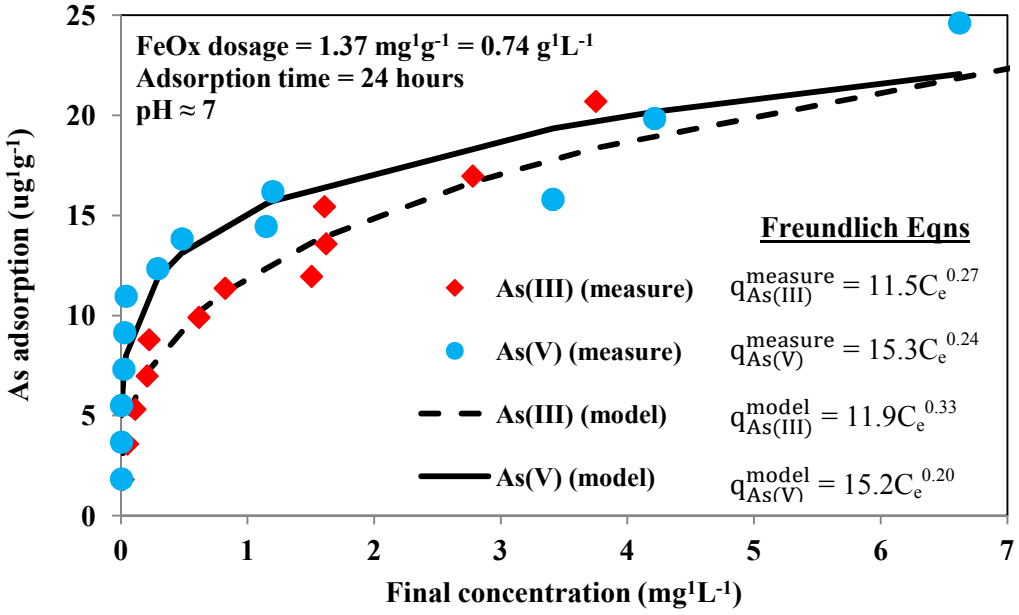

Figure 21: Freundlich Adsorption Isotherm of Arsenic via IOCS

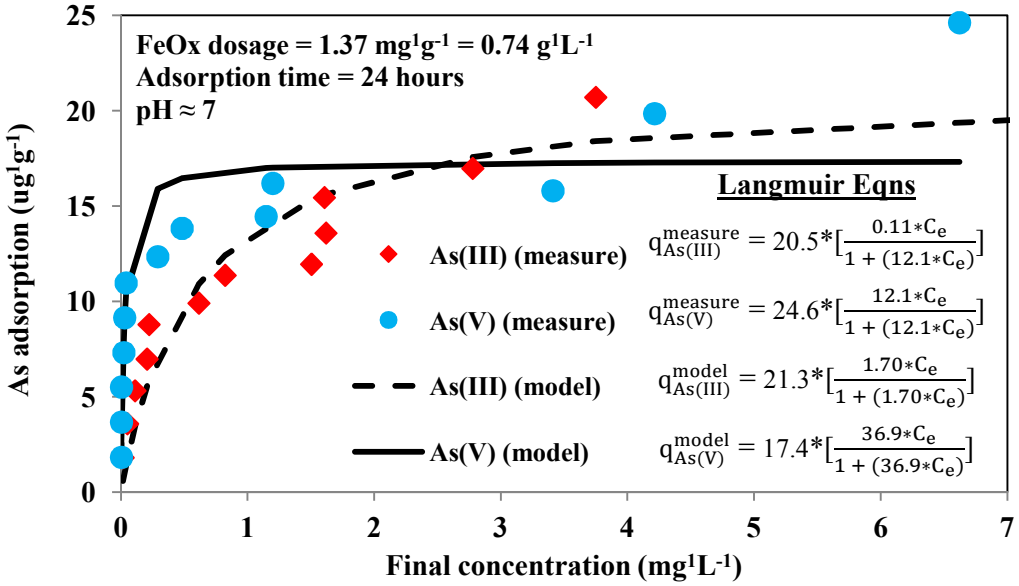

Figure 22: Langmuir Adsorption Isotherm of Arsenic via IOCS

Effects of Iron Oxide (FeOx) Dosage

In comparison to As uptake by uncoated sand, a rapid increase in arsenic adsorption efficiency was observed with an increase in adsorbent dose (0.74 – 1.34 mg^1g^{-1} FeOx) (Figure 23). Marginal improvements in As adsorption were observed on further increase in the adsorbent dose (1.34 – 2.25 mg^1g^{-1} FeOx), likely ensuing insufficient As loading from the influent (3 mg^1L^{-1}). The maximum adsorption efficiencies were recorded at 98.2% for As(III) (5.54 μg As per mg sand) and 99.9% for As(V) (5.63 μg As per g sand) each at 2.25 mg^1g^{-1} FeOx. The sharp elevation in the removal of As(III) and As(V) at 0.74 mg^1g^{-1} could be accredited to the enhancement of the FeOx emplacement (increased FeOx surface availability); effectively providing additional adsorption sites for the As ions. The additional FeOx coating and As adsorption could have increased the point of zero charge (pzc) and allowed for further As accumulation (Stumm, 1992).

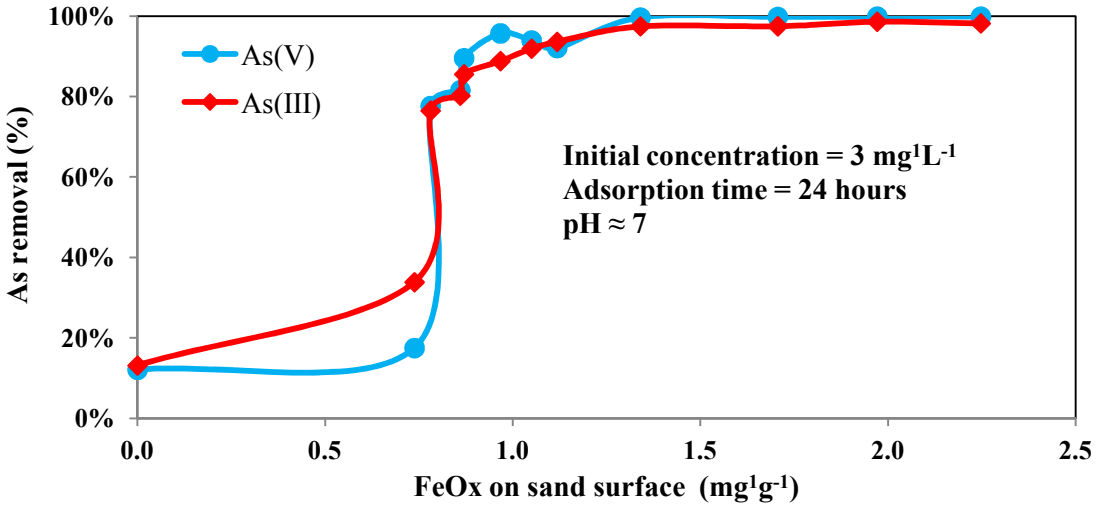

Figure 23: Effects of Adsorbent (FeOx) Dosage on As Adsorption

Effects of Groundwater Anions

The effects of variation of competing groundwater anions (0 – 300 mg^1L^{-1}) on As(III) and As(V) adsorption are illustrated in Figures 24 and 25. It was noted that bicarbonate (HCO_3^-), silicate (SiO_3^{2-}), and sulfate (SO_4^{2-}) posed no significant hindrance to As(III) adsorption at low concentrations. This observation was followed by the slightly gradual reduction in adsorption at higher levels that was likely a result of intensified adsorption competition between the anions and the As ions on the limited supply of adsorption sites on the iron oxide surface. Arsenic desorption was observed at 150 mg^1L^{-1} carbonate (CO_3^{2-}) for As(V) (-4.2% removal). While the assertion of elated adsorption competition may be genuine for the effects of carbonate (CO_3^{2-}) on As uptake, the elevated pH levels induced by concentration increases were also suspected of obstructing As adsorption. However, the initial reduction in As removal at near-neutral conditions ($pH_{As(III)}$ = 7.75 and $pH_{As(V)}$ = 7.23 at 30 mg^1L^{-1} CO_3^{2-}) affirmed that anionic

competition likely compromised the adsorption capacity of the FeOx more profoundly than the alkalinity of the system.

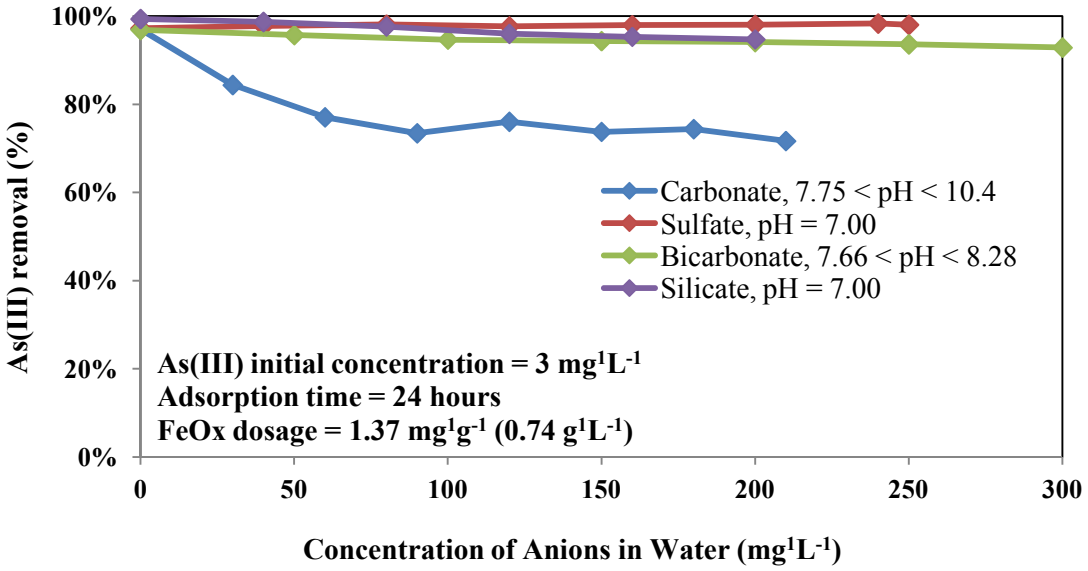

Figure 24: Groundwater Anion Effects on As(III) Adsorption onto IOCS

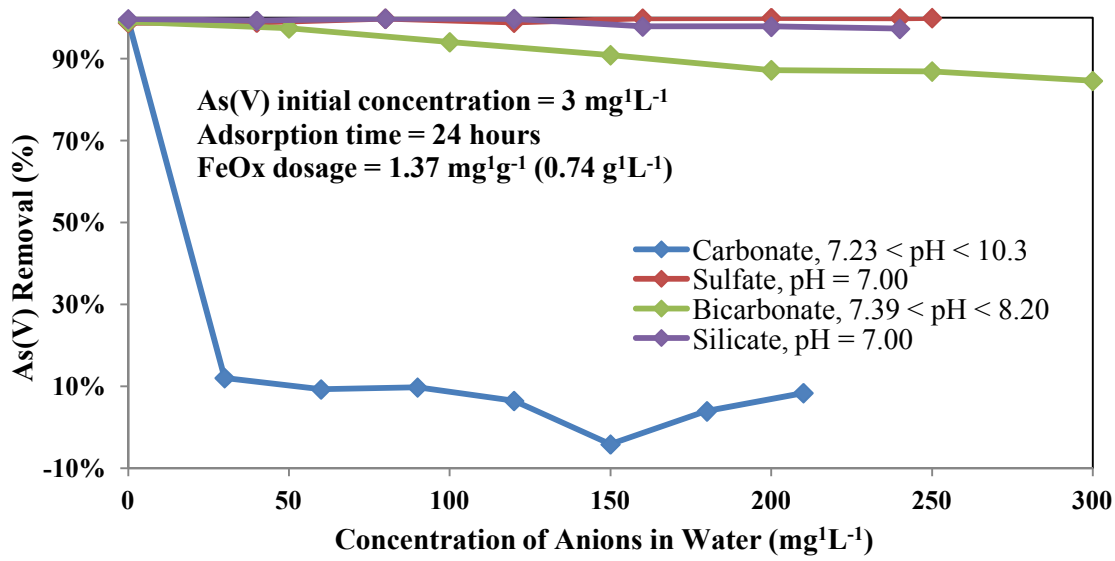

Figure 25: Groundwater Anion Effects on As(V) Adsorption onto IOCS

Column Tests

Evaluation of the As Adsorption Operation Format

Previously FeOx-coated sand columns preserved from Chapter II were commissioned for the proceeding operation platform:

$$(FeOx)_0 \rightarrow (As)_0 \rightarrow (t_{age})_0 \rightarrow (H_2O)_0 \rightarrow (FeOx)_n \quad (14)$$

where the iron oxide coating (FeOx), As adsorption (As), and water rinsing (H_2O) cycles could be repeated continuously until the sand hydraulic conductivity was significantly reduced (Figure 26). Adsorption activity accelerated within minutes of contact and plateaued at 200 minutes (Figure 18). Hence, all column experiments used a PVCT and ageing time (t_{age}) of 30 and at least 200 minutes, respectively. FeOx coating was immediately proceeded by As removal and IOCS ageing while the subsequent water rinsing (H_2O) simultaneously stabilized the system pH, alleviated the hydraulic conductivity, and flushed un-adsorbed As onto the IOCS due to saturation.

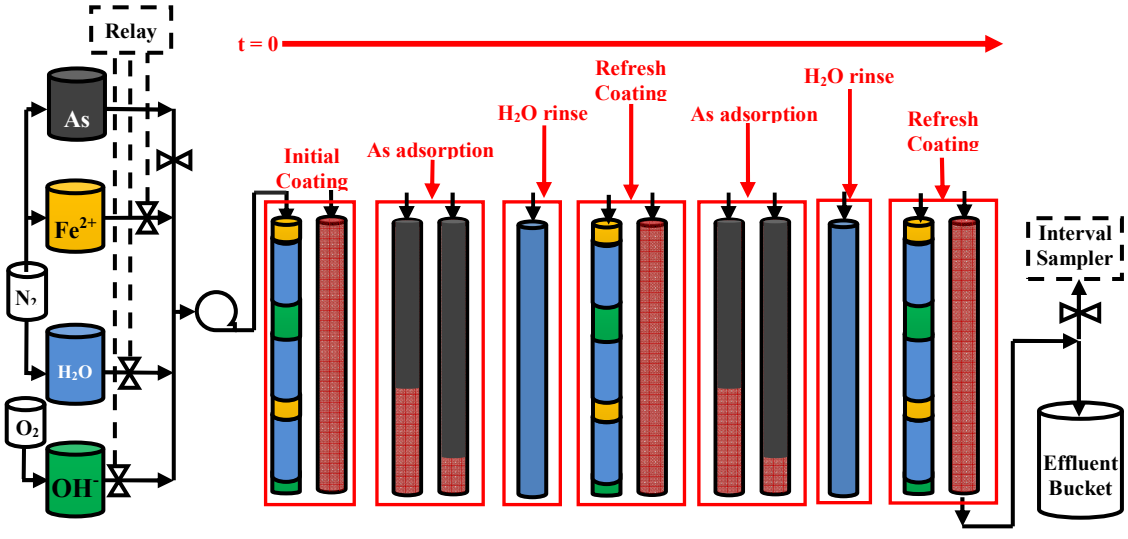

Figure 26: Operation of in situ FeOx Coating and Groundwater As Remediation

Two sand columns were pristinely coated in FeOx prior to the initial removal of As, followed by intermittent H_2O rinse/ageing cycles to re-calibrate the systems for an additional adsorption trial. The IOCS columns produced in this study were capable of recurrent FeOx coatings and As(III) adsorption or As(V) adsorption (Figures 27 and 28).

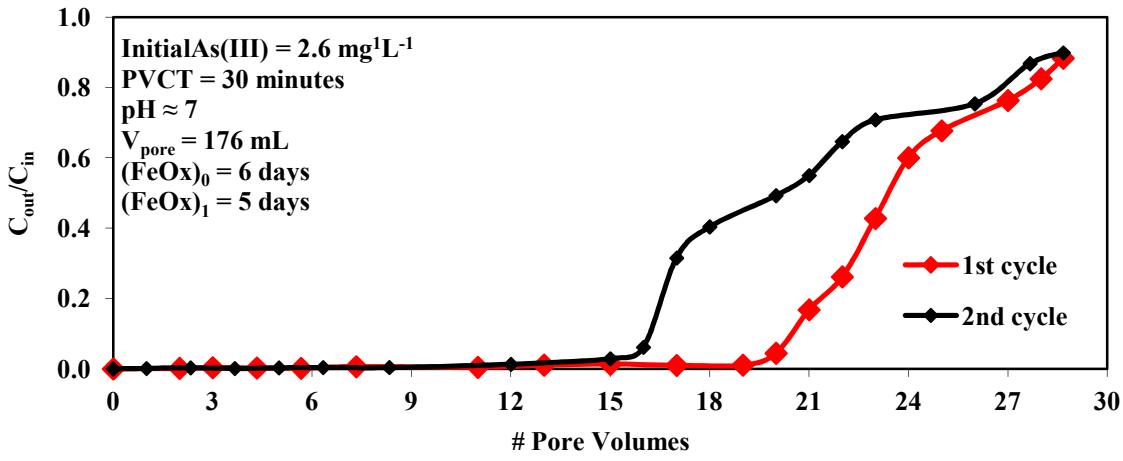

Figure 27: IOCS column As(III) Adsorption

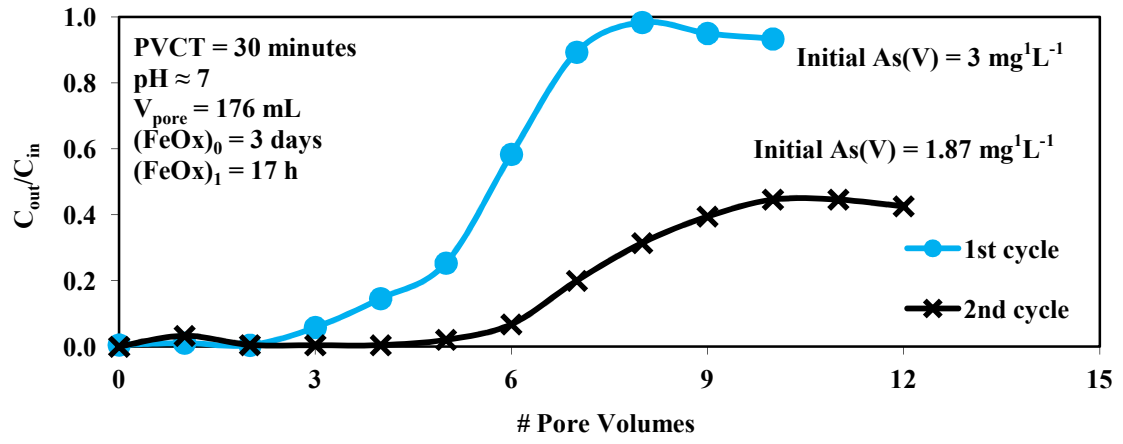

Figure 28: IOCS column As(V) Adsorption

As(III) was completely adsorbed up to the 20th and 15th pore volumes before reaching 10 $\mu g^1 L^{-1}$ in the first and second trials, respectively. Effluent As(V) detection was initially recorded at the 3rd and 5th pore volumes in the first and second trials, respectively (Table 8). The extended treatment life in the second cycle for As(V) ensued from the lower influent concentration despite a refresh coating period of 17 h.

Table 8: As(III) and As(V) Column Adsorption Summary

	As(III) adsorption trials				As(V) adsorption trials			
Parameter	**1st**	**2nd**	**Total**	**Units**	**1st**	**2nd**	**Total**	**Units**
$[As]_{feed}$	2.60	2.60	~	mg^1L^{-1}	3.00	1.87	~	mg^1L^{-1}
t_{MCL}[a]	600	480	1080	minutes	90	180	270	minutes
# $V_{pore, MCL}$	20	16	36	Pore volumes	3	5	8	Pore volumes
$V_{As, MCL}$[b]	3.52	2.82	6.34	L H_2O	0.53	0.88	1.41	L H_2O
$M_{As, total}$[c]	~	~	5.22	mg As(III)	~	~	1.09	mg As(V)
$V_{As, total}$[d]	5.05	5.05	10.1	L H_2O	1.76	2.11	3.87	L H_2O
UR_{IOCS}[e]	~	~	47.2	g^1L^{-1}	~	~	123	g^1L^{-1}
ST_{IOCS}[f]	~	~	21.2	L^1kg^{-1}	~	~	8.11	L^1kg^{-1}
$q_{As\text{-}IOCS}$[g]	~	~	10.9	μg^1g^{-1}	~	~	2.28	μg^1g^{-1}

[a] MCL breakthrough time recorded at arsenic effluent $\geq$ 10 $\mu g^1 L^{-1}$

[b] $V_{As, MCL}$ = volume of treated water at MCL breakthrough = (# $V_{pore, MCL}$)*(176 mL)

[c] Total mass of arsenic adsorbed in sand column acquired from extraction analyses

[d] $V_{As, total}$ = Total volume water treated in each adsorption trial = (# V_{pore})*(176 mL)

[e] UR_{IOCS} = IOCS usage rate = (M_{sand})*($V_{As, total}^{-1}$) where M_{sand} = 477 g

[f] ST_{IOCS} = specific throughput = ($V_{As, total}$)*1000*(M_{sand}^{-1}) as L H_2O per kg sand

[g] $q_{As\text{-}MCL}$ = MCL adsorption capacity = ($M_{As, total}$)*1000*(M_{sand}^{-1}) as $\mu g^1 g^{-1}$

Ageing was induced with 200 minutes of idleness before H_2O rinsing (2 h) and FeOx refreshment (5 days for As(III) and 17 h for As(V)) in between As adsorption trials, where samples were periodically collected and analyzed to determine As leaching during intermission. The maximum amount of As released from the FeOx during water rinsing

was 0.84 mg^1L^{-1} for As(III) and 0.54 mg^1L^{-1} for As(V). For re-coating, the arsenic leached from the spent IOCS did not exceed 0.39 mg^1L^{-1} for As(III) and 0.16 mg^1L^{-1} for As(V). The working water pressure in the As(III) IOCS column (10.3 $\pm$ 0.5 kPa) increased during the second FeOx coating cycle (12.8 $\pm$ 0.7 kPa) while no significant water pressure elevation was observed in the As(V) IOCS column. This response was likely due to the gradual pore volume reduction induced by the emplacement of supplemental FeOx crystals and additional As ions. The H_2O rinsing procedure stabilized the water pressure to 11.8 $\pm$ 0.3 kPa after removing suspended debris from the system for 1 h. The data highlights the stability of the adsorbed As between the initial and refresh FeOx coatings while concurrently treating additional contaminated water; thus substantiating the devised operation format as a practical method for recurrent water arsenic remediation in subsurface environments.

TCLP Classification of Spent Iron Oxide-Coated Sand

To assess the potential environmental impacts of the spent IOCS, the TCLP method was employed using two approaches to assess the hazard potential of the waste sorbent. All tests herein were carried out separately on As(III)-saturated and As(V)-saturated sorbents. The first test (batch TCLP) comprised of 60 mL of 0.09 M acetic acid (CH_3COOH at 5.81 mg^1L^{-1} and pH = 2.88) agitated with 3 g IOCS for 18 h and analyzed for As thereafter. The second experiment (column TCLP) applied 9.22 L of the same acetic acid to each As-saturated IOCS column at a PVCT of 60 minutes following multiple trials of As adsorption and supplementary FeOx coating cycles. Hourly samples were collected and subsequently analyzed for As leaching. An additional third test (HCl

extraction) replicated the configuration of the first procedure while mixing 5 g IOCS with 9 mL of 6 M hydrochloric acid (HCl at 216 mg^1L^{-1} and pH = 0.78 $\pm$ 0.04). The results concluded that the maximum leachates from the batch TCLP, column TCLP, and HCl extraction experiments were 0.05, 0.14, and 4.38 mg^1L^{-1}, respectively for As(III), and 0.04, 0.07, and 1.97 mg^1L^{-1}, respectively for As(V). Figure 29 shows the As leached from the IOCS during the column TCLP tests.

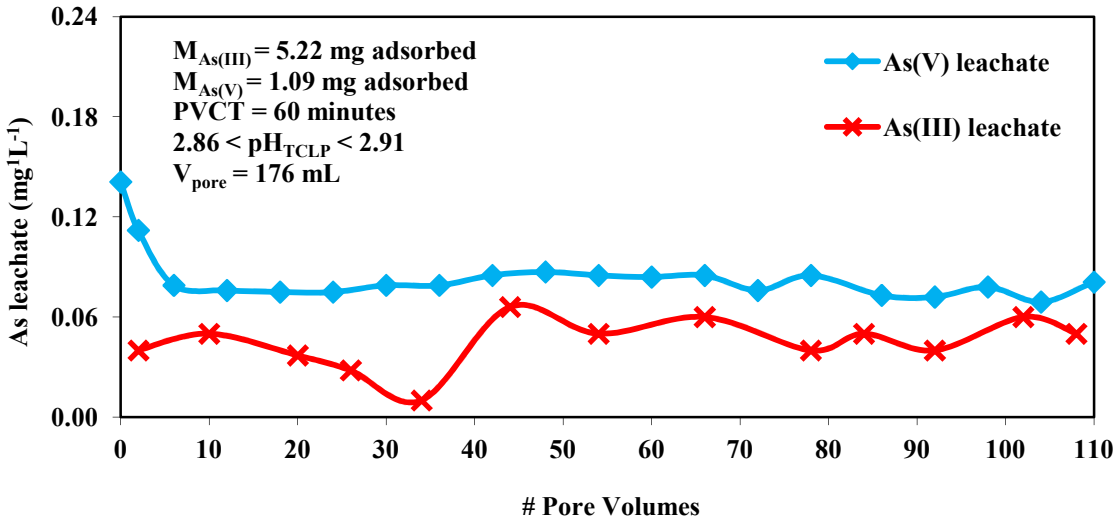

Figure 29: Arsenic-saturated IOCS Column TCLP Performance

The increased leaching of As(V) despite a higher mass adsorption of As(III) on the IOCS columns could be a result of the shorter FeOx re-coating period (17 h for As(V) versus 5 days for As(III)). Notwithstanding the HCl extraction results, these findings suggest that either (1) the adsorbed As was increasingly bounded to the FeOx by prolonged co-precipitation as a structural component onto the oxide/hydroxide minerals

or (2) the As became encapsulated between the saturated FeOx and refresh FeOx layers on the sand surface. The dissolution of the As during the HCl extraction tests indicated the strength of the As-FeOx bond being insufficient in strong acidic environments. Most importantly, the spent adsorbent failed to leach sufficient As to exceed the established USEPA standard of 5 $mg^{1}L^{-1}$, thus categorizing the As-saturated IOCS as inert and suitable for landfill application.

SUMMARY

As(III) and As(V) adsorption by iron oxide-coated sand (IOCS) was significantly impacted by the pH of the water. At alkaline conditions, As(V) uptake was severely retarded while As(III) removal was moderately hindered. pH levels shifted towards neutral conditions from initially extreme values; indicating that the adsorption process was optimal when acidity and alkalinity were balanced. Furthermore, optimal removal for As(III) and As(V) was observed at pH 7, where there was no reported change in pH. The effects of sulfate and silicate were found to have no significantly adverse impacts on arsenic adsorption. Carbonate and bicarbonate are forms of alkalinity and thus were associated with elevated pH levels as the prevalent hindrance to As adsorption. The uptake of arsenic onto the IOCS exhibited Langmuir adsorption behavior and was dominated by film diffusion up to 200 minutes, followed by a gradual surface complexation process. The maximum As adsorption onto the IOCS was 22.0 and 24.6 $\mu g^{1}g^{-1}$ for As(III) and As(V), respectively, at a feed concentration of 20 $mg^{1}L^{-1}$ and FeOx dosage of 1.37 $mg^{1}g^{-1}$. At an influent concentration of 3 $mg^{1}L^{-1}$ influent, the As uptake capacity peaked at an FeOx dosage of 1.34 $mg^{1}g^{-1}$ and leveled off thereafter. The

IOCS columns effectively reduced influent As (1.86 to 3.00 $mg^{1}L^{-1}$) to less than 10 $\mu g^{1}L^{-1}$ at near-neutral conditions before gradually becoming saturated. The slow reduction in As removal in all experiments was attributed to the imminent depletion of the limited supply of adsorption sites on the iron oxides. The installation of intermittent ageing and water rinsing procedures in the column tests contributed to the stability of the adsorbed arsenic and head loss resulting from refresh coatings; thus extending the treatment capacity for As(III) and As(V).

With the exception of the HCl tests, the As(III) and As(V)-saturated columns effectively immobilized the pollutants throughout the remaining configurations of the TCLP experiments. The HCl tests for As(III) and As(V) reveal that the FeOx and adsorbed As were significantly detached from the sand; insinuating the lack of immunity to high acidity shock loadings. Nonetheless, the batch and column TCLP tests showed that the spent IOCS could be classified as inert waste and landfilled upon complete exhaustion of As adsorption.

CHAPTER IV

ANALYSES OF WATER ARSENIC SORPTION ONTO IOCS USING KINETIC AND DIFFUSION MODELING

LITERATURE REVIEW

Sorption of Pollutants on Iron Oxides

The sorption of ions and molecules from solid and aqueous phases has been intertwined in various parts of the environment. In soils, the fate and transport of assorted nutrients (i.e. nitrogen and phosphorous) and pollutants (i.e. pesticides and heavy metals) are regulated in part by the uptake of plant roots and the transfer from soils to aquatic environments, respectively (Cornell and Schwertmann, 2003). In aqueous systems, the mobility of hydrophobic organic compounds (HOCs) (i.e. DDT) is partially controlled by sorption onto neighboring mineral surfaces (Murphy et al., 1994). In water treatment, the significance of metallic sorption is supported by the (1) elimination of supplementary sludge-handling processes; thus minimizing operating costs and (2) restoration of the adsorbent for maintaining superior treatment capacity upon exhaustion; hence extending the life cycle of the technology. The adsorption of pollutants onto FeOx has been studied extensively (USEPA, 1978; Dzombak and Morel, 1990; Raven et al., 1998; Goldberg and Johnstony, 2001; Xu and Axe, 2005; Guo et al., 2007); accruing critical acclaim as an acceptable water treatment alternative. According to Cornell and Schwertmann (2003), studies on iron oxides (FeOx) as sorbents have historically abided by two concepts: (1) quantification of a substance removed from a

liquid or gaseous phase and (2) spectroscopic examinations to identify the interaction between the adsorbed pollutant and the FeOx surface (i.e. co-mineralization, co-precipitation, surface complexation).

RESEARCH OBJECTIVE

The study described in this chapter was aimed at elucidating the fate and transport of As(III) and As(V) onto iron oxide-coated sand (IOCS) via kinetics and diffusion modeling. The analyses herein could apprise the sorption properties and augment the applicability of fresh IOCS developed via in situ oxidative precipitation (Chapter II).

MATERIALS AND METHODS

Materials, Equipment, and Wet Chemistry Analyses

IOCS produced in Chapter II was used for the batch experiments and all equipment and wet chemistry analyses were duplicated in the same manner from Chapter III.

Preparation of Synthetic Arsenic Samples

1.25, 3.75, and 11.3 mL of aqueous sodium hydrogen arsenate ($Na_2HAsO_4 \cdot 7H_2O$ at 1000 mg^1L^{-1}) were individually dissolved in beakers each filled with 300 mL DI H_2O to produce respective stock solutions of 1, 3, and 9 mg^1L^{-1} As(V). 0.10, 0.31, and 0.94 mL of sodium arsenite ($NaAsO_2$ at 0.5% w^1v^{-1} or 5,000 mg^1L^{-1}) were also discretely diluted in 300 mL DI H_2O to make As(III) stock supplies of 1, 3, and 9 mg^1L^{-1}, respectively.

Design of Modeling Experiments

Selection of Sorption Kinetic Systems for Iron Oxides

Several kinetic models have been investigated to characterize the adsorption capabilities of a variety of sorbents. Some of these models describe the reactions

between the sorbate and sorbent (chemical), while others approximate the diffusive behavior of the sorbate particles onto the adsorbing surface (physical). The double-diffuse layer model (DDLM) Freundlich isotherm, pseudo second-order, bed depth service time (BDST), Langmuir isotherm, intra-particle diffusion model (IPDM), constant capacitance model (CCM), triple layer model (TLM), and empty bed residence time (EBRT) models have been widely used for assessing the adsorption of pollutants onto iron oxides. Table 9 lists the experimental platforms of the aforementioned models employed for iron oxides in previous studies and Figure 30 illustrates the selection criteria for the model system design (Ho et al., 2000).

Table 9: Review of Iron Oxide Adsorption Models

Sorption model	Model basis/assumptions	Reference(s)
BDST[a]	Links service time to sorbent mass & depth	Lehmann et al., 2001
CCM[b, d]	Surface complexation	Hohl and Stumm, 1976
DDLM[b, d]	Surface complexation	Stumm et al., 1970
EBRT[a]	Links service time to sorbate effluent	Ko et al., 2000
Freundlich[b, d]	Sorbate-sorbent affinity, heterogenous	Cornell and Schwertmann, 2003
IPDM[b, e]	$t^{0.5}$ function, based on Fick's Law	Cheung et al., 2007
Langmuir[b, d]	Homogeneous, single-layer, inert sorbate	Cornell and Schwertmann, 2003
Psuedo 1st order[b,e]	Isolates sorbate at [sorbent] >> [sorbate]	Corbett, 1972
Psuedo 2nd order[b,e]	Good at short t_{eq} and $IR_{sorbent} > IR_{sorbate}$[c]	Ho and McKay, 1999
TLM[b, d]	Surface complexation	Cornell and Schwertmann, 2003

[a] Pertains to macro-sorption analyses (i.e. fixed-bed operation assessment)

[b] Pertains to micro-sorption analyses (i.e. liquid-solid interface assessment)

[c] t_{eq} = equilibrium sorption time and IR = ionic radius

[d] Equilibrium adsorption models

[e] Kinetic adsorption models

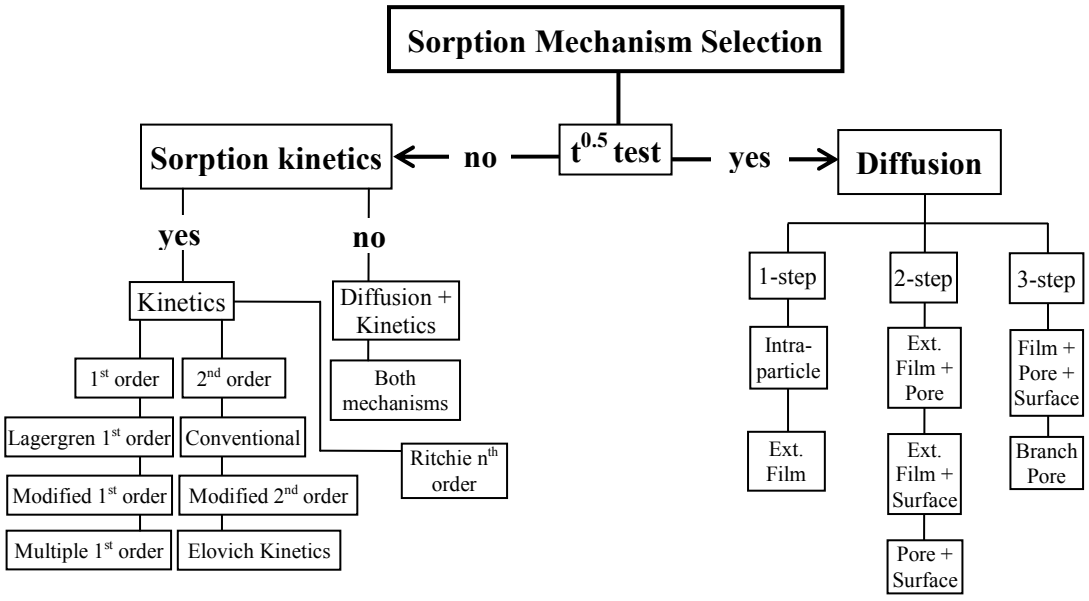

Figure 30: Sorption Model Selection Diagram (Ho et al., 2000)

Although the BDST and EBRT models could develop the minimum and maximum adsorption equilibrium times (Hutchins, 1974; Anastasios and Katsoyiannis, 2002), they are merely restricted to column tests and are incapable of accommodating surface hot-spot assessments. Moreover, the macro-sorption analyses of ions would assume that the sorbent surface in the column is entirely uniform; reducing the accuracy of the adsorption rate constant. The Freundlich and Langmuir isotherm models describe the affinity between the iron oxides and the sorbates in equilibrium (Navasivayan and Ranganathan, 1993 and Szecsody et al., 1994). Nonetheless, the use of a presumed sorption equilibrium time may not accurately predict the rate constant of adsorption. The TLM, DDLM, and CCM programs associate adsorption with sorbent surface parameters such as ionization constants and sorbate properties such as binding and capacitance

constants; thus delivering all-inclusive physical platforms for modeling the uptake rate constant for the adsorbing species (Zachara et al., 1987 and Ainsworth et al., 1989). However, these surface complexation also presume the system to be in equilibrium.

The pseudo first-order approximation model has been used on a variety of investigations studying the sorption of metals (Sharma et al., 1990; Ho and McKay, 1999; Chiron et al., 2003; Ibezim-Ezeani and Anusiem, 2010). The procedure is especially useful when characterizing the behavior of one arbitrary reactant in a 2-reactant system. Corbett (1972) used pseudo-first order kinetics to mathematically demonstrate the feasibility of second-order reaction studies ([reactant A] = 10^{-3} M, [reactant B] = 10^{-4} M, and k = 100 $M^{1}min^{-1}$) under first-order kinetic conditions ($A^{1}B^{-1}$ > 5). Although the depletion of the excess reactant was assumed to be negligible, the literature highlighted the reliability of the data throughout progressive stages of the overall reaction (error yields of <1.1% and <2.5% at 60% and 80% reaction conversion, respectively).

The pseudo second-order kinetic model, which is based on the sorption equilibrium capacity, has also been widely applied in a variety of sorption studies (Khare et al., 1987; Sharma et al., 1990; Kaur et al., 1991; Singh et al., 1998; Ho and Ofomaja, 2006). The procedure operates under the assumption that the uptake capacity of a liquid-phase substance is directly proportional to the amount of available adsorption sites on the surface of the solid sorbent (Zhuang et al., 2008). The availability of adsorption sites on the FeOx surface based on the size(s) of As(III) and As(V) ions could be an attribute of the uptake capacity. Case in point: the variation in the ionic radius (IR) between As and

Fe^{3+} ($IR_{As(V)}$ = 46 picometers < $IR_{As(III)}$ = 58 pm < $IR_{Fe(III)}$ = 64.5 pm) (Shannon, 1976) may appropriate pseudo-second order kinetics as a suitable modeling platform for the uptake of As onto FeOx (Ho et al., 2000).

The adsorption of pollutants onto sorbents via diffusion modeling has been thoroughly investigated (Ganesh et al., 1994; Chu and Tsui, 1999; Choy et al, 2004; Gupta et al., 2005; Cheung et al., 2007). Ho et al. (2000) described the diffusive behavior of a substance in a liquid-solid interface using four steps: (1) transport of the solute in the solution bulk, (2) diffusion of the solute across the liquid engulfing the sorbent particles, (3) particle diffusion of the sorbate into the sorbent pore structure, and (4) sorption and desorption on the pore surface. The intra-particle diffusion model (IPDM), developed from Fick's Law, analyzes the mass transfer rate of substances at varying times and initial concentrations. As such, the IPDM has been widely acceptable in adsorption studies of color and dyes in wastewater treatment (Lin and Lin, 1993; Walker and Weatherley, 2000; Chu and Ma, 2000). Using the square root of time ($t^{0.5}$) function and incorporating the aforementioned processes, the IPDM could effectively elucidate the mass transfer for arsenic from a solution to the solid-based FeOx surface.

In essence, the pseudo-first order, pseudo-second order, and diffusion models allow for discreet, isolated examinations on the transfer of dissolved sorbates onto a solid-phase sorbent; eliminating the need for comprehensive surface characterization of the adsorbing species while accommodating time-dependent analyses. The mathematical reliability of these models further validates their applicability for patterning the fate and transport of pollutants at a liquid-solid interface.

Sorption Modeling Data Evaluation

The amount of arsenic (As) adsorbed onto the sand, q_{As} (μg As per g IOCS), was determined using the initial and final As concentrations during the batch experiments and accounting for the sand mass using the following equation:

$$q_{As} = ((C_o - C_e)*V_s)/M_{IOCS} \quad (15)$$

where C_o and C_e are the influent and effluent As concentrations (mg^1L^{-1}), V_s is the sample volume ($9.2\ E^{-3}$ L), and M_{IOCS} is the mass of the FeOx-coated sand (5 g).

Lagergren (1898) developed a pseudo-first order sorption equation describing the mass transfer of a substance from a liquid phase to a solid medium:

$$dq_t/dt = k_1*(q_e - q_t) \quad (16)$$

A non-linearized form of Equation 16 was generated by integrating and solving for q_t at boundaries t = 0 to t = t and $q_t = 0$ to $q_t = q_t$:

$$q_t = q_e*(1 - e^{-k_1 t}) \quad (17)$$

where q_e and q_t are the mass-based adsorption capacities ($\mu g^1 g^{-1}$) at equilibrium and time t (min), respectively. The term k_1 is known as the pseudo-first order rate constant (min^{-1}). By executing several adsorption experiments and composing a plot of the As reaction rates (q_t vs. t) with respect to different FeOx concentrations, the non-linear regression of the data gives the overall rate constant of the adsorption process. Equation 17 is based on the uptake capacity of the dissolved solute by the excess solid sorbent. In order to simplify the observation of the reaction, the As concentration change was closely followed while the fixed FeOx concentration was presumed to be in a surplus. Only a

negligible amount of FeOx was consumed; sustaining a constant sorbent mass throughout the process.

The pseudo-second order equation is written as followed (Ho and Mckay, 1999):

$$dq_t/dt = k_2*(q_e - q_t)^2 \quad (18)$$

where k_2 is the rate constant of adsorption ($g^1\mu g^{-1}min^{-1}$), q_t is the adsorption capacity ($\mu g^1 g^{-1}$) at time t (min), and q_e is the equilibrium adsorption ($\mu g^1 g^{-1}$). Knowing that $q_t = 0$ at $t = 0$, Equation 18 can be converted to the initial adsorption rate, r_i:

$$r_i = k_2*q_e^2 \quad (19)$$

Equation 18 could also be integrated at the boundaries $t = 0$ to $t = t$ and $q_t = 0$ to $q_t = q_t$ to yield a non-linear relationship between time-specific and equilibrium adsorption:

$$q_t = q_e - 1/((1/q_e) + k_2*t) \quad (20)$$

where t is on the x-axis and q_t is on the y-axis. The experimental (measured) values of q_t were calculated using Equation 15 at the recorded time t and were plotted against non-linear pseudo-second order model values derived from Equation 20. The correlation between the experimental and model values (r) was squared to determine the suitability of the data in a non-linear regression analysis.

As adsorption and contact time can be correlated for diffusion using the following expression (Weber and Morris, 1963):

$$q_t = k_3*(t)^{0.5} + C_i \quad (21)$$

where k_3 is the intra-particle diffusion rate constant ($ug^1g^{-1}min^{-0.5}$), q_t is the time-dependent adsorption capacity ($\mu g^1 g^{-1}$), C_i (unitless) is associated with the boundary layer thickness, and t is the adsorption time (minutes).

Experimental Conditions of the Selected Models

The batch experiments were designed to accommodate the experimental conditions of the models applied in this study. To approximate As diffusion onto IOCS, initial concentrations of 1, 3, and 9 $mg^{1}L^{-1}$ As(III) or As(V) were used to determine their respective variable mass transfer rates onto the FeOx-coated sand. The resulting set-up also provided pseudo first-order (FeOx/As $\geq$ 5) and pseudo second-order kinetic conditions for all samples by sustaining appropriately high sorbent-sorbate concentration ratios ($[(FeOx = 728\ ppm)/(As = 1\ ppm)]_{batch\ \#1} \approx 730$, $[(FeOx = 745\ ppm)/(As = 3\ ppm)]_{batch\ \#2} \approx 250$, and $[(FeOx = 728\ ppm)/(As = 9\ ppm)]_{batch\ \#3} \approx 81$) and preserving a fixed FeOx concentration on the sand ($1.34\ mg^{1}g^{-1} \leq [FeOx]_{sand} \leq 1.37\ mg^{1}g^{-1}$), respectively. To eliminate potential ionic interference to adsorption, the solution media of the samples were composed of near-neutral DI H_2O (pH = 7.0 $\pm$ 0.3). All samples were placed in 12-mL glass vials (solution volume = 9.4 mL), sealed with rubber stoppers, and agitated indoors (22 $\pm$ 3 ^{o}C at 101 kPa) in a rotating arm shaker (29 rpm) for mixing. After arm-shaking agitation, the supernatant was extracted (sample volume $\approx$ 8.8 mL) using a syringe (samples collected at 5, 10, 20, 30, 40, 50, 60, 70, 80, 90, 100, 120, 210 510, 1230, 2670, and 4110 minutes), filtered through a 0.22-micrometer (μm) cellulose acetate filter, and analyzed for final As(III) or As(V) concentrations via atomic absorption. Table 10 summarizes the specifications of the batch experiments used for kinetic and diffusion modeling.

Table 10: Experimental Conditions of Batch Tests

Parameters	Label	Low	High	Units	# levels
Sand particle size	$D_{particle}$	0.42	0.59	mm	~
Iron oxide dosage	$[FeOx]_{sand}$	1.34	1.37	mg^1g^{-1}	2
	$[FeOx]_{sand}$	728	745	mg^1L^{-1}	2
pH of solution	$pH_{solution}$	6.7	7.3	~	~
As(III) influent	$[As(III)]_{inf}$	1.00	9.00	mg^1L^{-1}	3
As(V) influent	$[As(V)]_{inf}$	1.00	9.00	mg^1L^{-1}	3
Adsorption time	t	5	4110	minutes	17

Parameters solely pertaining to the FeOx emplacement process such as drying time (t_{dry}), drying temperature (T_{dry}), ageing time (t_{age}), and ageing temperature (T_{ageing}) were kept constant. The coating temperature (T_{coat} = 23 $\pm$ 2 ^oC), coating pH (pH_{coat}), and coating time (t_{coat}) also remained unchanged in the model. Other physical parameters associated with the experiments such as sand mass (M_{sand} = 5 g), sand particle size (0.42 mm $\leq D_{particle} \leq$ 0.59 mm), and adsorption temperature (T_{ads} = 23 $\pm$ 2 ^oC) also remained steady in the experiment. The resulting consistency would significantly reduce, if not eliminate, the effects of varying pore size distribution of the adsorbent that would have otherwise limited the uptake of arsenic.

RESULTS AND DISCUSSION

Kinetic Modeling

The Generalized Reduced Gradient (GRG) method was employed for conducting non-linear optimization modeling of the pseudo-first order and pseudo-second order adsorption kinetics (Ho, 2006; Chowdhury and Saha, 2010; Lin and Wang, 2009). The rate constants from the kinetic models are presented in Table 11 while the application of

the experimental data to non-linear first and second order kinetics are illustrated in Figures 31 through 34.

Table 11: Kinetic Model Parameters

				Pseudo 1st order		Pseudo 2nd order	
	[As]	q_e		rate (k_1)	r^2	rate (k_2)	r^2
	1 mg^1L^{-1}	2.02	ug^1g^{-1}	0.54 min^{-1}	0.45	1.18 $g^1ug^{-1}min^{-1}$	0.84
As(III)	3 mg^1L^{-1}	5.41	ug^1g^{-1}	0.46 min^{-1}	0.39	0.27 $g^1ug^{-1}min^{-1}$	0.78
	9 mg^1L^{-1}	14.9	ug^1g^{-1}	0.28 min^{-1}	0.25	0.03 $g^1ug^{-1}min^{-1}$	0.57
	1 mg^1L^{-1}	1.97	ug^1g^{-1}	0.70 min^{-1}	0.42	2.40 $g^1ug^{-1}min^{-1}$	0.85
As(V)	3 mg^1L^{-1}	5.50	ug^1g^{-1}	0.38 min^{-1}	0.20	0.15 $g^1ug^{-1}min^{-1}$	0.60
	9 mg^1L^{-1}	15.6	ug^1g^{-1}	0.29 min^{-1}	0.32	0.03 $g^1ug^{-1}min^{-1}$	0.64

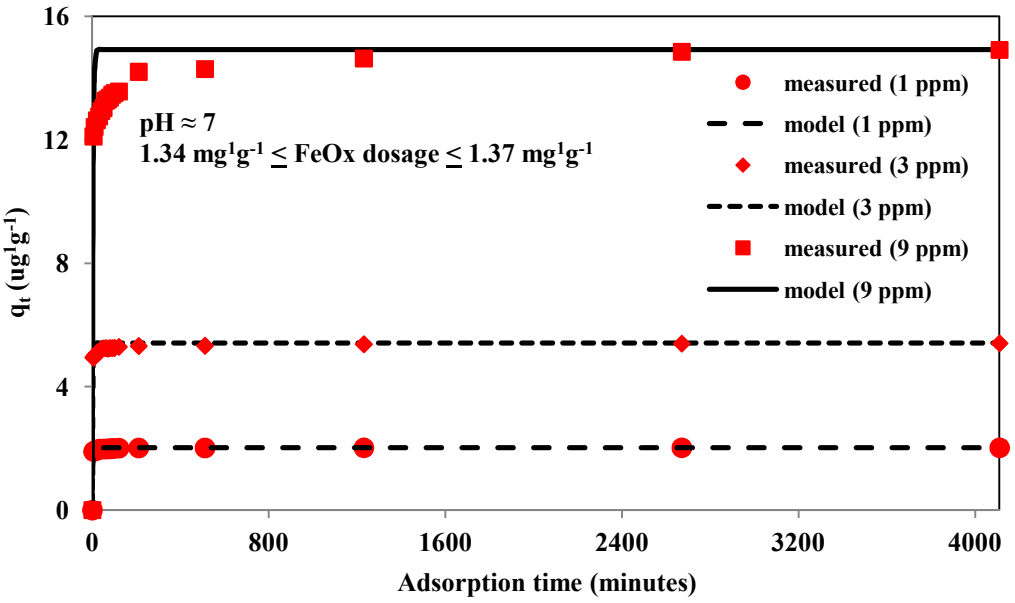

Figure 31: Plot for Pseudo-first order As(III) Adsorption

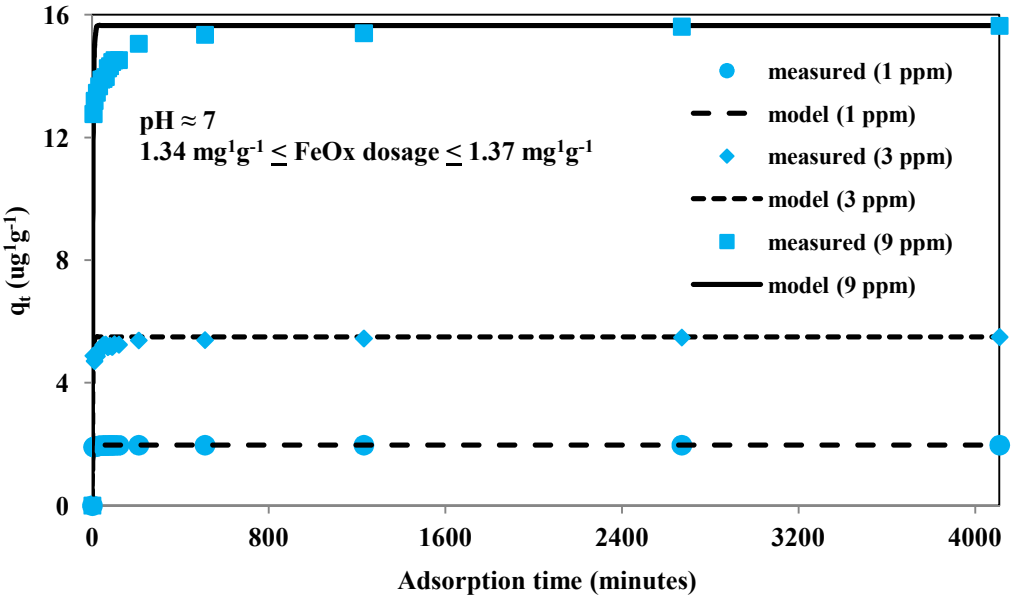

Figure 32: Plot for Pseudo-first order As(V) Adsorption

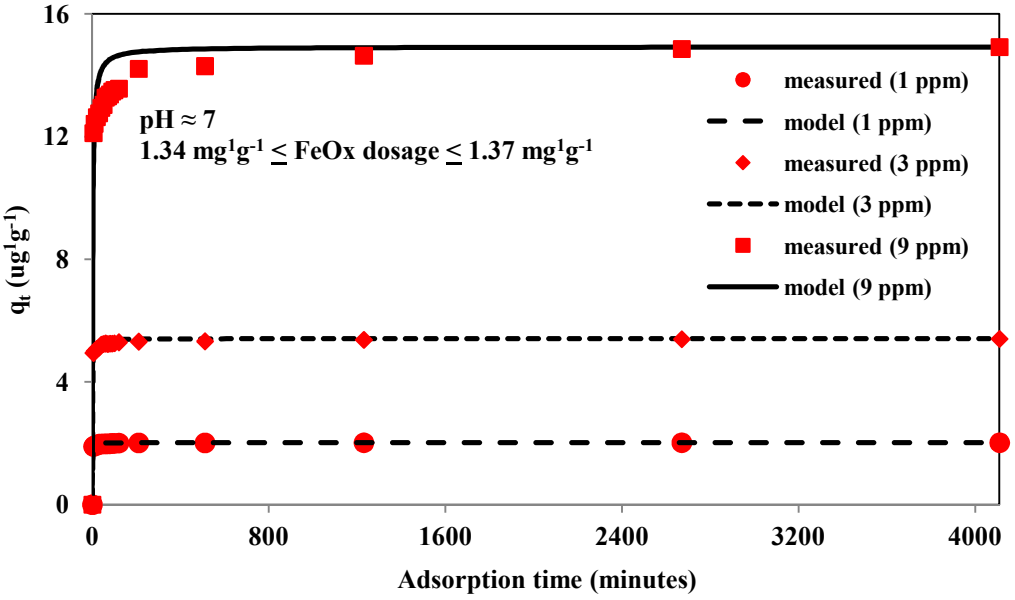

Figure 33: Plot for Pseudo-second order As(III) Adsorption

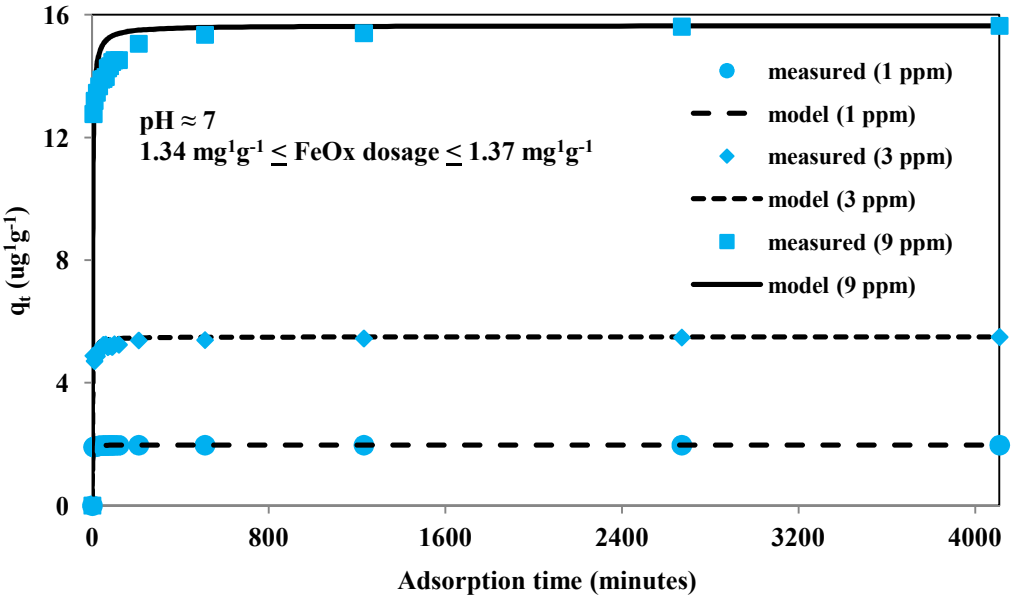

Figure 34: Plot for Pseudo-second order As(V) adsorption

Although the q_t vs t adsorption plots were similar, the pseudo-first order parameters were the least representative of the kinetic uptake of As(III) and As(V) at all initial concentrations in this study. The curves in Figures 33 and 34 reveal stronger correlation coefficients for As(III) and As(V) adsorption than the pseudo-first order reactions; concluding that As uptake via IOCS follows pseudo-second order kinetics.

Intra-particle Diffusion Modeling

The plots of q_t vs $t^{0.5}$ for As(III) and As(V) at different concentrations (1, 3, and 9 mg^{1}L^{-1}) identified several adsorption mechanisms through a multitude of linearities (Figure 35). The sharp increase of the line slope in the first step was attributed to the rapid diffusion of the arsenic in bulk phase onto the exterior surface of the FeOx, or boundary layer diffusion (BLD). As the process progressed, the adsorption of the As by

FeOx decreased to mesopore intra-particle diffusion before transitioning to micropore diffusion at equilibrium. The reduction in the rate of adsorption over time likely resulted from the depleted arsenic in the system.

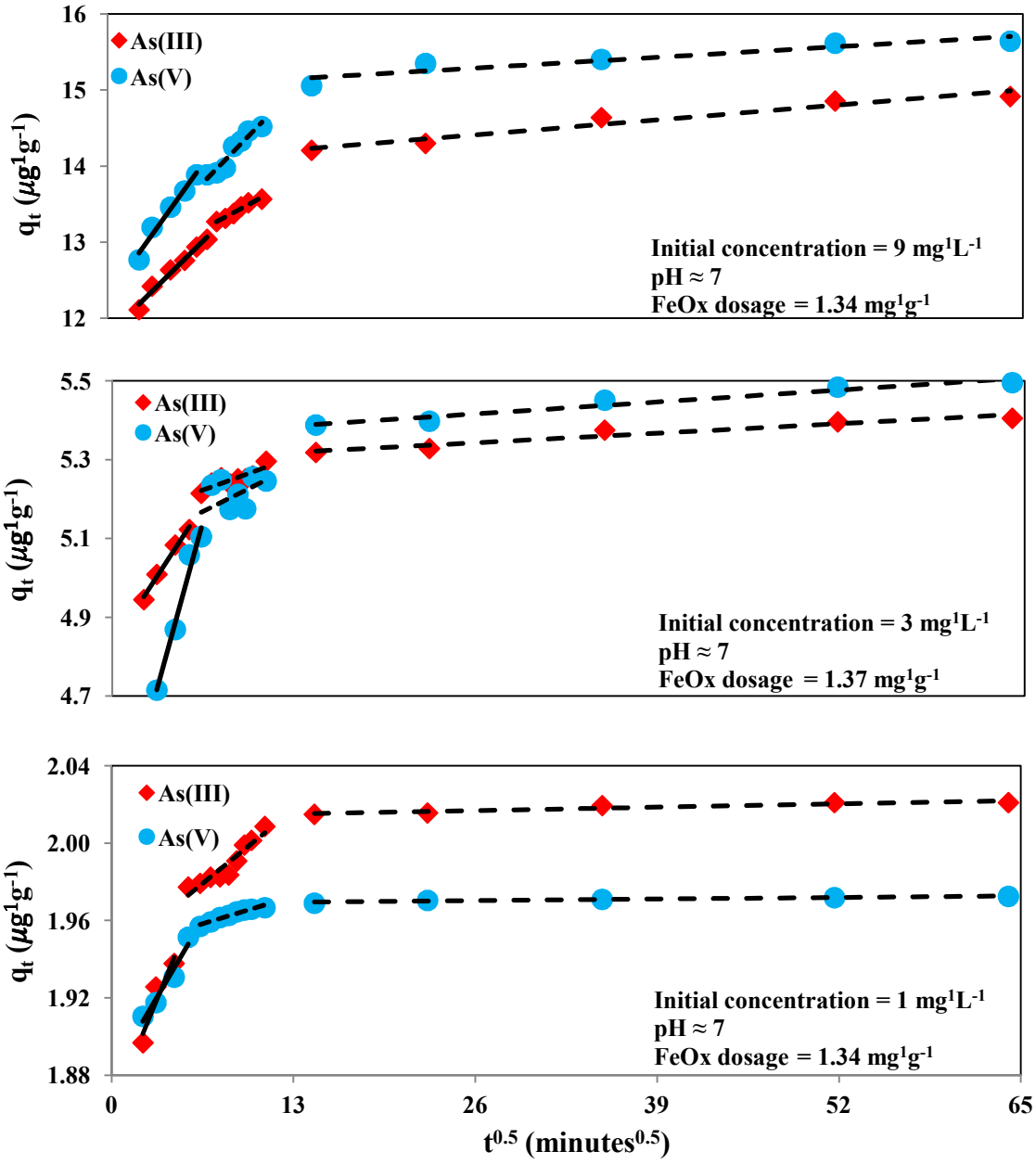

Figure 35: Intra-particle Diffusion Modeling of As Adsorption onto IOCS

Although the plots were not entirely linear, the uptake of As at different initial concentrations onto the fixed sorbent conformed to the following pattern: (1) rapid adhesion of As(III) and As(V) via boundary layer diffusion at the onset of the process followed by (2) slower, 2-step intra-particle diffusion. The rate of As accumulation varying with the square root of time not only illustrated the multi-step model, but also identified the rate-determining step of adsorption. The adsorption cycles in this study were not depicted as functions of $t^{0.5}$; suggesting that As migration across the liquid-solid interface was not exclusively limited by intra-particle diffusion. Moreover, the plots did not pass through the origin, possibly due to the difference in mass transfer between the rapid sorption stage and the subsequent prolonged complexation phase of the overall adsorption process (Panday et al., 1986). Such deviation from the origin further substantiates that boundary layer diffusion may have also controlled the sorption process to some extent (Poots et al., 1978). Excluding boundary layer diffusion, pore diffusion appeared as the rate-limiting step, mostly over extended contact time periods.

Effect of Initial Concentration on Diffusion Rate Parameter

To solely assess the effect of initial concentration on intra-particle diffusion, the differences in the arsenic molecule size, molecular structure, and As-FeOx affinity were assumed to be negligible. As demonstrated in Table 12, the increase in the initial As(III) and As(V) concentrations resulted in increased rate parameters for boundary layer diffusion and the subsequent 2-step intra-particle diffusion processes, respectively. The equilibrium portions of the plots in Figure 35 were not parallel; suggesting an enhanced diffusion of the arsenic molecules with increasing initial concentration. This

phenomenon might arise from (1) the differences in ionic charge densities resulting from As accumulation on the sorbent and (2) the intra-particle diffusion model originating from Fick's Law, which suggests that a rise in the arsenic concentration gradient subsequently hastened diffusion and adsorption onto the fixed FeOx surface.

Table 12: As Diffusion Rate Parameters at Different Concentrations

		Boundary Layer Diffusion		Mesopore Diffusion		Micropore Diffusion	
	[As]	slope (k_1)	r^2	slope (k_2)	r^2	slope (k_3)	r^2
	1 mg^1L^{-1}	0.018 $ug^1g^{-1}min^{-0.5}$	0.89	0.006 $ug^1g^{-1}min^{-0.5}$	0.90	1E-04 $ug^1g^{-1}min^{-0.5}$	0.88
As(III)	3 mg^1L^{-1}	0.055 $ug^1g^{-1}min^{-0.5}$	0.99	0.013 $ug^1g^{-1}min^{-0.5}$	0.75	0.002 $ug^1g^{-1}min^{-0.5}$	0.93
	9 mg^1L^{-1}	0.182 $ug^1g^{-1}min^{-0.5}$	0.98	0.100 $ug^1g^{-1}min^{-0.5}$	0.97	0.015 $ug^1g^{-1}min^{-0.5}$	0.95
	1 mg^1L^{-1}	0.012 $ug^1g^{-1}min^{-0.5}$	0.95	0.002 $ug^1g^{-1}min^{-0.5}$	0.94	8E-05 $ug^1g^{-1}min^{-0.5}$	0.95
As(V)	3 mg^1L^{-1}	0.130 $ug^1g^{-1}min^{-0.5}$	0.97	0.018 $ug^1g^{-1}min^{-0.5}$	0.27	0.002 $ug^1g^{-1}min^{-0.5}$	0.95
	9 mg^1L^{-1}	0.258 $ug^1g^{-1}min^{-0.5}$	0.97	0.191 $ug^1g^{-1}min^{-0.5}$	0.93	0.011 $ug^1g^{-1}min^{-0.5}$	0.88

SUMMARY

The GRG non-linear method was applied to adsorption kinetic modeling to assay the uptake of As(III) and As(V) onto iron oxide-coated sand (IOCS). The intra-particle diffusion model was also utilized to the adsorption data to elucidate the multi-step accumulation of As(III) and As(V) onto the IOCS. Regression analyses concluded that As(III) and As(V) adsorption was predominantly pseudo-second order kinetics. Three adsorption (diffusion) mechanisms were observed during As collection. The rates of macropore (boundary layer diffusion), mesopore (intra-particle diffusion), and micropore (intra-particle diffusion at equilibrium) adsorption of As(III) and As(V) onto FeOx were augmented by the increase in initial concentrations.

CHAPTER V

EVALUATION OF 2-DIMENSIONAL IN SITU IRON OXIDE EMPLACEMENT AND ARSENIC REMEDIATION USING A SIMULATED SINGLE-LINE GROUNDWATER WELL

LITERATURE REVIEW

Conventional Preparation of IOCS

Previously known IOCS preparation methods are operationally complex and require the utilization of heat and hazardous chemicals (Ramakrishna et al., 2006). A variety of approaches have been used to produce iron oxide-coated sand for small-scale heavy metal remediation. Several reports have discussed coating silica sand with Fe^{3+} chemicals such as ferric nitrate ($Fe(NO_3)_3$) and ferric chloride ($FeCl_3$) (Edwards and Benjamin, 1989; Bailey et al., 1992; Benjamin et al., 1996; Gupta et al., 2005). In those studies, various sand samples were mixed with the anhydrated Fe^{3+} and aqueous alkalinity reagents. The resulting IOCS samples were heated to at least 100 ^{o}C for extended periods of time and required additional reagents to ensure Fe^{3+} fixation on the sand. Table 13 reviews a list of reported coating methods for lab-scale use. Table 14 calculates the chemical consumption rates for each reviewed method to predict small-scale and large-scale IOCS chemical consumption rates. The large-scale (industrial-size) values were derived from the smaller (lab-scale) chemical demand.

Table 13: Review of Lab-scale Iron Oxide Coating Methods for Sand

Method	M_{sand}	Fe^{3+} (V_{Fe} and $[Fe^{3+}]$)	Alkalinity	Drying	Reference
1	200 g	50 mL, 1.65 M $Fe(NO_3)_3$	no alkalinity used	20 hrs at 110 ^oC	Edwards and Benjamin, 1989
2	321 g	80 mL, 2.00 M $Fe(NO_3)_3$	1.85 mL, 10 M NaOH	14 hrs at 110 ^oC	Bailey et al., 1992
3	321 g	80 mL, 2.70 M $Fe(NO_3)_3$	1.20 mL, 10 M NaOH	16 hrs at 110 ^oC	Stenkamp and Benjamin, 1994
4	321 g	80 mL, 2.50 M $FeCl_3$	no alkalinity used	3 hrs at 110 ^oC	Benjamin et al., 1996
5	250 g	150 mL, 0.69 M $Fe(NO_3)_3$	no alkalinity used	24 hrs at 100 ^oC	Vaishya and Gupta, 2004
6	200 g	80 mL, 2.00 M $Fe(NO_3)_3$	no alklainity used	14 hrs at 110 ^oC	Gupta et al., 2005
7	200 g	80 mL, 2.00 M $Fe(NO_3)_3$	2.00 mL, 10 M NaOH	9 hrs at 800 ^oC	Ramakrishna et al., 2006

Table 14: Small-scale and Large-scale Chemical Consumption Rates

		Small-scale (mg chemical per g sand)[a]		Large-scale (kg chemical per ton sand)[b]	
Method	**M_{sand}**	**Fe^{3+} demand**	**Alkalinity demand**	**Fe^{3+} demand**	**Alkalinity demand**
1	200 g	100 mg^1g^{-1} $Fe(NO_3)_3$	~	91 kg^1ton^{-1} $Fe(NO_3)_3$	~
2	321 g	121 mg^1g^{-1} $Fe(NO_3)_3$	2.31 mg^1g^{-1} NaOH	110 kg^1ton^{-1} $Fe(NO_3)_3$	2.1 kg^1ton^{-1} NaOH
3	321 g	163 mg^1g^{-1} $Fe(NO_3)_3$	1.50 mg^1g^{-1} NaOH	148 kg^1ton^{-1} $Fe(NO_3)_3$	1.36 kg^1ton^{-1} NaOH
4	321 g	101 mg^1g^{-1} $FeCl_3$	~	92 kg^1ton^{-1} $Fe(NO_3)_3$	~
5	250 g	100 mg^1g^{-1} $Fe(NO_3)_3$	~	91 kg^1ton^{-1} $Fe(NO_3)_3$	~
6	200 g	194 mg^1g^{-1} $Fe(NO_3)_3$	~	176 kg^1ton^{-1} $Fe(NO_3)_3$	~
7	200 g	194 mg^1g^{-1} $Fe(NO_3)_3$	4.00 mg^1g^{-1} NaOH	176 kg^1ton^{-1} $Fe(NO_3)_3$	3.64 kg^1ton^{-1} NaOH

[a] Small-scale demand = $V_{Fe}*[Fe^{3+}]*MW_{Fe}*(M_{sand}^{-1})$ where V_{Fe} (mL), $[Fe^{3+}]$ (M), and M_{sand} (g) are from table 6

[b] Large-scale demand = (small-scale demand)*(10^{-6})*1000*2000*(2.2^{-1}) in units of kg reagent per ton of sand

From an application standpoint, the above-mentioned procedures are not feasible as they pose significant economical and health risks. The nitrate (NO_3^-) ions from the ferric nitrate compound may cause blue baby syndrome when dissociated and ingested at high concentrations (USEPA, 2006). Furthermore, the capital and operating costs associated with elevating the temperature to favor coating large amounts of sand in aqueous iron

oxide would exceed the projected value of the research and render the technique impractical.

Conventional As Treatment Costs

Installation and operational costs associated with conventional As remediation technology have put them out of reach for many small communities who cannot afford above-surface groundwater arsenic treatment. Tables 15 and 16 compare the costs of reducing drinking water As from 50 μg^1L^{-1} to 10 μg^1L^{-1} for a population of 501 – 1,000 people through a variety of treatment technologies (NDWAC, 2001 and USEPA, 2000).

Table 15: As Treatment Cost Comparison (NDWAC, 2001)

Treatment Process	Treatment Costs (USD)
Coagulation-filtration	$11,325
Lime Softening (LS)	$19,681
Reverse Osmosis (RO)	$143,199
Ion Exchange (IX)	$169,273
Activated Alumina (AA)	$83,871

EPA system size category: 501 – 1,000 (population)
Inlet As concentration = 50 μg^1L^{-1}
Outlet As concentration = 10 μg^1L^{-1}
Single contaminated entry point

Table 16: As Treatment Cost Comparison with Modeling (USEPA, 2000)

Treatment Process	Treatment Costs (USD)	Model Used
Coagulation-filtration	~	~
Lime Softening (LS)	$310,500 per 1 mgd	Water model for package lime softening
Reverse Osmosis (RO)	$775,820 per 1 mgd	Water cost model
	$1,157,600 per 1 mgd	Water model for package reverse osmosis
Ion Exchange (IX)	$253,930 per 1.1 mgd	Water cost model
Activated Alumina (AA)	$90,400 per 0.7 mgd	Water cost model

EPA system size category: 501 – 1,000 (population)
Inlet As concentration = 50 μg^1L^{-1}
Outlet As concentration = 10 μg^1L^{-1}
Single contaminated entry point
mgd = million gallons of water per day

Although coagulation-filtration and lime softening are the two cheapest technologies for As treatment to according to Table 4, there have been reports that consistently rate their removal efficiencies at less than 90% (Mondal et al., 2006; Mohan and Pittman, 2007; and Ghosh, 1993). Furthermore, all of the aforementioned processes produce As-laden sludge during treatment and/or regeneration; complicating operation configuration and requiring extensive sludge handling.

RESEARCH OBJECTIVE

The objective of this undertaking was to assess the performance of in situ iron oxide sand coating and arsenic (As) removal on a single-line simulated groundwater well. The results herein could highlight the applicability of in situ groundwater As remediation.

MATERIALS AND METHODS

Materials, Equipment, and Wet Chemistry Analyses

Fine play sand was procured from two indigenous manufacturers for this study (Quikrete International, Atlanta, Georgia, United States and Short Mountain Silica, Mooresburg, Tennessee, United States). The sands each had a bulk density of 1605 $kg^{1}m^{-3}$ and porosity 38%. Four separate 50-L Nalgene carboys filled with tap water were first titrated to their desired pH ranges and purged with 95%-purity compressed nitrogen. Concentrated reagents in granular and/or aqueous form were added to the batches prior to experimentation. All other materials, equipment, and wet chemistry analyses were duplicated from Chapters II and III.

Preparation of Iron Oxide Chemical Components

The iron oxide reagent concentrations were calculated using Equation 22:

$$2Fe^{2+} + H_2O_2 + 4OH^- \rightarrow 2Fe(OH)_3 \quad (22)$$

$$2Fe(OH)_3 \rightarrow Fe_2O_3 + 3H_2O \quad (23)$$

where the transformation of the precipitated $Fe(OH)_3$ to Fe_2O_3 in Equation 23 is induced by ageing and dehydration (Cornell and Schwertmann, 2003).

Ferrous Iron Solution

360 g of ferrous chloride tetrahydrate ($FeCl_2 \cdot 4H_2O$) was dissolved in 50 L of water to produce stock Fe^{2+} of 36 mM (2,000 mg^1L^{-1} at $3 \leq pH_{Fe(II)} \leq 4$).

Hydrogen Peroxide + Hydroxide Solution

50 L of water was enriched with 102 mL of hydrogen peroxide solution (H_2O_2 at 30% w^1w^{-1} or 300 g^1L^{-1}) and 189 mL sodium hydroxide (NaOH at 50% w^1w^{-1} or 19 M) to produce a stock mixture ($[H_2O_2 + OH^-]_{mix}$) comprising of 18 mM H_2O_2 (612 mg^1L^{-1}) and 72 mM OH^- (1,223 mg^1L^{-1}) at pH 13 $\pm$ 0.1.

Water Buffer Solution

100 L of water used as a contact barrier between the Fe^{2+} and $[H_2O_2 + OH^-]_{mix}$ plumes in the conveyance system was titrated with HCl to a pH of 5.5 $\pm$ 0.5.

Preparation of Synthetic Arsenic Samples

5.55 mL of sodium arsenite ($NaAsO_2$ at 0.5% w^1v^{-1} or 5,000 mg^1L^{-1}) and 66.6 mL of sodium hydrogen arsenate heptahydrate ($Na_2HAsO_4 \cdot 7H_2O$ at 1,000 mg^1L^{-1} As(V)) were collectively dissolved in 80 L water to make a 200 μg^1L^{-1} As(III) and 200 μg^1L^{-1} As(V) influent stock mixture (total As = 400 μg^1L^{-1}).

Design of Single-Well Experiment

A single-well aquifer made of polycarbonate was constructed to simulate two-dimensional iron oxide sand coating and groundwater arsenic removal (Figure 36). The injection well at height 30.5 cm and inside diameter (ID) 3.18 mm was encircled by a permeable sand barrier to treat inward-bound groundwater. 1.59-mm cavities and an end-plug were installed on the lower 10.2 cm and bottom of the well to inject chemicals into the surrounding sand. The holes were equilaterally placed 5.08 mm from each other. The inner wall of the water well containing the sand was 30.5 cm in depth with an ID of 61 cm. The lower 22.9 cm of the sand barricade was perforated with 0.51 cm holes that were separated 2.54 cm vertically, 5.08 cm horizontally, and covered in weed blocker to contain the sand and permit water seepage. The outer wall containing the arsenic-laden water was 30.5 cm in depth with an ID of 68.6 cm. The sand was 10.2-cm in depth; translating to a working saturated volume and mass of 30 L (pore volume = 11.4 L) and 47.6 kg, respectively. 6.4-mm ID-channels were placed on the outer wall at a height of 10.2 cm to simulate the horizontal flow of groundwater containing arsenic. The components of the water well were collectively supported by an acrylic sheet platform with length 91.4 cm, width 91.4 cm, and thickness 1.30 cm. A pore volume contact time (PVCT) of 6 h was sustained by pumping feed water through the well at 32 $mL^{1}min^{-1}$. Three 8-port, rubber-marker rings placed 7.6, 15, and 23 cm from the injection well, respectively, were installed in the sand to monitor FeOx sedimentation (Figure 37). A 1.27-cm ID polycarbonate tube was used to discreetly extract 15 cm of sand. A digital water pressure gauge (3.0 ± 0.3 kPa) was installed at the inlet for head loss monitoring.

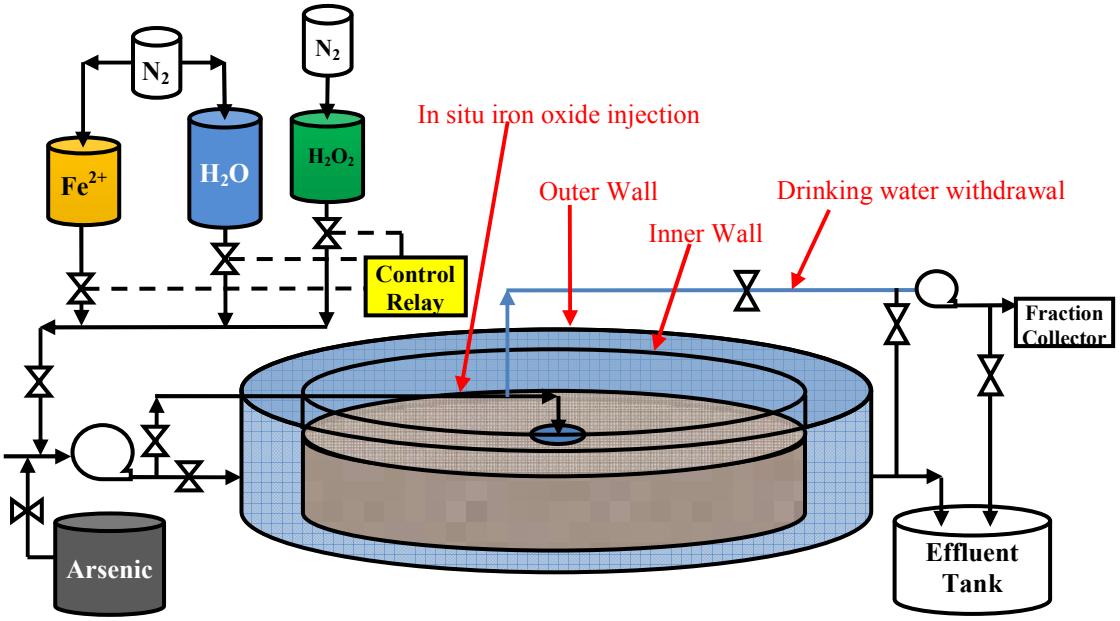

Figure 36: Single Well Study Design

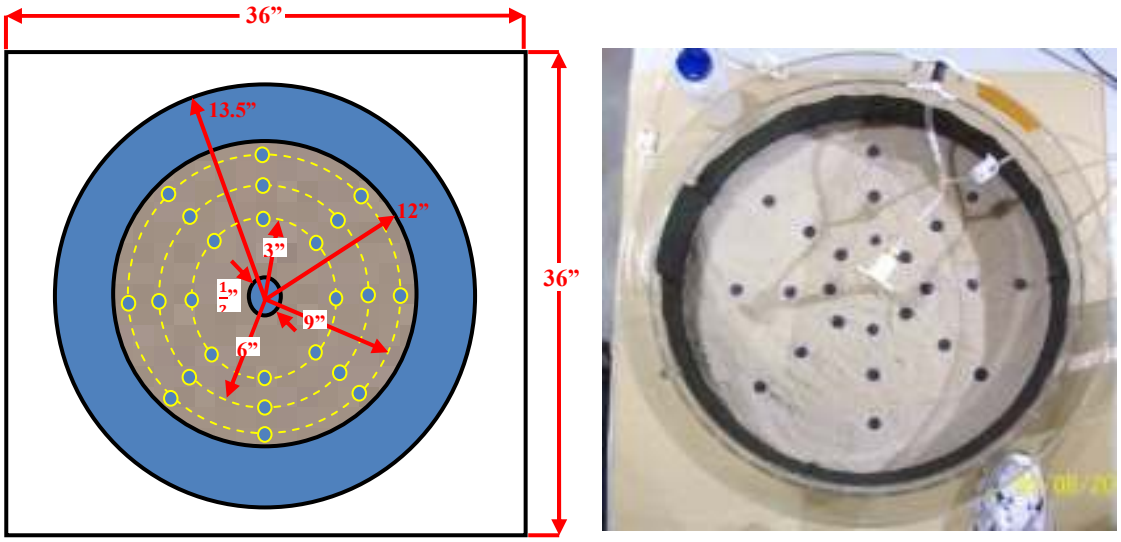

Figure 37: Single Well Study (top view)

Surface-bound Iron and Arsenic Characterization

Two extraction procedures were carried out to characterize (1) the surface-bound, pre-existing iron on the sand prior to iron oxide coating and (2) the subsequently emplaced iron oxide and adsorbed arsenic. Herein, a mass-based liquid-solid ratio of 10:1 was used to determine the proper amount of extraction liquid required for each sand batch (Lee et al., 2007 and Lee et al., 2009). 60 mL of hydrochloric acid (HCl at 6 M) was mixed with sand samples of 6 g; sustaining a pH of 0.78 $\pm$ 0.03. Iron extraction experiments were performed under constant agitation in rubber-sealed 70-mL beakers in a rotating arm shaker (29 rpm) for 24 h. Supernatant samples were individually filtered through a 0.45 μm cellulose acetate filter and analyzed for Fe^{2+} via UV/IVS Spectrometry. The iron oxide and arsenic accumulated on the sand in this study were extracted and analyzed in the same manner as derived from Chapter III.

Sorption Data Analyses

As adsorption data analyses methods were duplicated from Chapter III.

RESULTS AND DISCUSSION

Selection of Iron Oxide Reagents

Potential Fe^{2+} compounds that were considered for this study were ferrous chloride ($FeCl_2$), ferrous nitrate ($Fe(NO_3)_2$) and ferrous sulfate ($FeSO_4$). Table 17 compares the dosage levels of the compounds to their respective maximum concentration levels (MCLs) and highlights their side effects when applied in their respective amounts. A dissolved oxygen (DO) level of 39.6 mg^1L^{-1} was used as the weakest oxidant (control) to back-calculate the minimum Fe^{2+} dosage necessary for FeOx coating in this study.

Table 17: Comparison of Fe^{2+} Sources by Dosage and Side Effects

Fe^{2+} agent[a]	Fe^{2+} dose[b]	Agent Dose[c]	Anion Dose[d]	Anion MCL[e]	H_2O Effects	Health Impacts[f]
$FeCl_2$	275 mg^1L^{-1}	627 mg^1L^{-1}	352 mg^1L^{-1} Cl^-	250 mg^1L^{-1}	Color, odor, taste	Vital electrolyte
$FeSO_4$	275 mg^1L^{-1}	752 mg^1L^{-1}	477 mg^1L^{-1} SO_4^{2-}	250 mg^1L^{-1}	Color, odor, taste	Discomfort
$Fe(NO_3)_2$	275 mg^1L^{-1}	887 mg^1L^{-1}	612 mg^1L^{-1} NO_3^-	10.0 mg^1L^{-1}	O_2 depletion	Fatal above MCL

[a] Ferrous iron (Fe^{2+}) sources manufactured in industrial (anhydrous) form

[b] Fe^{2+} dose = [39.6 mg^1L^{-1} O_2]*[32 mg^1mmole^{-1} O_2]$^{-1}$*[4]*[56 mg^1mmole^{-1} Fe^{2+}]

[c] Agent dose = (Fe^{2+} dose)*(MW_{agent})*($MW_{Fe(II)}^{-1}$)

[d] Anion dose = (agent dose) – (Fe^{2+} dose)

[e] Maximum contaminant levels (MCLs) established by USEPA (primary and secondary)

[f] Reported toxicological outcomes for anions ingested at concentrations above MCLs (USEPA, 2006)

Nitrate (NO_3^-) is an oxygen-depleting water nutrient with known adverse effects on human health when ingested at concentrations above the enforceable MCL of 10 mg^1L^{-1} NO_3-N (nitrate as nitrogen) (USEPA, 2006). Pending the employment of $Fe(NO_3)_2$ for groundwater arsenic adsorption, supplementary treatment would be required to preserve the drinking water quality above 5.0 mg^1L^{-1} O_2 and under 10 mg^1L^{-1} NO_3-N. Hence, ferrous nitrate was eliminated as an Fe^{2+} source candidate for this study. Sulfate (SO_4^{2-}) and chloride (Cl^-) are secondary pollutants with aesthetic effects (color, odor, and taste of water) and identical recommended (non-enforceable) MCLs at 250 mg^1L^{-1} each. Chloride also has technical effects (corrositivity and staining of conveyance fixtures), which translate to potential economic implications over time (USEPA, 2006). However, the anions obstruct As adsorption onto iron oxides in the following order: $SO_4^{2-} > NO_3^- \approx Cl^-$ (Dzonmabk and Moral, 1990). In contrast to sulfate, chloride has no health-based guideline for drinking water standards (WHO, 1996). In fact, the electrolyte maintains osmotic pressure and proper liver functions in humans (Essig et al., 2008).

The oxidizing power of potential Fe^{2+} oxidants decreases in the following order: ozone (O_3) > hydrogen peroxide (H_2O_2) > permanganate (MnO_4^-) > hypochlorite (OCl^-) > chlorine gas (Cl_2) > chlorine dioxide (ClO_2) > O_2 (Bard, 1966 and Ozonia, 1977). The Fe^{2+} and oxidant dosages were calculated from a pre-set iron oxide (Fe_2O_3) concentration on saturated aquifer sand in a simulated groundwater well:

$$M_{Fe(III)\ total} = ([Fe_2O_3]_{sand})*(10^{-3})*(M_{sand})*(111.2/159.2) \quad (24)$$

$$Fe^{2+}_{demand} = (M_{Fe3+\ total})*[(\#\ mole\ Fe^{2+})/(\#\ mole\ Fe^{3+})]/(MW_{Fe3+}) \quad (25)$$

$$M_{oxidant\ demand} = (Fe^{2+}_{demand})*[(\#\ mole\ oxidant)/(\#\ mole\ Fe^{2+})]*MW_{oxidant} \quad (26)$$

$$C_{Fe2+} = ((Fe^{2+}_{demand})*(MW_{Fe2+}))/(\forall_{Fe2+,\ total}) \quad (27)$$

$$C_{oxidant} = ((M_{oxidant\ demand})*1000)/(\forall_{oxidant,\ total}) \quad (28)$$

where Equations 24, 25, 26, 27, and 28 determine the total Fe^{3+} accumulated on the sand ($M_{Fe(III)\ total}$) (g), total Fe^{2+} required for FeOx coating (Fe^{2+}_{demand}) (moles), total mass of oxidant required to oxidize the Fe^{2+} demand to the amassed Fe^{3+} on the sand ($M_{oxidant\ demand}$) (g), Fe^{2+} concentration (C_{Fe2+}) (mg^1L^{-1}), and oxidant concentration ($C_{oxidant}$) (mg^1L^{-1}), respectively. The $[FeOx]_{sand}$ is the FeOx concentration on the sand (1.5 mg^1g^{-1}), M_{sand} is the total sand mass in the filter (47.6 x 10^3 g), MW_{Fe2+} and MW_{Fe3+} are the respective molar masses of Fe^{2+} and Fe^{3+} (55.6 g^1mole^{-1}), $MW_{oxidant}$ is the molar mass of the oxidant used in the oxidation process (g^1mole^{-1}), and $\forall_{inj,\ total}$ is the pre-set injection volume for each chemical for the entire coating procedure (50 L). The molar ratios [(# mole Fe^{2+})/(# mole Fe^{3+})] and [(# mole oxidant)/(# mole Fe^{2+})] are determined from oxidation-reduction reactions (Tchobanoglous et al., 2003) while the Fe^{3+} mass composition ratio (111.2/159.2) was based on the precipitation of Fe_2O_3. In the case of

using oxygen to oxidize Fe^{2+}, the dissolved oxygen (DO) concentration in water dictates the FeOx coating scheme:

$$C_{Fe2+,\ DO} = (C_{DO})*(10^{-3})*[(\#\ mole\ Fe^{2+})/(\#\ mole\ DO)]*(MW_{Fe2+})/(MW_{DO}) \quad (29)$$

$$\forall_{Fe2+\ total} = (Fe^{2+}{}_{demand})*(MW_{Fe2+})/(C_{Fe2+,\ DO}) \quad (30)$$

$$\forall_{DO,\ total} = (M_{DO\ demand})*(10^{3})/(C_{DO}) \quad (31)$$

where C_{DO} (mg^1L^{-1}) is the temperature-dependent O_2 concentration in water, $C_{Fe(II),\ DO}$ is the maximum Fe^{2+} concentration permissible by the C_{DO} (g^1L^{-1}), $\forall_{Fe2+\ total}$ and $\forall_{DO,\ total}$ are the respective injection volumes for Fe^{2+} and O_2 (L), and $M_{DO\ demand}$ is the mass of O_2 needed to generate the targeted $[Fe_2O_3]_{sand}$ (g). Table 18 summarizes the dosage levels of conventional oxidants and their respective regulatory guidelines.

Table 18: Comparison of Oxidant Sources by Dosage and Side Effects

Oxidant	$C_{Fe(II)}$[a]	(Ox:Fe^{2+})[b]	$C_{oxidant}$	Oxidant MCL[c]	H_2O Effects	Health Impacts[d]
O_3	2,000 mg^1L^{-1}	1:2	863 mg^1L^{-1}	None	Disinfectant	None
H_2O_2	2,000 mg^1L^{-1}	1:2	612 mg^1L^{-1}	None	Color, odor, taste	Oral damage
MnO_4^-	2,000 mg^1L^{-1}	1:5	396 mg^1L^{-1} Mn	0.05 mg^1L^{-1} Mn	Metallic taste	Vital nutrient
OCl^-	2,000 mg^1L^{-1}	1:2	917 mg^1L^{-1}	0.8 mg^1L^{-1}	Disinfectant	Anemia
Cl_2	2,000 mg^1L^{-1}	1:2	1,259 mg^1L^{-1}	4.0 mg^1L^{-1}	Disinfectant	Eyes, nose, stomach
ClO_2^-	2,000 mg^1L^{-1}	1:4	603 mg^1L^{-1}	0.8 mg^1L^{-1}	Disinfectant	Anemia
O_2[e]	275 mg^1L^{-1}	1:4	39.6 mg^1L^{-1}	$\geq$ 5.0 mg^1L^{-1}	Improved quality	Vital element

[a] $[Fe_2O_3]_{sand}$ = 1.5 mg^1g^{-1}, M_{sand} = 47.6 x 10^3 g, and $\forall_{chemcial}$ = 50 L from Equation 1

[b] Molar ratios derived from oxidation-reduction reactions (Tchobanoglous et al., 2003)

[c] Primary or secondary maximum contaminant levels established by USEPA (USEPA, 2006)

[d] Reported toxicological outcomes for anions ingested at concentrations above MCLs (USEPA, 2006)

[e] O_2 concentration in water at Temperature = 25 ^oC and $\forall_{Fe(II),\ total} = \forall_{DO,\ total}$ = 363 L

Although ozone (O_3) has a short temperature-induced half-life in water (i.e. 30 min. at 15 ^oC, 20 min. at 20 ^oC, 15 min. at 25 ^oC, 12 min. at 30 ^oC, and 8 min. at 35 ^oC) (Lenntech, 2009) and no enforceable MCL, it is highly reactive and has been implicated with occupational pulmonary edema resulting from long-term inhalation (Kleinfeld et al., 1957). The burdensome storage control requirements (occupational and environmental) for long-term ozonation, combined with the need for supplementary personal protective equipment (PPE), could possibly outweigh the applicability of ozone in laboratory and industrial settings alike. As such, the utilization of O_3 was eliminated in this study. Hydrogen peroxide (H_2O_2), like O_3, has no regulatory drinking water standard in the United States. Yet, ingestion of food-grade H_2O_2 (30 mg^1L^{-1}) has been linked to severe damage of the mouth, esophagus, and stomach (Hathway et al., 1991). Manganese (Mn) is a non-lethal metal that is vital for human bodily functions. However, when reduced from permanganate (MnO_4^-) at high concentrations following Fe^{2+} oxidation, Mn^{7+} causes a metallic taste in drinking water. Hence, a secondary (non-enforceable) MCL of 0.05 mg^1L^{-1} was mandated to protect the taste of the water. As such, MnO_4^- was removed from the list of oxidants in this research due to its potentially undesirable aesthetic effects. Hypochlorite (OCl^-) and chlorine dioxide (ClO_2^-) have been associated with anemia and nervous system damage resulting from considerable intake. Chlorine gas (Cl_2) causes irritation in the eyes, nose, and stomach when consumed at elevated levels in water. Without supplementary neutralization, the side effects of the chlorine-based oxidants could potentially undermine the feasibility of this study in its entirety and thus were eliminated as Fe^{2+} oxidant candidates. Unlike other

oxidants in consideration, oxygen is widely available (Emsley, 2001) and has no enforceable MCL or health advisory for drinking water standards (USEPA, 2006). In fact, a higher DO concentration in water improves odor and taste (Tchobanoglous et al., 2003). Nonetheless, the injection volume of the DO significantly exceeds the other oxidants ($\forall_{DO,\ total}$ = 363 L >>> $\forall_{oxidant,\ total}$ = 50 L) due to the limited solubility of oxygen in water. This translates to higher operating costs (energy, chemicals, etc.) resulting from using DO to achieve $[Fe_2O_3]_{sand}$ = 1.5 mg^1g^{-1} instead of alternative chemicals. Accordingly, hydrogen peroxide was employed as the Fe^{2+} oxidant in this study to control costs, minimize coating time, and maximize FeOx emplacement.

Tap Water Chemistry Profile

The water used in this study originated from sand formations in the Carrizo-Wilcox aquifer (Thorkildsen and Price, 1991). The relative abundance of several water constituents, and their resistivity to synthetic alteration, primarily rely on their chemical mobility. Cornell and Schwertmann (2003) concluded that the mobility of an ion is governed by (1) the solubility of its elemental components, (2) its affinity towards sorption and ion exchange by various mediums in the hydrosphere, and (3) the extent of uptake in the biosphere. Hence, the presence of assorted ions in the groundwater is directly related to their respective mechanisms of fate and transport. The chemical modification of native groundwater for in situ remediation is essentially dictated by the pre-existing condition of the water. Chebotarev (1950) and Hem (1989) analyzed the compositions and relative hydrochemical mobilities of several dissolved elements in groundwater, which were compared to the tap water quality (Table 19).

Table 19: College Station Water Quality Profile

Item	Mobility[a]	Range (mg^1L^{-1})[b]	Tap Water Quality (mg^1L^{-1}) 2005[c]	2008[d]	Experiment[e]	MCL (mg^1L^{-1})[f]
Al	N/A	1 - 2	0.008	N/A	ND	0.05 - 0.2
Ca^{2+}	3	10 - 200	3	N/A	< 0.1	N/A
Cl^-	100	1 - 150	34	51	71	250
F^-	N/A	0.1 - 2	1.1	0.32	0.63	2
Fe^{2+}	N/A	0 - 5	ND	ND	0.008	0.3
HCO_3^-	N/A	80 - 400	459	431	447	N/A
Mg^{2+}	1.3	1 - 100	0.65	NA	< 0.1	N/A
Na^+	2.4	1 - 300	200	200	252	N/A
O_2	N/A	N/A	> 5	> 5	> 5	$\geq$ 5
pH	N/A	N/A	7.8	8.3	8.6 ± 0.1	7.5 ± 1
Si	0.2	1 - 30	N/A	N/A	10	N/A
SO_4^{2-}	57	10 - 100	9	12	7	250
TDS	N/A	100 - 1000	523	489	496	500

N/A = not available or applicable, TDS = total dissolved solids, ND = non-detectable

[a] Constituent hydrochemical mobility in groundwater (Chebotarev 1950 and Hem 1989)

[b] Groundwater quality range of constituents (Chebotarev 1950 and Hem 1989)

[c] 2005 College Station water quality report (College Station Utilities, 2005)

[d] 2008 College Station water quality report (College Station Utilities, 2008)

[e] Experimental water quality profile (sampled and analyzed prior to investigation)

[f] USEPA Drinking Water Secondary MCL (USEPA, 2006)

Prior to distribution, the source water is pumped through cooling towers, disinfected with chlorine gas (Cl_2), and fluoridated to a maximum residual of 1 mg^1L^{-1} (College Station Utilities, 2011). The tap water quality preceded the secondary drinking water MCLs mandated by the USEPA. For reagent preparation, the water quality components of concern were the initial pH and oxygen (O_2) as the solutions required variable ionic conditions ($pH_{Fe(II)} = 3.5 \pm 0.5$, $pH_{H2O} = 5.5 \pm 0.5$, and $pH_{H2O2} \approx 13$) in anoxic environments. The water pH likely resulted from the prevalence of alkalinity (HCO_3^-), salinity (Na^+), and silicon (Si). These constituents conceivably destabilized tap water titration and complicated ensuing pH adjustments. Furthermore, the occurrence of multiple anions (SO_4^{2-}, Si, and HCO_3^-) may significantly decelerate As adsorption.

Iron Oxide Coating Performance

Several trials were performed to (1) elucidate the operating parameters and (2) optimize FeOx coating and As adsorption in 2-dimensional settings. The coating scheme devised from Chapter II was replicated in this study. The injection schedule was adjusted to accommodate a larger pore volume by computing the projected plume size based on the PVCT and filter radius:

$$r_{plume} = (t_{injection}/PVCT)*(r_{sand}) \quad (32)$$

where an upsurge in the chemical injection time (minutes) consequently increased the plume radius (r_{plume}) (cm) from the injection point according to a steady PVCT (360 minutes) and sand radius (r_{sand} = 30.5 cm). Additional sand in the well was became immersed in the chemicals as the injection plume expanded. Hence, the injection schedule accounted for the increasing distances from the injection well (Table 20).

Table 20: FeOx Reagent Chemistry, Injection Format, and Plume Radius

Chemical(s)	pH	Molar Conc.	Mass Conc.	Injection Time[a]	r_{plume}[b]
Fe^{2+}	~3.15	36.0 10^{-3} M	2,000 mg^1L^{-1}	90 minutes	7.63 cm
HCl		100 10^{-5} M	1.00 mg^1L^{-1}		
H_2O #1	~5.13	10.0 10^{-6} M	10.0 μg^1L^{-1}	90 minutes	7.63 cm
H_2O_2	~13	18.0 10^{-3} M	612 mg^1L^{-1}	90 minutes	7.63 cm
OH^-		72.0 10^{-3} M	1,223 mg^1L^{-1}		
H_2O #2	~5.13	10.0 10^{-6} M	10.0 μg^1L^{-1}	90 minutes	7.63 cm
[a]	Sum of injection times is equal to one FeOx injection cycle (PVCT = 360 min.)				
[b]	$r_{plume} = (t_{injection})*(PVCT^{-1})*(r_{sand})$ where sand diameter = r_{sand} = 30.5 cm				

The play sands were analyzed for initial Fe^{2+} and Fe^{3+} content prior to coating. The results reveal surface-bound Fe^{2+} and Fe^{3+} compositions at 0.03 mg^1kg^{-1} and 0.24 mg^1g^{-1}, respectively, for the Short Mountain white play sand (high quality grade). Surface-bound

Fe^{3+} precipitation was not observed on the sand until after 4 days of coating. Conversely, Fe^{3+} accumulation was established on the Qiukrete brown play sand (low quality grade) after 6 hours of coating, which initially consisted of 0.61 mg^1kg^{-1} Fe^{2+} and 1.25 mg^1g^{-1} Fe^{3+}. The brown sand contained significantly more surface-bound iron content; thus qualifying as the sand of choice for all further experiments in this study.

Multi-point extraction and wet chemistry analyses were conducted on the sand to quantify the FeOx accumulation ($[FeOx]_{sand}$) at three marked radius points. Of the 15-cm sand extraction depth, the lower (saturated) 10.2 cm was analyzed for Fe^{3+} since the easily desorbed FeOx observed at the top likely resulted from upward capillary action during the coating process. The FeOx coating configured to a symmetrical distribution on the sand (Figure 38). The injection scheme devised in Table 19 emplaced a concentrated FeOx ring (1.17 mg^1g^{-1}) at 15 cm from the injection well. The ring was engulfed by weaker and/or partial Fe^{3+} deposit zones; amassing average concentrations of 0.49 and 0.55 mg^1g^{-1} at 7.6 and 23 cm, respectively (Figure 39). The FeOx content between the inner and outer wall was found to comprise of ferrous hydroxide ($Fe(OH)_2$ at 0.74 mg^1g^{-1}); likely resulting from alkalinity-induced Fe^{2+} precipitation. Despite the ample variation of $[FeOx]_{sand}$ between the radii, the widespread dispersion of Fe^{3+} sedimentation corroborated equilateral Fe^{3+} dissemination. The positioning of the reactive barrier was influenced by control factors associated with the chemical and physical properties of the reagents and the operation of the water well. More specifically, the pH levels, reagent solubility, and the injection schedule of the chemicals were suspected of influencing the deposit radius of the precipitated FeOx in the sand filter.

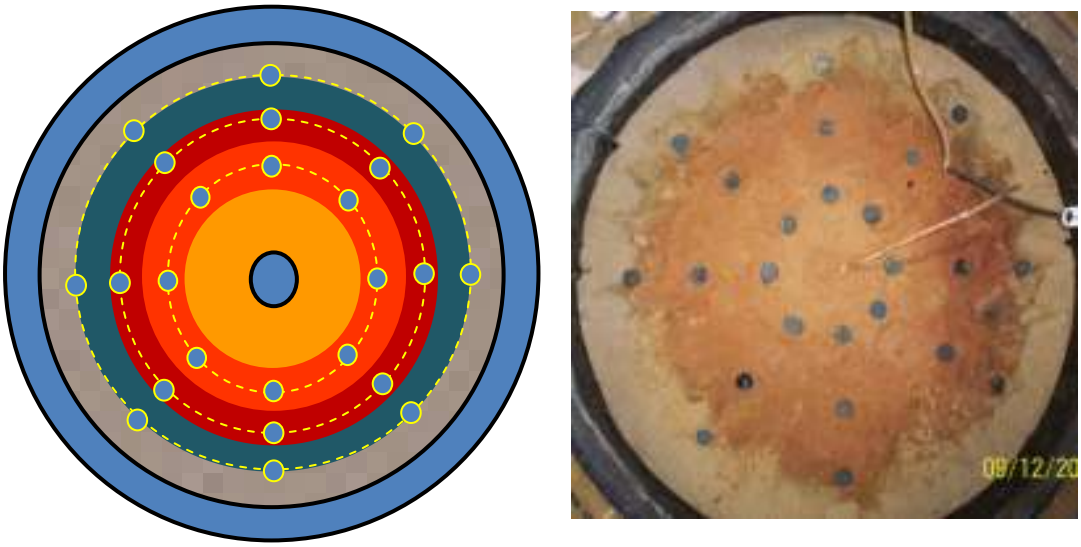

Figure 38: FeOx Precipitation Profile (top view, not drawn to scale)

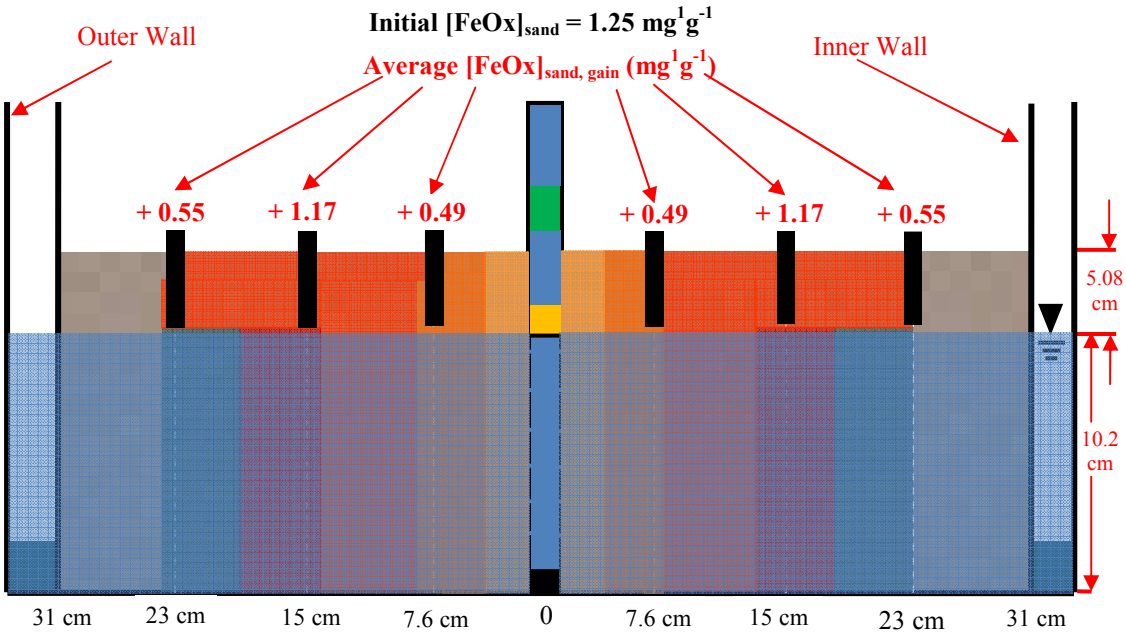

Figure 39: FeOx Precipitation Profile (based on depth and radius)

With a pH of 5.92 $\pm$ 0.03 and an injection time of 60 minutes in the initial stages of the experiment, the water buffer ($5 \leq pH_{H2O} \leq 6$) formed an contact zone for Fe^{2+} and H_2O_2 within close proximity of the injection well; accounting for the moderate FeOx sedimentation inside the inner 15-cm barrier radius. This occurrence probably resulted from the near-neutral pH_{H2O} providing insufficient H^+ to expand the Fe^{2+}-H_2O_2 reaction perimeter. The buffer pH and injection time were subsequently reduced to 5.05 $\pm$ 0.05 and protracted to 90 minutes, respectively, to delay Fe^{3+} precipitation until reaching remoter distances from the injection well. Additionally, the ferrous chloride solution ($3 \leq pH_{Fe(II)} \leq 4$) had an initial pH of 3.90 $\pm$ 0.3; consequently decelerating the dispersive capacity of Fe^{2+} as the proceeding H_2O and H_2O_2 elutions expanded the overall plume diameter in the well. The initial $pH_{Fe(II)}$, accompanied by the limited solubility of the ferrous chloride in water (625 g^1L^{-1} at 20 ^oC, 670 g^1L^{-1} at 25 ^oC, and 700 g^1L^{-1} at 30 ^oC) (NIST, 2007), could have reduced Fe^{2+} dispersion in the water well; thus allowing the infinitely miscible H_2O_2 to imbricate the Fe^{2+} plume and deposit Fe^{3+} on the sand prematurely. Hence, the $pH_{Fe(II)}$ was reduced to 3.10 $\pm$ 0.05 to improve Fe^{2+} mobility through the system and drive the reaction zone away from the point of injection. As a result of the Fe^{2+} and H_2O buffer reagent modifications, Fe^{3+} precipitation was effectively facilitated remotely from the injection well throughout the system. No Fe^{2+} or Fe^{3+} was detected at the well outlet following these operational modifications; corroborating the prevalence of iron retention on the sand. The evidence to date suggests that the manipulation of the chemical pHs and injection schedules allow for controlled

FeOx formation at selected distances from the point of injection while simultaneously retaining all Fe^{3+} ions in the system.

Although H_2O_2 is more soluble than the Fe^{2+} source, the oxidant was susceptible to decomposition induced by temperature increases and the presence of water impurities in alkaline conditions (Petrucci, 2007). This vulnerability likely caused the formation of $Fe(OH)_2$ in the well. Equation 33 shows the exothermic disproportionation of H_2O_2:

$$2H_2O_2 \rightarrow 2H_2O + O_2 \quad (33)$$

where the decomposition process could also be catalyzed by contact with light, metals, or dust (US Peroxide, 2011). Intermittent H_2O_2 level readings were recorded during the experiment to observe concentration reductions. The H_2O_2 composition (initially 612 mg^1L^{-1}) declined to 509, 442, and 271 mg^1L^{-1} following 2, 3, and 8 hours of storage (pH $\approx$ 13, T = 23 $\pm$ 2 ^oC, and P = 1 atm), respectively. The rapid reduction in H_2O_2 was apparently accelerated by the (1) elevated alkalinity of the $[H_2O_2 + OH^-]_{mix}$, (2) interactions with residual metals in the mixture originating from the alkalinity source (0.03 mg^1L^{-1} Fe, 0.03 mg^1L^{-1} Ni, and 0.29 mg^1L^{-1} Hg), and (3) heterogeneous reactions with the pre-existing impurity content of the tap water used to prepare the reagent. Additionally, continuous exposure to illumination (indoor lighting) may have also influenced H_2O_2 putrefaction to a lighter extent. The rate of deterioration during storage (28% reduction prior to injection into the water well) ultimately undermined the oxidation capacity of H_2O_2 and would require overstock in future investigations.

Another suspected variable affecting the FeOx radius was the physical design of the conveyance system and water well. Each chemical traveled a linear distance of 4.57 m

from storage to the injection well. With a volumetric flow rate of 32 mL^1min^{-1} passing through 3.18-mm ID tubing, the linear flow velocity and conveyance time were 4.03 m^1min^{-1} and 68 s, respectively; translating to a 0.32% delay of the PVCT (360 minutes) due to transport. Conclusively, conveyance of the reagents was determined to be insignificant when compared to the diminished mobility of Fe^{2+} at increased gaps from the well. All injections were adjusted to improve FeOx formation at greater plume sizes without regard to conveyance time.

Evaluation of As(III) and As(V) Remediation

Following FeOx coating, the sand filter and outer wall were filled with radially-inbound arsenic-laden tap water (total As = 400 μg^1L^{-1}) to commence As remediation. Figures 40 and 41 illustrate that the FeOx-coated in the water well was capable of repetitiously removing As(III) and As(V) from the polluted drinking water.

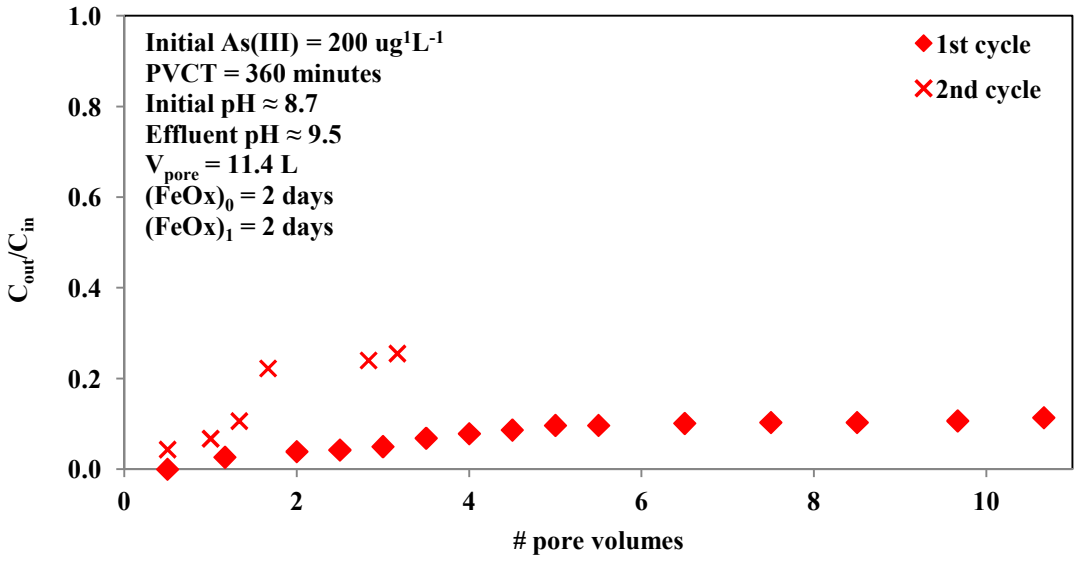

Figure 40: IOCS Water Well As(III) Adsorption

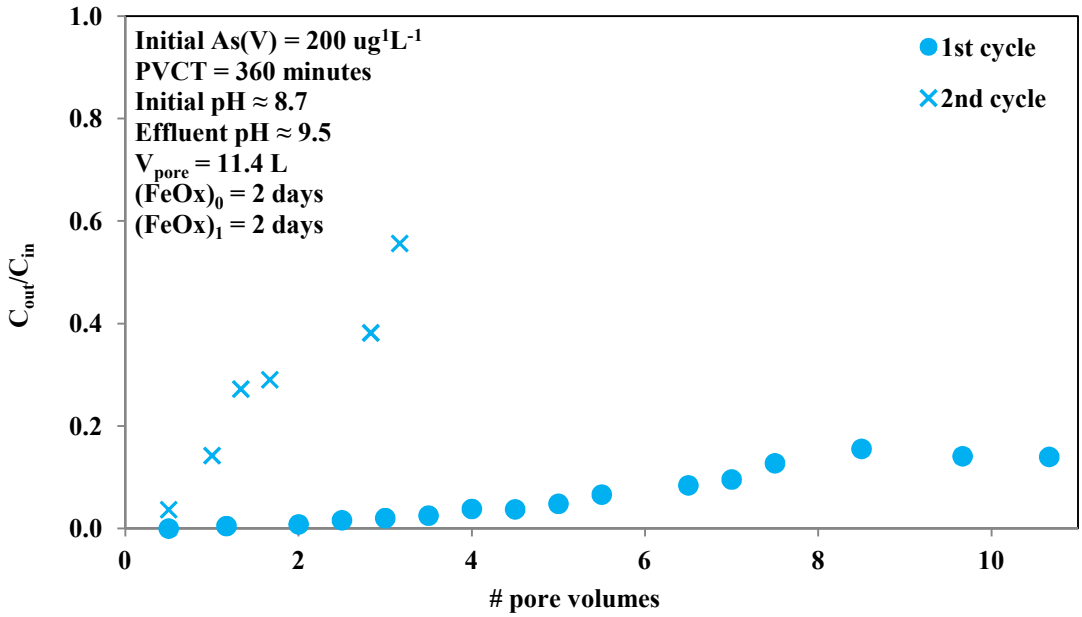

Figure 41: IOCS Water Well As(V) Adsorption

MCL-compliance for As(III) and As(V) ($\leq$ 10 $ug^{1}L^{-1}$) in the first round prevailed up the 5^{th} and 7^{th} pore volume, respectively. Although the second round of As adsorption ended prematurely, the IOCS filter produced safe drinking water up to the 1^{st} pore volume for As(III) and less than 1 pore volume for As(V). The diminished adsorption capacity for As(III) and As(V) apparently resulted from the insufficient replenishment of FeOx during the second coating phase; which was caused by the recurring deterioration of the H_2O_2 (Table 21). The water pH and competition for adsorption sites between As(III), As(V), and other dissolved constituents could have also reduced As uptake in both cycles. Nonetheless, the initial surface-bound Fe^{3+} on the sand (1.25 $mg^{1}g^{-1}$) provided adsorption sites for accumulated As(III) and As(V) along with the additional Fe^{3+} deposits; thus facilitating the extension of the first As remediation cycle.

Table 21: Water Well As(III) and As(V) Adsorption Summary

	As(III) adsorption trials				As(V) adsorption trials			
Parameter	**1st**	**2nd**	**Total**	**Units**	**1st**	**2nd**	**Total**	**Units**
$[As]_{feed}$	200	200	~	μg^1L^{-1}	200	200	~	μg^1L^{-1}
t_{MCL} [a]	33	6	39	hours	42	3	45	hours
# $V_{pore, MCL}$	5.5	1	6.5	Pore volumes	7	0.5	7.5	Pore volumes
$V_{As, MCL}$ [b]	63	11.4	74.4	L H_2O	80	5.7	85.7	L H_2O
$V_{As, total}$ [c]	122	36	158	L H_2O	122	36	158	L H_2O
UR_{MCL} [d]	756	4175	~	g^1L^{-1}	595	8351	~	g^1L^{-1}
ST_{MCL} [e]	1.32	0.24	~	L^1kg^{-1}	1.68	0.12	~	L^1kg^{-1}

[a] MCL breakthrough time recorded at arsenic effluent $\geq$ 10 μg^1L^{-1}

[b] $V_{As, MCL}$ = volume of treated water at MCL breakthrough = (# $V_{pore, MCL}$)*(11.4 L)

[c] $V_{As, total}$ = Total volume water treated in each trial derived from Figures 40 and 41

[d] UR_{MCL} = IOCS usage rate at MCL = $(M_{sand})*(10^3)*(V_{As, MCL}^{-1})$ where M_{sand} = 47.6 kg

[e] ST_{MCL} = MCL specific throughput = $(V_{As, MCL})*(M_{sand}^{-1})$

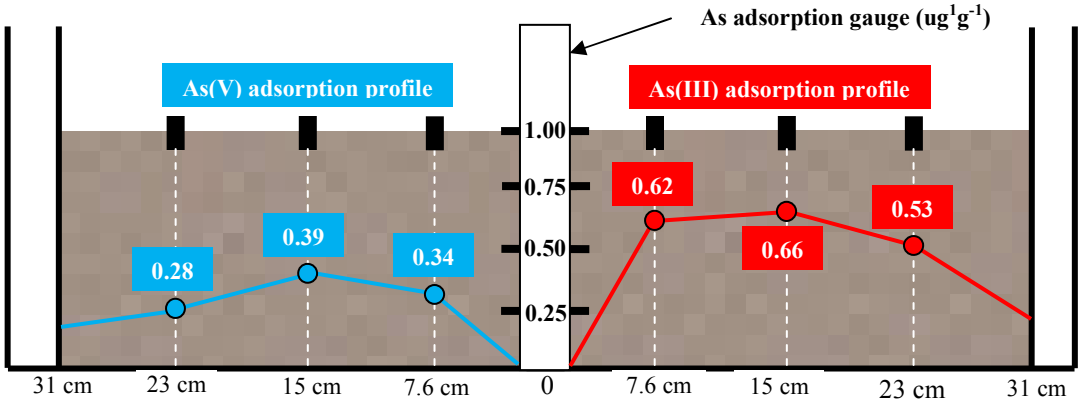

Figure 42: Water Well Arsenic Adsorption Profile

Multiple sand samples were collected to quantify surface-bound As(III) and total As content and the average accumulation was plotted with respect to each radius (Figure 42). The profile revealed an asymmetrical distribution of As collection on the sand where As(III) adsorption significantly exceeded As(V) adhesion. Two possible

explanations of the low surface-bound As(V) concentration may be (1) the reduction of previously adsorbed As(V) to As(III) by organic matter in the water and adsorbed onto the sand (Bauer and Blodau, 2005) and (2) trace amounts of Fe^{2+} reducing As(V) to As(III) in an anoxic environment (Kent et al., 2001). Furthermore, the initial pH of the water (8.6 $\pm$ 0.1) was elevated during adsorption (9.4 $\pm$ 0.1); ensuing a shift in titration (Stumm, 1992) and leading to the results acquired in Figure 16. These mechanisms, combined with the sorption competition of other anions, may have severely diminished As(V) adsorption on the sand; thus yielding higher As(III) accumulation on the iron oxide surface.

The FeOx coating/As adsorption operation format (Figure 26) devised in Chapter III was applied in this study to replenish the IOCS upon breaching the 10 ug^1L^{-1} effluent As limit. The working water pressure in the injection well (3.0 $\pm$ 0.2 kPa) increased with less stability during the second FeOx emplacement cycle (3.9 $\pm$ 0.4 kPa). The resistance to flow likely increased as the pore volume was displaced by the ongoing accumulation and suspension of FeOx and As. The intermittent H_2O rinsing procedure briefly stabilized the water pressure to 2.8 $\pm$ 0.3 kPa after removing suspended debris from the system for 6 h. However, groundwater withdrawal was severely impeded (32 mL^1min^{-1} reduced to < 5 mL^1min^{-1}) shortly after commencing the second As adsorption cycle. This outcome was caused by congestion of the well casing (amassed FeOx on the weed blocker covering). The obstruction of well casing and imminent porosity attenuation appeared to have confined the effective life cycle of this study; prompting early shutdown and limiting its applicability. Notwithstanding its complications and

shortcomings, the data accentuates recurrent water arsenic remediation using in situ iron oxide-coated sand as an emerging alternative to conventional groundwater As treatment.

SUMMARY

Play sand packed in a simulated aquifer well was coated in iron oxide and used to remove As(III) and As(V) from contaminated groundwater. The iron oxide was precipitated from the interaction between Fe^{2+} and H_2O_2 on the sand surface using imbibition flow. The reagent pH, solubility, stability, and injection schedule were found to facilitate the emplacement of the FeOx barrier at remote distances from the point of injection. The initial condition of the native groundwater used to prepare the reagents was found to significantly impact the overall performance of FeOx sedimentation by accelerating oxidant degradation. The resulting IOCS could remove As from water; however, the treatment capacity was profoundly limited by the loss of hydraulic conductivity ensuing from congestion at the injection well and in the sand.

CHAPTER VI

CONCLUSIONS

SUMMARY

Iron Oxide Emplacement

A specially-designed injection scheme effectively coated silica sand in iron oxides. The emplacement was dictated by (1) the preparation of the chemicals, (2) the initial surface condition of the sand (initial surface area and pre-existing iron content), and (3) the injection schedule of the procedure. The first FeOx layer originated from the pre-existing iron content on the surface colloids of the sand grain; effectively initiating an auto-catalytic sedimentation process thereafter. The physical, chemical, and operational manipulation of the reagents was shown to have delayed iron oxide (FeOx) precipitation in the storage and conveyance systems, but encouraged depth-specific sedimentation in the sand column.

As Adsorption by IOCS

A neutral environment with ionic balance was found to be the most stable condition by which superior arsenic adsorption could be achieved. The anions in the water were shown to have no adverse impact on As(III) and As(V) adsorption, except when present as a function of alkalinity. The uptake of arsenic onto IOCS was affected by adsorbent dosage to a lesser extent than the effects of adsorption time and influent concentration. The impending saturation of the limited adsorption sites by the FeOx dosage was accelerated by increasing the influent As concentrations. The dynamics of the adsorption

complied with pseudo-second order kinetics that was dominated by film diffusion, followed by surface reactions that strengthened the bond between the arsenic and iron oxides. Despite its vulnerability to ultra-acidic conditions, the bond between the pollutant and the FeOx surface withstood acetic acid loadings and was rendered suitable for landfilling upon breaching the operational life cycle.

Modeling As Adsorption by IOCS

The adsorptive behavior of arsenic onto iron oxide-coated sand (IOCS) followed a multi-step pattern in which the process was dominated by bulk transport through the liquid phase. The rapid uptake of As(III) and As(V) was succeeded by the gradual diffusion into the iron oxide mesopores and micropores. The increase in mass transfer of the arsenic was initiated by the increase in initial concentrations. The adsorption mechanism reached equilibrium when the depleted As in the system reduced the rate of intra-particle diffusion.

Evaluation of Single Well Study

The coating scheme devised in Chapter II was successfully replicated for coating play sand in a 2-dimensional simulated groundwater well. The diffusion of Fe^{2+} was inhibited at greater distances from the well; allowing the H_2O_2 to oxidize the Fe^{2+} before leaving the aquifer system. The manipulation of the reagent pH and injection configuration precipitated an iron oxide barrier that was capable of removing large quantities of arsenic from groundwater.

RECOMMENDATIONS

Expansion of IOCS Production

The use of simple chemicals in this study to produce large quantities of IOCS in the ambient environment has exhibited substantial applicability. However, the technique could be enhanced with the implementation of a novel modeling mechanism that could predict the chemical demand and coating efficiency (FeOx accumulation) on the sand; thus forecasting the operational platform needed for optimum performance. This supplemental tool could allow the consumer to minimize input (operating costs, chemical usage, and capital) while meeting drinking water demand and regulations.

Although oxygen is an effective Fe^{2+} oxidant, its limited strength could be substituted with a stronger oxidizing agent such as hydrogen peroxide; yielding a higher Fe^{3+} precipitation efficiency. Additionally, the technique could be optimized with common ions such as calcium (Ca^{2+}), magnesium (Mg^{2+}), and sodium (Na^{+}) coexisting with Fe^{2+} in anoxic groundwater. While Chapter V used tap water, the performance was not compared to using DI H_2O. Lowson (1982) and Stumm and Morgan (1996) concluded that silica (Si) and phosphate (PO_4^{3-}) facilitated the oxidation of Fe^{2+} by materializing into complexes with Fe^{3+}. Houben (2004) found that trace amounts of cobalt (Co) and copper (Cu) accelerated the reaction of ferrous iron (Fe^{2+}). Tamura et al., (1976) also determined that Fe^{2+} oxidation was enhanced by the fluoride ion (F^{-}), but was lowered by perchlorate (ClO_4^{-}), nitrate (NO_3^{-}), chloride (Cl^{-}), bromide (Br^{-}), iodide (I^{-}), and sulfate (SO_4^{2-}). Hence, it is possible that further optimization of the FeOx emplacement technique using trace catalysts from native groundwater could eliminate

the demand for specially-prepared components such as de-ionized water; thus simplifying the developed procedure for large scale production. The resulting amendment, combined with the installment of a superior oxidant and modeling tool, could establish a new platform for in situ and ex situ IOCS manufacturing; effectively highlighting its feasibility and commercial value for other water treatment applications.

Expansion of Remediation Studies pertaining to IOCS

The primary focus of this study was to demonstrate and optimize the emplacement of iron oxides on sand using specially-prepared ferrous iron, water, and oxidant solutions in a newly devised coating procedure. However, the development of this technique also increases accessibility and efficiency for additional research opportunities to explore the versatility of this technology in water treatment. As such, future investigations on the uptake of pollutants such as radionuclides, inorganics, dissolved metals, and other drinking water-related contaminants should be considered. Such developments could supplement the social, fiscal, and environmental benefits of using IOCS to produce drinking water for domestic consumption and/or disaster relief efforts.

Pilot Study Implementation

The evidence gathered from this study provides proof of concept for IOCS as an adsorption medium for As. However, additional examinations on the ever-changing physical, biological, and chemical complexities of a groundwater well (heterogeneities in sand permeability, nuisance bacteria accumulation in the well, potential injection well congestion, variable water quality, pre-existing levels of reductants in the native groundwater, reductive dissolution of Fe^{3+} in anoxic environments, etc.) should be

conducted to replicate the outcomes that would be encountered in an actual aquifer. The complications associated with the varying porosities of an aquifer were briefly addressed in Chapter V by using play sand as the media; however, no extensive correlation between FeOx coating and hydraulic conductivity was observed in this study. Furthermore, the critically unsteady state of the groundwater arsenic (concentration, oxidation state, organic vs. synthetic nature, mobility, stability, etc.) should be extensively profiled with respect to the feasibility of this technology. The FeOx coating process was not significantly impacted by the conveyance of the reagents in this investigation. However, the effect of transference in a scale-up study, especially with the use of high-maintenance chemicals at elevated dosages, should be examined and accommodated. The outcomes of these investigations, combined with the results of Chapter V could warrant a pilot study to validate the commercial value of in situ groundwater arsenic remediation using iron oxide-coated sand. A demonstration at an existing groundwater well (high priority given to USEPA Superfund sites) incorporating the data acquired from current and future studies would be the first step in making this technology accessible to the public and hence would be recommended in the near future.

REFERENCES

Ainsworth C.C., Girvin D.C., Zachara J.M., and Smith C.C. (1989) Chromate adsorption on geothite: effects of aluminum substitution. Soil Science Society of America Journal 53, 411 – 418.

American Public Health Association (APHA), American Water Works Association (AWWA), and Water Environment Federation (WEF) (1995) Standard methods for the examination of water and wastewater. 19th edition. American Public Health Association Washington, DC.

American Water Works Association Committee (AWWA). (1985) An AWWA survey of inorganic contaminants in water supplies. Journal American Water Works Association 77(5), 67 – 72.

Anastasios I.Z. and Katsoyiannis I.A. (2002) Arsenic removal using iron oxide loaded alginate beads. Industrial and Engineering Chemistry Research 41, 6149 – 6155.

Anderson, L.C.D. and Bruland, K.D. (1991) Biochemistry of arsenic in natural waters: the importance of methylated species. Environmental Science and Technology 25, 420 – 429.

Anderson P.R. and Benjamin M.M. (1985) Effect of silicon on the crystallization properties of ferric oxides. Environmental Science and Technology 19(11), 1048 – 1053.

Bailey R.P., Bennett T., and Benjamin M.M. (1992) Sorption onto and recovery of Cr(IV) using iron oxide-coated sand. Water Science and Technology 26, 1239 – 1244.

Bard, A.J. (1966). Chemical Equilibrium. Harper and Row Publisher, Inc., New York.

Bauer M. and Blodau C. (2005) Mobilization of arsenic by dissolved organic matter from iron oxides, soils, and sediments. Science of the Total Environment 354, 179 – 190.

Benjamin M.M., Sletten R.S., Bailey R.P., and Bennett, T. (1996) Sorption and filtration of metals using iron oxide-coated sand. Water Research 30(11), 2609 – 2620.

Bureau of Reclamation, Technical Service Center. (2001) Water Treatment Engineering and Research Group. United States Department of the Interior. Denver, CO.

Chebotarev N.G. (1950) Fundamentals of Galois Theory. 1st edition. Nordhoff Publishing. Kandern, Germany.

Chen S.L., Yeh S.J., Yang M.H., and Lin T.H. (1995) Trace element concentration and arsenic speciation in the well water of a taiwan area with endemic blackfoot disease. Biological Trace Elements Research 48, 263 – 274.

Cheung W.H., Szeto Y.S., and McKay G. (2007) Intraparticle diffusion processes during acid dye adsorption onto chitosan. Bioresource Technology 98, 2897 – 2904.

Chiron N, Guilet R., and Deydier E. (2003) Adsorption of Cu(II) and Pb(II) onto a grafted silica: isotherms and kinetic models. Water Research 37, 3079 – 3086.

Chowdhury S. and Saha P (2010) Pseudo-second order kinetic model for sorption of malachite green onto sea shell: comparison of linear and non-linear methods. Research: Biophysics 1(3), 3 – 7.

Choy K.K.H., Porter J.F., and McKay G. (2004) Film-surface diffusion during the adsorption of acid dyes onto activated carbon. Journal of Chemical Technology and Biotechnology 79, 1181 – 1188.

Chu W. and Ma C.W. (2000) Quantitative prediction of direct and indirect dye ozonation kinetics. Water Research 34(12), 3153 – 3160.

Chu W. and Tsui S.M. (1999) Photo-sensitization of diazo disperse dye in aqueous acetone. Chemosphere 39(10), 1667 – 1677.

College Station Utilities (2005) Water Quality Test Results. City of College Station Water Quality Report. College Station, Texas.

College Station Utilities (2008) Water Quality Test Results. City of College Station Water Quality Report. College Station, Texas.

College Station Utilities (2011) Water Production and Treatment. City of College Station Water Services. College Station, Texas.

Cook G.A. and Lauer C.M. (1968) The Encyclopedia of the Chemical Elements. Reinhold Book Corporation. New York.

Corbett J.F. (1972) Psuedo first-order kinetics. Journal of Chemical Education 49(10), 663.

Cornell, R. M. and Schwertmann, U. (2003) The iron oxides: structure, properties, reactions, occurrences, and uses. 2nd Edition. Wiley-VCH GmbH and Company KGaA. Weinheim, Germany.

Cotruvo, J. A. (1988) Drinking water standards and risk assessment. Regulatory Toxicology and Pharmacology 8(3), 288-299.

Cotton F.A. and Wilkinson G. (1972) Advanced Inorganic Chemistry: A Comprehensive Text. 3rd edition. Interscience Publishers. New York.

Dole M. (1965) The natural history of oxygen. Journal General Physiology 49, 5 - 27

Dzombak, D. A. and Morel, F. M. (1990) Surface complexation modeling: hydrous ferric oxide. Wiley-Interscience. New York.

Eckenfelder, Jr. W.W. (2000) Industrial Water Pollution Control. 3rd edition. McGraw Hill, Inc. New York.

Edwards, M. and Benjamin, M.M. (1989) Adsorptive filtration using coated sand: a new approach for treatment of metal-bearing wastes. Research Journal of Water Pollution Control Federation 61(9), 1523 – 1533.

Ellis, E. A. and Pendleton, M. (2007) Vapor coating: a simple, economical procedure for preparing difficult specimens for scanning electron microscopy. Microscopy Today 15(3), 44.

Emsley J. (2001) Nature's Building Blocks: An A-Z Guide to the Elements. Oxford University Press. Oxford, England.

Essig, M.G. (2008) Chloride (Cl). WebMD Information and Resources. Van Houten S. and Landauer T. (eds). Online. URL: http://www.webmd.com/a-to-z-guides/chloride-cl. Updated on April 17, 2009. Accessed on April 3, 2011.

Fuller C.C., Davis J.A., and Waychunas G.A. (1993) Surface chemistry of ferrihydrite: part 2. kinetics of arsenate adsorption and co-precipitation. Geochimica et Cosmochimica Acta 57, 2271 – 2282.

Ganesh R., Boardman G.D., and Michelsen D. (1994) Fate of azo dyes in sludges. Water Research 28(6), 1367 – 1376.

Ghosh, M. (1993) Committee report: research needs for inorganic contaminants. Journal American Water Works Association 5, 106 – 113.

Goldberg S. and Johnstony C.T. (2001) Mechanisms of arsenic adsorption on amorphous oxides evaluated using macropscopic measurements, vibrational spectroscopy, and surface complexation modeling. Journal of Colloid Interfacial Science 234, 204 – 216.

Guo H., Stuben D., and Berner Z. (2007) Arsenic removal from water using natural iron mineral-quartz sand columns. Science of the Total Environment 377, 142 – 151.

Gupta V.K., Saini V.K., and Jain N. (2005) Adsorption of As(III) from aqueous solutions by iron oxide-coated sand. Journal of Colloid and Interface Science, 288, 55 – 60.

Hathway G.J., Proctor N.H., Hughes J.P., and Fischman M.L. (1991) Proctor and Hughes' Chemical Hazards of the Workplace. 3rd edition. Van Nostrand Reinhold. New York, NY.

Hem J.D. (1989) Study and interpretation of the chemical characteristics of natural water. US Geological Survey (USGS) Water-Supply Paper 2254, 263.

Ho Y.S. (2006) Second-order kinetic model for the sorption of cadmium onto tree fern: A comparison of linear and non-linear methods. Water Research 40(1), 119 – 125.

Ho Y.S., Ng J.C.Y., and McKay G. (2000) Kinetics of pollutant sorption by biosorbents: review. Separation and Purification Methods 29(2), 189–232.

Ho Y.S. and McKay G. (1999) Pseudo-second order model for sorption process. Process Biochemical 34, 451 – 465.

Ho Y.S. and Ofomaja A.E. (2006) Psuedo-second order model for lead ion sorption from aqueous solutions onto palm kernel fiber. Journal of Hazardous Materials B129, 137 - 142

Hohl H. and Stumm W. (1976) Interaction of Pb^{2+} with hydrous α-Al_2O_3. Journal of Colloid Interface Science 55, 281 – 288.

Huang Y.H. (2009) Induced migration of surface colloids by acid and base elutions. Personal Communication.

Houben G.J. (2004) Modeling the buildup of iron oxide encrustations in wells. Ground Water 42(1), 78 – 82.

Hutchins R.A. (1974) New method simplifies design of activated carbon systems. Chemical Engineering 80, 133 – 138.

Hutton M. (1987) Human Health Concerns of Lead, Mercury, Cadmium, and Arsenic. Lead, Mercury, Cadmium, and Arsenic in the Environment. John Wiley and Sons. New York.

Ibezim-Ezeani M.U. and Anusiem A.C.I. (2010) Kinetic studies of adsorption of palmitate and laurate soaps onto some metal ores in aqueous media. International Journal of Physical Sciences 5(1), 62 – 67.

Jambor J.L. and Dutrizac J.E. (1998) Occurrence and Constitution of Natural and Synthetic Ferrihydrite, a Widespread Iron Oxyhydroxide. Chemical Review 98, 2549 - 2585

Kaur A., Malik A.K., Verma N., and Rao A.L.J. (1991) Removal of copper and lead from wastewater by adsorption on bottom ash. Indian Journal of Environmental Protection 11, 433 – 435.

Kent D.B., Niedan V.W., Isenbeck-Schroter M., Stadler S., Jahn S., Hohn R., and Davis J.A. (2001) The influence of oxidation-reduction and adsorption reactions on arsenic transport in the oxic, suboxic, and anoxic zones of a mildly acidic sand and gravel aquifer. Abstract in United States Geological Survey (USGS) Workshop on Arsenic in the Environment, Denver, CO.

Khare S.K. Panday K.K., Srivastava R.M., and Singh V.N. Removal of victoria blue from aqueous solution by fly ash. Journal of Chemical Technology and Biotechnology A – Chemical Technology 38, 99 – 104.

Kleinfeld M., Giel C., and Tabershaw I.R. (1957) Health hazards associated with inert-gas-shielded metal arc welding. AMA Archives of Industrial Health 15(1), 27-31.

Ko D., Porter J., and McKay G. (2000) Optimized correlations for the fixed-bed adsorption of metal ions on bone char. Chemical Engineering Science 55, 5819.

Korte N.E., and Fernando Q. (1991) A Review of arsenic(III) in groundwater. Critical Review of Environmental Control 21, 1 – 39.

Lagergren S. (1898) To the theory of so-called adsorption of dissolved substances. Kungliga Svenska Vetenskapsakadeiens. Handlingar 24(4) 1 – 39.

LaGrega M.D., Buckingham P.L., Evans J.C., and Environmental Resources Management (ERM) (2001) Hazardous Waste Management. 2nd edition. McGraw-Hill Companies. New York.

Lalvani S.B., Wiltowski T., Hubner A., Weston A., and Mandich N. (1998) Removal of hexavalent chromium and metal cations by a novel carbon adsorbent. Carbon 36, 1219 – 1269.

Lee K.Y., Yoon Y.Y., Jeong S.B., Chae Y.B., and Ko K.S. (2009) Acid leaching purification and neutron activation analysis of high purity silicas. Journal of Radioanalytical and Nuclear Chemistry 282, 629 – 633.

Lee S.O., Tran T., Jung B.H., Kim S.J., and Kim M.J. (2007) Dissolution of iron using oxalic acid. Hydrometallurgy 87, 91 – 99.

Lehmann M., Zouboulis A., and Matis K. (2001) Modeling the sorption of metals from aqueous solutions on goethite fixed beds. Environmental Pollution 113, 121.

Leist M., Casey R.J., and Caridi D. (2000) The Management of Arsenic Wastes: Problems and Prospects. Journal Hazardous Materials 76, 125 – 138.

Lenntech (2009) Water treatment solutions: ozone decomposition. Online. Accessed 25 May 2011. URL: http://www.lenntech.com/library/ozone/decomposition/ozone-decomposition.htm.

Life Systems, Inc. (1989) Toxicological Profile for Arsenic. Agency for Toxic Substances and Disease Registry, Report No. ATSDR/TP-88/02. Atlanta, GA.

Lin J. and Wang L. (2009) Comparison between linear and non-linear forms of pseudo-first order and pseudo-second order adsorption kinetic models for the removal of methylene blue by activated carbon. Environmental Science and Engineering 3(3), 320 – 324.

Lin S.H. and Lin C.M. (1993) Treatment of textile waste effluents by ozonation and chemical coagulation. Water Research 27(12), 1743 – 1748.

Lowson R.T. (1982) Aqueous oxidation of pyrite by molecular oxygen. Chemical Review 82(5), 461 – 497.

MacKenzie F.T., Lanzy R.J., and Paterson V. (1979) Global trace metal cycles and predictions. Journal of International Association of Mathematics and Geology 6, 99 – 142.

Mandal B.K. and Suzuki K.T. (2002) Arsenic around the world: A review. Talanta 58, 201 – 235.

McNeill L.S. and Edwards M. (1997) Arsenic removal during precipitative softening. Journal Environmental Engineering 123, 800 – 807.

Meng X., Cheng Z., Van Geen A., Jing C., Seddique A., and Kazi Matin A. (2004) Performance of a household-level arsenic removal system during 4-month deployments in Bangladesh. Environmental Science and Technology 38(12), 3442 – 3448.

Millero F.J., Hubinger S., and Fernandez M. (1987) Oxidation of H_2S in seawater as a function of temperature, pH, and ionic strength. Environmental Science and Technology 21, 439 – 443.

Mohan D. and Pittman Jr., C.U. (2007) Arsenic removal from water/wastewater using adsorbents: a critical review. Journal Hazardous Materials 142, 1 – 53.

Mondal P., Majumder C.B., and Mohanty B. (2006) Laboratory based approaches for arsenic remediation from contaminated water: recent developments. Journal Hazardous Materials B137, 464 – 479.

Morel, F. M. M. and Hering, J. G. (1993) Principles and Applications of Aquatic Chemistry. 1st edition. Wiley-Interscience. New York.

Murphy E.M., Zachara J.M., Smith S.C., Phillips J.L., and Thomas W.W. (1994) Interaction of hydrophobic organic compounds with mineral-bound humic substances. Environmental Science and Technology 28, 1291 – 1299.

Namasivayam C. and Ranganathan K. (1993) Waste Fe(III)/Cr(III) hydroxide as adsorbent for the removal of Cr(IV) from aqueous solution and chromium plating industry wastewater. Environmental Pollution 82(3), 255 – 261.

National Academy of Science (NAS). (1999) Risk Estimate. USA.

National Drinking Water Advisory Council (NDWAC) (2001) Final Report of the Arsenic Cost Working Group to the National Drinking Water Advisory Council. United States Environmental Protection Agency (USEPA) USA.

National Institute of Standards and Technology (NIST) (2007) IUPAC-NIST Solubility Database: Ferrous Chloride. Accessed 9 September 2011.

Nordstrom D.K., and Alpers C.N. (1999) Negative pH, Efflorescent Mineralogy, and Consequences for Environmental Restoration at the Iron Mountain Superfund Site, California. Proceedings of the National Academy of Science USA 96, 3455 – 3462.

Onishi H. and Wedepohl K.H. (1969) Handbook of Geochemistry. Volume 2. Springer-Verlag. New York. Chapter 33.

Oremland S. and Stolz J.F. (2003) Ecology of arsenic. Science 300(5621), 939 – 944.

Ozonia, Ltd (1977). The Ozat™ Compact Ozone Generation Units. Technical Paper. Ozone North America. Elmwood Park, New Jersey.

Panday K.K., Prasad G., and Singh V.N. (1986) Mixed adsorbent for Cu(II) removal from aqueous solutions. Environmental Technology Letters 7, 547 – 554.

Petrucci, R.H. (2007) General Chemistry: Principles and Modern Applications. 9th edition. Prentice Hall, Inc. New Jersey.

Pontius F.W., Brown K.G., and Chen C.J. (1994) Health implication of arsenic in drinking water. Journal American Water Works Association 86(9), 52 – 63.

Poots V.J.P., McKay G., and Healy J.J. (1978) Removal of basic dye from effluent using wood as an adsorbent. Journal of Water Pollution Control Federation 50, 926 – 931.

Ramakrishna D.M., Viraraghavan T., and Jin Y.C. (2006) Iron oxide coated sand for arsenic removal: investigation of coating parameters using factorial design approach. Practice Periodical of Hazardous, Toxic, and Radioactive Waste Management 10(4), 198 – 206.

Raven K.P., Jain A., and Loeppert R.H. (1998) Arsenite and arsenate adsorption on ferrihydrite: kinetics, equilibrium, and adsorption envelopes. Environmental Science and Technology 32, 344 – 349.

Rose A.L. and Waite T.D. (2002) Kinetic model for Fe(II) oxidation in seawater in the absence and presence of natural organic matter. Environmental Science and Technology 36, 433 – 444.

Ryker S.J. (2001) Mapping arsenic in groundwater. Geotimes 46(11), 34-36.

Sarkar S., Lee M.B., Gupta A., Ghosh D., and Segupta A.K. (2008) Arsenic removal from groundwater and its safe containment in a rural environment: validation of a sustainable approach. Environmental Science and Technology 42(12), 4268 - 4273

Shannon R.D. (1976) Revised effective ionic radii and systematic studies of interatomic distances in halides and chalcogenides. Acta Crystallographica A32, 751 – 767.

Sharma Y.C., Gupta G.S., Prasad G. and Rupainwar D.C. (1990) Use of wallastonite in the removal of Ni(II) from aqueous solutions. Water, Air, and Soil Pollution 49, 69 – 79.

Singh A.K., Singh D.P., Panday K.K., and Singh V.N. (1998) Wollastonite as adsorbent for removal of Fe(II) from water. Journal of Chemical Technology and Biotechnology 42, 39 – 49.

Smith A.H., Arroyo A.P., Mazumdar D.N.G., Konsnett, Harnandez A.L., Lingas E.O., Beeris M., Smith M.M., and Moore L.E. (2000) Arsenic induced skin lesions among atacameno people in northern chile despite good nutrition and centuries of exposure. Environmental Health Perspectives 108, 617 – 620.

Smith A.H., Hopenhayn-Rich C., Bates M.N., Goeden H.M., Picciotto I.H., Duggan H.M., Wood R., Kosnett M.J., and Smith M.T. (1992) Cancer risks from arsenic in drinking water. Environmental Health Perspectives 97, 259–267.

Stenkamp V.S. and Benjamin M.M. (1994) Effect of iron oxide coating on sand filtration. Journal American Water Works Association. 86(8), 37 – 50.

Stumm W. (1992) Chemistry of solid-water interface. Wiley and Sons, Inc. New York.

Stumm W., Huang C.P., and Jenkins S.R. (1970) Specific chemical interactions affecting the stability of dispersed systems. Croatica Chemica Acta 42, 223 – 245.

Stumm W. and Lee G.F. (1961) Oxygenation of ferrous iron. Industrial Engineering and Chemistry Research 53, 143 – 146.

Stumm W. and Morgan J.L. (1996) Aquatic Chemistry. Wiley and Sons, Inc. New York.

Subramnian K.S. (1988) Arsenic in Quantitative Trace Analysis of Biological Materials. McKenzie H.A. and Smythe L.E. (eds). Elsevier Science Publishers. Amsterdam.

Sung W., and Morgan J.L. (1980) Kinetics and product of ferrous iron oxygenation in aqueous systems. Environmental Science and Technology 14, 561 – 568.

Tamura H., Goto K., and Nagayama M. (1976) The effect of ferric hydroxide on the oxygenation of ferrous irons in neutral systems. Corrosion Science 16, 197 – 207.

Tchobanoglous G., Burton F., and Stensel D.H. (2003) Wastewater Engineering: Treatment and Reuse. 4th edition. McGraw-Hill, Inc. New York.

Thirunavukkarasu O.S., Viraraghavan T., and Subramanian K.S. (2003) Arsenic removal from drinking water using iron oxide-coated sand. Water, Air, Soil Pollution 142, 95 – 111.

Thorkildsen D. and Price R.D. (1991) Groundwater resources of the Carrizo-Wilcox aquifer in the Central Texas region. Texas Water Development Board 332, 73.

Tondel M., Rahman M., Magnuson A., Chowdhury I.A., Faruquee M.H., and Ahmad S.A. (1999) The relationship of arsenic levels in drinking water and the prevalence of skin lesions in Bangladesh. Environmental Health Perspectives 107, 727 – 729.

US Environmental Protection Agency (USEPA) (1978) Manual of Treatment Techniques for Meeting the Interim Primary Drinking Water Regulations. EPA-600/8-77-005

US Environmental Protection Agency (USEPA) (1986) Method 1311: Toxicity Characteristic Leaching Procedure. SW-846: Test Methods for Evaluating Solid Waste. 3rd edition. Washington D.C.

US Environmental Protection Agency (USEPA) (1988) Special Report on Ingested Arsenic: Skin Cancer; Nutritional Essentiality. Risk Assessment Forum, Washington, DC. EPA/625/3-87/013.

US Environmental Protection Agency (USEPA) (2000) Technologies and Costs for Removal of Arsenic from Drinking Water. Washington, D.C. EPA 815-R-00-028.

US Environmental Protection Agency (USEPA) (2006) Drinking Water Standards and Health Advisories. Washington, D.C. EPA 822-R-09-011.

US Environmental Protection Agency (USEPA) (2009) Steam Electric Power Generating Point Source Category. Electronic Code of Federal Regulations. USEPA Washington D.C. EPA Title 40, Part 423.

USEPA Office of Emergency and Remedial Response (USEPA OERR) (2009) Environmental Response Comprehensive and Liability Information System database (CERCLIS 3). USEPA. Washington D.C.

US Peroxide. Hydrogen peroxide technical library: decomposition. Online. Accessed 9 September 2011. URL: http://www.h2o2.com/faqs/FaqDetail.aspx?fId=5

Vaishya R.C. and Gupta S.K. (2003) Coated sand filtration: An emerging technology for water treatment. Journal of Water Supply: Research and Technology-AQUA 52(4), 299 – 306.

Viraraghavan T., Subramanian K.S., and Aruldoss J.A. (1999) Arsenic in drinking water: problems and solutions. Water Science and Technology, 40(2), 69-76.

Vracar R.Z. and Cerovic K.P. (1997) Kinetics of oxidation of Fe(II) ions by gaseous oxygen at high temperatures in an autoclave. Hydromettalurgy 44, 113 – 124.

Walker G.M. and Weatherley, L.R. (2000) Prediction of bisolute dye adsorption isotherms on activated carbon. Process Safety and Environmental Protection 78(B3), 219 – 223.

Weber W.J.Jr. and Morris S.C. (1963) Intra-particle diffusion during the sorption of surfactants onto activated carbon. Journal. Sanitation Engineering Division. Proceedings. American Society of Civil Engineers 89(1), 53 – 61.

Wehrli, B. (1990) Redox reactions of metal ions at mineral surfaces. Aquatic Chemical Kinetics. Stumm W. (ed). John Wiley and Sons. New York. 311 - 336

Willet I.R., Chartres C.J., and Nguyen T.T. (1988) Migration of phosphate into aggregated particles of ferrihydrite. Journal of Soil Science 39, 275 – 282.

World Health Organization (WHO) (1996). Guidelines for Drinking Water Quality. 2nd edition. Health Criteria and Other Supporting Information. World Health Organization, Geneva.

Xu Y. and Axe L. (2005) Synthesis and characterization of iron oxide-coated silica and its effect on metal adsorption. Journal of Colloid and Interface Science 282, 11 – 19.

Zachara J.M., Girvin D.C., Schmidt R.L., and Resch C.T. (1987) Chromate adsorption on amorphous iron oxyhydroxide in the presence of major groundwater ions. Environmental Science and Technology 21, 589 – 594.

Zeng, L. (2003) A method for preparing silica-containing iron (III) oxide adsorbents for arsenic removal. Water Resources Research, 37(18), 4351 – 4358.

Zhuang J.M., Hobenshield E., and Walsh T. (2008) Arsenate sorption by hydrous ferric oxide incorporated onto granular activated carbon with phenol formaldehyde resins coating. Environmental Technology 29, 401 – 411.

VITA

Name:	Thomas Sunday Abia II
Address:	201 Scoates Hall, TAMU 2117, College Station, TX 77843
Email Address:	tsabia2@gmail.com
Education:	B.S., Environmental Engineering, California State University – San Luis Obispo, 2008
	M.S., Civil/Environmental Engineering, California State University – San Luis Obispo, 2008
Specialties:	Applied Water Treatment Research: permeable reactive barrier (PRB) technology R&D, black and grey water management, and natural disaster impaired water remediation
	In Situ Engineering: on-site inventory availability and conversion
	Disaster Relief Technology: assistive living and water resources
	Water Research Efficiency: control systems and automation
	Process Research and Development: proof-of-concept testing, life cycle assessments, prototype development, operational optimization, and sustainable commercialization